AN AUTOMATIC GLIOMA DETECTION AND EXTRACTION FRAMEWORK FOR THE REMOVAL OF SHRINKAGE IN SEGMENTATION

Thesis submitted in fulfillment of the requirements for the Degree of

DOCTOR OF PHILOSOPHY

By

JYOTSNA DOGRA
(166004)

Department of Electronics and Communication Engineering

JAYPEE UNIVERSITY OF INFORMATION TECHNOLOGY
WAKHNAGHAT, SOLAN-173234, HIMACHAL PRADESH, INDIA

JUNE, 2020

TABLE OF CONTENTS

CHAPTER 4

AUTOMATED FRAMEWORK DESIGN FOR REMOVAL OF FALLACIOUS SEGMENTATION

CHAPTER 5

ROBUST DESIGN FOR BIAS FIELD EFFECTED MR IMAGE FOR GLIOMA SEGMENTATION

CHAPTER 6

DESIGN OF MR SEQUENCE DETECTOR FOR EFFECTIVE GLIOMA GRADING

CHAPTER 7

CONCLUSION AND FUTIRE WORK   **177**

DECLARATION BY THE SCHOLAR

I hereby declare that the work reported in the Ph.D. thesis entitled **"An Automatic Glioma Detection and Extraction Framework for the Removal of Shrinkage in Segmentation"** submitted at **Jaypee University of Information Technology, Wakhnaghat, India,** is an authentic record of my work carried out under the supervision of **Dr. Meenakshi Sood** and **Dr. Shruti Jain**. I have not submitted this work elsewhere for any other degree or diploma. I am fully responsible for the contents of my Ph.D. Thesis.

Jyotsna Dogra

Department of Electronics and Communication Engineering
Jaypee University of Information Technology, Wakhnaghat, India

SUPERVISOR'S CERTIFICATE

This is to certify that the work reported in the Ph.D. thesis entitled **"An Automatic Glioma Detection and Extraction Framework for the Removal of Shrinkage in Segmentation"**, submitted by **Jyotsna Dogra** at **Jaypee University of Information Technology, Wakhnaghat, India,** is a bonafide record of her original work carried out under my supervision. This work has not been submitted elsewhere for any other degree or diploma.

Dr. Meenakshi Sood

Associate Professor
Department of CDC
National Institute of Technical Teachers Training & Research, Chandigarh, India

Dr. Shruti Jain

Associate Professor
Department of Electronics and Communication Engineering
Jaypee University of Information Technology, Wakhnaghat, India

ACKNOWLEDGEMENT

LIST OF ACRONYMS & ABBREVIATIONS

ABC	Artificial Bee Colony
ACC	Accuracy
ANN	Artificial Neural Network
AUC	Area Under the Curve
BRATS	Brain Tumor Segmentation
CAD	Computer Assisted Diagnosis
CBICA	Center of Biomedical Image Computing and Analytics
CBSS	Centroid Based Seed Selection
CC	Correlation Coefficient
CHCN	Competitive Hopfield clustering network
CNS	Central Nervous System
CSF	Cerebrospinal Fluid
CT	Computer Tomography
DSC	Dice Similarity Coefficient
ERR	Error Rate
FCM	Fuzzy c Mean
FFT	Fast Fourier Transform
FLAIR	Fluid Attenuated Inversion Recovery
FN	False Negative
FP	False Positive
GBKS GC	Gradient Based Kernel Selection Graph Cut
GBM	Glioblastoma Multiforme
GC	Graph Cut
GLCM	Gray Level Co-occurrence Matrix
GLN	Gray Level Non-Uniformity
GLRM	Generalized Low Rank Models
GM	Gray Matter
GRFs	Gibbs Random Fields

HBBTR	Hospital Based Brain Tumor Registry
HGG	High Grade Gliomas
IBSR	Internet Brain Segmentation Repository
ICM	Iterated Conditional Mode
IGMC	Indra Gandhi Medical College
IDM	Inverse Difference Moment
IIH	Intensity Inhomogeneity
JI	Jaccard Index
KMSS	k-Mean Seed Selection
KNN	k-Nearest Neighbor
LACM	Localized Active Contour Model
LBP	Loopy Belief Propagation
LGG	Low Grade Gliomas
LRE	Long Run Emphasis
LSF	Level Set Function
MAL	Major Axis Length
MAP	Maximum a Posteriori
MiAL	Minor Axis Length
MICCAI	Medical Image Computing and Computer Assisted Intervention
MRF	Markov Random Field
MRI	Magnetic Resonance Imaging
MRMR	Minimal Redundancy Maximal Relevance
MSE	Mean Square Error
NBTF	National Brain Tumor Foundation
NM	Nuclear medicine
NMR	Nuclear Magnetic Resonance
NMV	Net Magnetization Vector
NP	Nondeterministic Polynomial
OCT	Optical coherence tomography
PCA	Principle Component Analysis
PET	Positron Emission Tomography

PPV	Positive Predicted Value
PSNR	Peak Signal-To-Noise Ratio
PSO	Particle Swarm Optimization
QCT	Quantitative computed tomography
RANO	Response Assessment in Neuro-Oncology
RF	Radio Frequency
RGB	Red Green Blue
RLN	Run Length Non-Uniformity
RMSE	Root Mean Square Error
ROI	Region of Interest
RP	Run Percentage
RW	Random Walk
SBIA	Section for Biomedical Image Analysis
SENS	Sensitivity
SOM	Self Organizing Maps
SPEC	Specificity
SPECT	Single-Photon Emission Computed Tomography
SPSS	Statistical Package for Social Sciences Statistics
SRE	Short Run Emphasis
SVM	Support Vector Machine
TE	Echo Time
TN	True Negative
TP	True Positive
TR	Repetition Time
UAV	Unmanned Aerial Vehicle
UECS	Ultimate Erosion for Convex Sets
US	Ultrasound
WHO	World Health Organization
WM	White Matter

LIST OF FIGURES

LIST OF TABLE

ABSTRACT

Medical image analysis is an essential part of clinical and laboratory research that has led to development of techniques for various medical applications. These techniques improve the sensitivity, specificity and provide complete characterization and grading of tumors. One of the tumor type that is a major threat to human population is Glioma found in adults. A lot of registered cases of malignant and benign tumor have been found. The technological advancement in images analysis techniques has gain popularity, as they provide a second opinion to the experts for making a better decision in treatment planning. They also help in avoiding biopsy that causes patient to go through post physiological stress. Image segmentation and classification of glioma tumors is an eminent research area that provides assistance to radiologist that aid in early detection and treatment planning of patient. For tumor extraction from MR Images, Graph Cut technique is a ubiquitous method in the medical image segmentation field. It is an energy based technique that is determined from region based statistics of the posterior probabilities. Graph cut energy minimization framework is popularly adopted for tumor segmentation in MRI.

In previous years the initialization of this technique has remained manual due to lack of priori information. This priori information is the most essential requirement for constructing accurate seed values in order to extract tumor region through an automatic process. MRIs are constructed with various spatial parameters, topology and pixel intensities. Different regions in brain consists of different properties and their identification is mostly provided by the expert radiologist. Hence, understanding, selection and identification of these values becomes difficult with the complex brain structure. In this thesis, we propose that the quality of image segmentation is improved by developing an intelligent framework that is able to internally feed this prior information.

The tumor extraction completely depends on these selected seed values but a better framework is developed by automatizing this process. As graph cut portrays the segmentation as labelling problem and depends on intensity values so, there is a chance that similar intensity values if found in normal part of brain may also get labeled as object region. This problem of graph cut

is called as Shrinkage problem that has been addressed in this research work. The fallacious segmentation caused by shrinkage problem changes tumor characterization and increases ambiguity in diagnosis. Hence, a technique is developed in this research work that is able to provide simultaneous goals like automatic initialization, accurate seed selection and removal of shrinkage problem.

More advanced MRI machines are able to provide human body scan at magnetic field above 3T. These scans have higher spatial resolution but may hinder with the imaging properties. Hence, a noise is created that is called as intensity inhomogeneity (IIH). It is a low frequency surface that change the image pixels through a smooth gradation by variation of the radio frequency pulses. These changes are also observed by the histogram of images. Two types of bias field cause IIH that are longitudinal (RF at 90º) and circular (caused RF at 45º). We demonstrate that by taking into account the higher magnetic field application, we not only able to achieve better extraction and segmentation of glioma, but also potentially resolve certain ambiguities of graph cut technique.

Finally, we consider the problem of automatically determining the sequence from MRI scans. The MRI scans consists of different sequences that highlight different property of brain and tumor region. The different sequences are: T1, T1ce, T2 and Flair that are obtained by varying different parameter in MR machine. A tumor consists of different regions like tumor core, enhancing and non-enhancing regions. Each sequence of MRI scan provides diverse information regarding these regions. Extraction of tumor is done on Flair image as it provides high contrast difference between the tumor and non-tumor region. But, to have the knowledge of best sequence that is able to define the type of glioma with highest accuracy is a big issue. Machine learning is used for binary classification of each sequence in order to identify the optimal sequence for glioma grading.

This research work aims at developing a system design for providing better diagnosis and prognosis.

CHAPTER 1

INTRODUCTION

CHAPTER 1

INTRODUCTION

Brain is the most important part of the human body with an intricate structure that controls all the vital functions such as: motor skills, touch, speech and other body movement. A large amount of communication is done through trillions of connections inside this complex organ. Brain is encapsulated inside the skull consisting: i) Gray Matter (GM), ii) White Matter (WM) and iii) Cerebrospinal Fluid (CSF). The GM is the darker tissue of the brain and spinal cord that contains nerve cells and dendrites. The paler tissue that comprise myelin sheaths and nerve fibers is the WM. CSF is a transparent liquid composed of oxygen, ion and glucose that help in providing a barrier against shocks. It also helps in removing the waste product from nervous tissue.
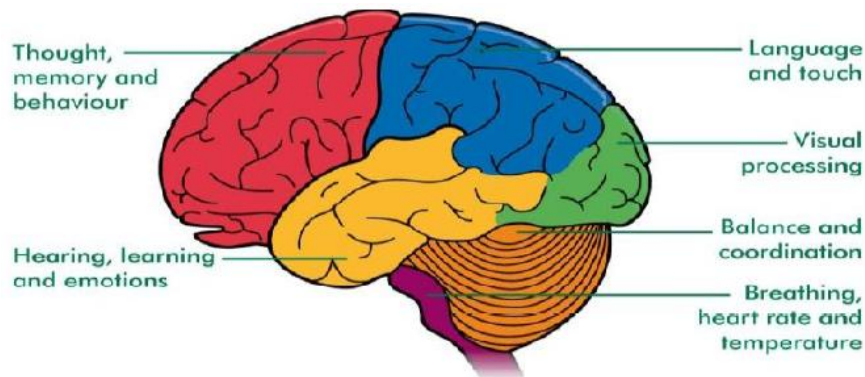
Figure 1.1 Brain anatomy [2]

The main parts of brain are shown in Figure 1.1 that consists of Cerebrum, Frontal lobe, Occipital lobe, Cerebellum, Brain stem, Temporal lobe and Parietal lobe. Cerebrum controls function such as creativity, logic and reasoning and is divided in two hemispheres. The right hemisphere controls function of left side of body and left hemisphere controls functions of right side of body. Both the hemispheres are further divided into subparts of different lobes.

Below the cerebrum lies Cerebellum with the main feature of coordinating the muscles. If any problem occurs in this region affects the motor skills of the human body.

Even with such a fascinating organization of brain some portion of the brain has been affected by the abnormal growth of cells called Tumor. Hence, tumors are the most fatal disease for human body and has become very prevalent. In this chapter we will study the most common type of tumor known as Glioma that is caused due to uncontrolled growth of glial cell.

1.1   OVERVIEW OF GLIOMA

The prevalence of brain tumors among the human population has caused an increased threat as most of the tumors are fatal cancers [1]. The most common type of primary tumor is Glioma that is caused due to the abnormal growth of the tissue. An uncontrolled multiplication of tissue causes this growth and a mass is formed in the brain that has no physiological function. Gliomas start in the glial cells that are supporting cells of the brain and spinal cord. They affect the functioning of the brain and can be life threatening depending on its growth and location. Glioma form a 24.7% of all the primary tumor as broadly categorized in Figure 1.2 [2].
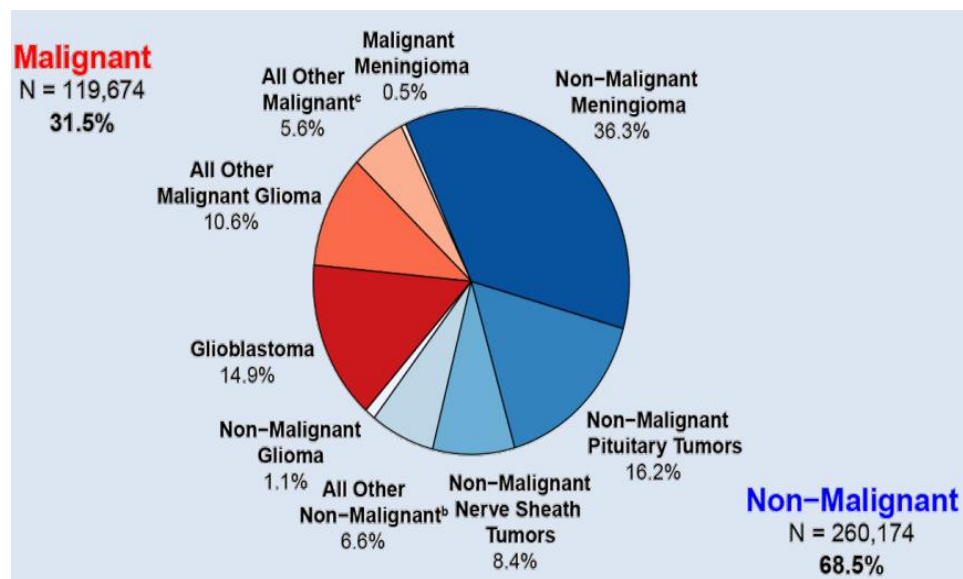
Figure 1. 2 Primary brain tumor distribution [2]

Depending on the origin and the growth of the tumor, they are classified in two types primary and secondary (metastasis) tumors. The primary tumors are benign and the secondary tumors are malignant in nature. In the primary tumors the cells are originally brain cell that are not active cancer cell and has a uniformity in structure. These include the Low Grade Gliomas (LGG) such as Meningiomas. On the other hand, secondary tumors contain active cancer cell and a non-uniform structure. In these tumors the cancerous cell spread into the brain from other infected regions. These are also called as high grade glioma including tumor classes of Glioblastoma and Astrocytoma.

In 2018, new cases of brain and Central Nervous System (CNS) tumors that were recorded in United States were 23,880 and the recorded deaths were 16,830 [3]. In a study done by Kohler *et al.* in 2011 [4] US incidence rate for primary tumor was estimated to be 25 per 100,000 adults among which the malignant tumors were one third. The national Brain Tumor Foundation (NBTF) projected that in the developed countries the people dying because of brain tumor are more than 300% [5-6]. Also in the US 29000 population underwent diagnosis for the primary brain tumor diagnosis [7]. Among malignant tumors Glioblastoma has the highest number of estimated cases that from the 46.6% [2] of primary and CNS tumors. The incidence of this tumor has been commonly seen in the age group of 75 to 84 years.

World Health Organization (WHO) has classified the tumors in different grades. Based in the predicted behavior the tumors are classified in different stages named as Grade I-This distribution is done according to the evolution of the neuroepithelial tissue (also known as glioma). The Grade I and II are the LGG that include tumors like astrocytoma. The Grade III and IV are the High Grade Gliomas (HGG) that include tumors like: Glioblastoma, Oligodendroglioma and Ependymoma. Mostly the study is concentrated on the Glioma tumors as vast majority of the population is affected with this disease. The incidence of CNS tumors in India is increasing with 2% of malignancy and ranges 5 to 10 per 100,000 population [8]. The cases registered by hospital over a year show 38.7% of Astrocytoma among which 59.7% are high grade glioma. A tertiary care center

of South India [9] reported 1043 patients with CNS tumor over past 15 years. Among these the most frequent tumors were nerve sheath tumor of 4.1%, astrocytoma of 47.3%, caraniopharymgioma of 9.7%. Jha *et al.* [11] reported registered cases for different cases as shown in Table 1.1.

In a survey based on the studies of Hospital Based Brain Tumor Registry (HBBTR) [10] that examines the Indian population has registered 4295 cases in the year 2010-2014. In this period the tumors registered are given in the Table 1.1. An estimated case of 38% and 24.5% have been reported of glioblastoma and anaplastic oligodendroglioma respectively as the most common type of tumor among the adults.

Table 1. 1 Survey done by different center for Indian population

		Grade I	Grade II	Grade III	Grade IV
2010-2014	HBBTR [10]	36.3%	11.4%	20%	18.9%
2016	Jha *et al.* [11]	-	68.8%	85.7%	12.8%

Tumor prognosis has a critical step in patient's treatment planning that depends on various factors like shape, type, enhancement of the tumor. Similarly, some other factors are considered like symptoms occurring prior to diagnosis and the extent to which a patient's functionality is affected by tumor. Depending on all these factors and severity preeminent treatment is done that includes surgery, radiation therapy and chemotherapy. But, to get a clear picture of the treatment and initial diagnosis of tumor imaging techniques are required. These techniques are non-invasive and prove to be most efficient way of providing diagnosis.

1.2   IMAGING MODALITIES OF BRAIN

The commonly used modalities for image acquisition are: X-ray, Computer Tomography (CT), Magnetic Resonance Imaging (MRI), Ultrasound (US) and Nuclear

medicine (NM). All these imaging techniques used for initial diagnosis with their application in brain tumor imaging is depicted in Figure 1.3 [12].
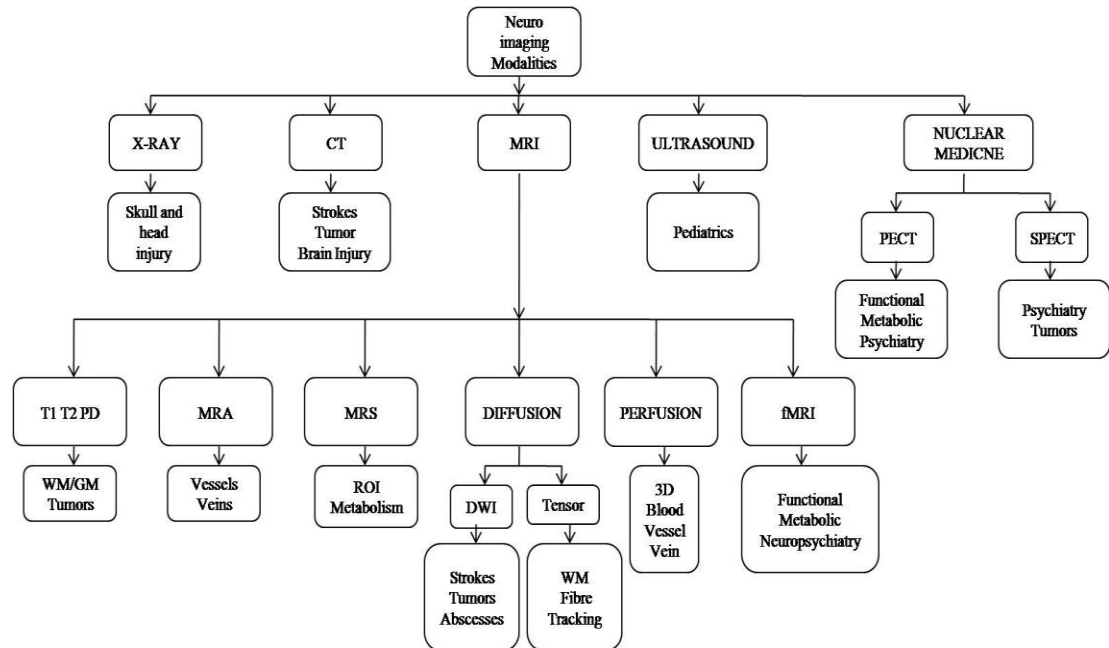
Figure 1. 3 Imaging modalities of brain with their application [12]

The X-ray and CT imaging use series of X-ray scans that constructs the structural view of the body. But an over exposure of these rays proves to be harmful for the human body. US imaging use high frequency waves to look indie the organs and structures. They provide real time visualization that shows structure and movement of organs. These scans are also harmful with the over exposure of the waves and develop heat that gets absorbed by the tissues. Nuclear medicine consists Positron Emission Tomography (PET) and Single-Photon Emission Computed Tomography (SPECT) that are invasive techniques as a small amount of material is injected in the body. This modality provides only functional view of brain. The pros and cons of these imaging modality is given in Table 1.2.

Table 1. 2 Comparison of different image modalities

	Detection	Advantage	Disadvantage
X-ray	Bones	Cheap	Over exposure of X-ray is harmful
CT	Soft tissue and bones	Useful for boney architecture, guide biopsy	Radiation exposure
MRI	Soft tissue and bones	Non-invasive, specific for acute and chronic osteomyelitis, anatomic	High cost, requires anesthesia
US	Soft tissue and some bones	Specific and anatomic	Require sedation (invasive)
NM	Bone related pathology	Highly specific	High cost, limited availability

1.2.1 Magnetic Resonance Imaging

MRI modality is the best choice for a non-invasive test essential for brain tumor analysis [13]. It provides more accurate results for analysis of metastases in comparison to other modalities. In 1973, Lauerbur [14] and Mansfield [15] explored MRI as an application of imaging modality in field of medicine. It is based on theory of Nuclear Magnetic Resonance (NMR) that uses a combination of high magnetic field caused by strong magnets and radio frequency that develops images with high detailed information. The commonly used magnetic field strength of these magnets is 1.5T and 3T as at higher fields these cause high signal-to noise ratio (SNR). MRIs are able to control various contrast parameters enabling an inclusive assessment of normal and abnormal physiology of brain. Corresponding to these controls sequences of different brain region show different contrast as listed in Table 1.3 [16].

The main advantages of MRI are absence of harmful ionizing radiation, being a non-invasive technique, painless, possibly also performed without contrast, showing great soft tissue contrast along with high spatial resolution, direct multi planar imaging sagittal, coronal and axial planes, displaying many images and oblique cuts [17].

Table 1. 3 Imaging sequences of brain with their application

Tissue	T1	T2	FLAIR
CSF	Dark	Bright	Dark
WM	Light	Dark Gray	Dark Gray
Cortex	Gray	Light Gray	Light Gray
Fat	Bright	Light	Light
Inflammation	Dark	Bright	Bright
TR	500	4000	9000
TE	14	90	114

1.2.2 Image sequences

In recent clinical routine MRI has a grown popularity for brain tumor diagnosis as it uses sequences for better analysis and delineation of tumor compartments. The different sequences include following sequences as depicted in Figure 1.4: a. T1-weighted (T1), b. T1-weighted with contrast enhancement (T1ce), c. T2-weighted (T2), d. Fluid Attenuated Inversion Recovery (FLAIR).

The most commonly used sequence for easy remarks of healthy tissue is T1 weighted sequence. The tumor borders are brighter in T1ce sequence as contrast agent accumulates there due to disruption of blood-brain barrier in proliferative brain tumor region. Hence, it becomes easier to distinguish necrotic and active cell region. In comparison to other sequences edema region appears brighter in T2 sequence. The most effective sequence is regarded as FLAIR sequence because water molecule signals are suppressed that allow tumor region to appear brighter than any sequence.
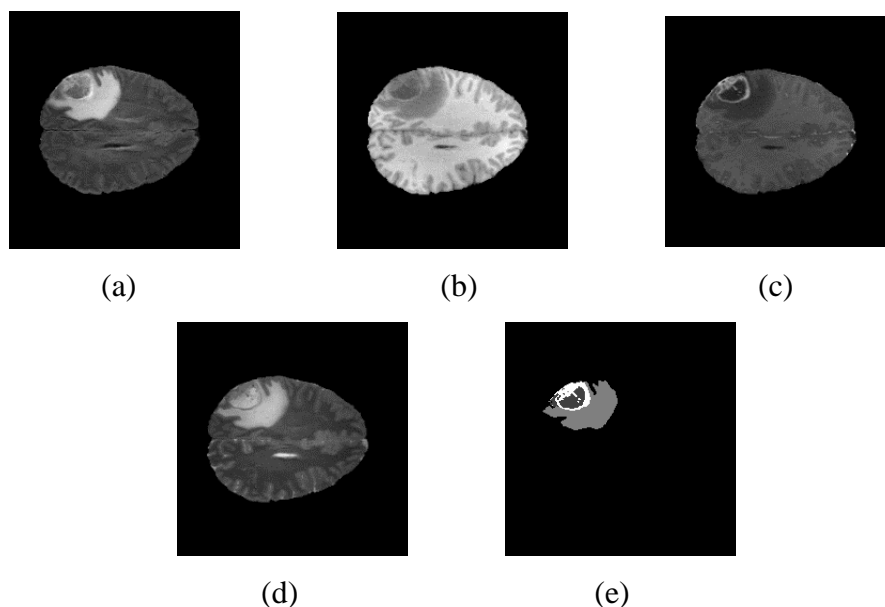
Figure 1. 4 Axial view of brain tumor MR Images with all sequences and ground truth. (a) FLAIR, (b) T1, (c) T1ce, (d) T2 and e) Ground truth.

1.3   IMAGE SEGMENTATION

The MRI are capable of describing brain accurately but medical image segmentation is difficult due to poor spatial resolution, inhomogeneity and ill-defined boundaries. These problems along with complex brain anatomy capture possible deformation of entire structure making segmentation a tough tack. Also, enormous amount of brain tumor images that are generated in clinics for annotation and segmentation of tumors in a particular time becomes laborious for clinicians. So, popularity and research work in the field of automatic segmentation is inevitable. Segmentation partitions an image in mutual exclusive homogeneous subsets according to predefined criterion. Brain has an intricate structure in itself and occurrence of tumor in such a complex structure increases difficulty level of segmentation. The anatomy of tumors is complex in its shape, size and position and considerable amount of variation is seen from patient to patient. Complex brain tumors have different tissue type found in it such as edema, necrotic core, active cells as shown in Figure 1.5 [18].
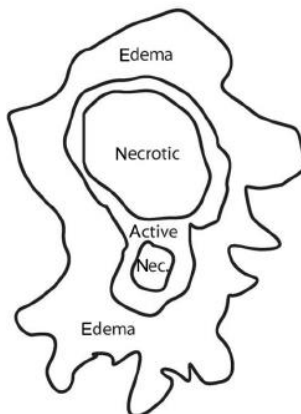
Figure 1. 5 Different region existing in glioma tumor

The complex structure of brain develops major limitations in classification of tumor as measurement of enhancing tumor that defines glioma progression is difficult. This even leads in providing patient's treatment response. Some of the limitations are: i) gliomas have irregular shape and it can change anisotropically or differently, ii) any tissue/component that show contrast enhancement are not essentially indicators of any active tumor volume and iii) active tumor that are non-enhancing and show enhancement are well recognized.

Some of the limitations or problem occurring in diagnosis of tumor are explained as follows:

i.   **Tumor shape heterogeneity:** It is difficult to perform linear measurement of the gliomas due to irregular shape that they acquire especially after surgery. The differential growth of tumor and surrounding brain tissues cause an anisotropical growth of tumor. After surgery there are any multifocal enhancement or presence of small lesions it may cause tumor assessment difficult [19]. Lesions such as Necrotic and cystic cause huge amount of ambiguity in tumor assessment as they are closely related [20].

ii. **Evaluation of non-enhancing tumor:** The Response Assessment in Neuro-Oncology (RANO) have highlighted some of the major challenges for tumor assessment [21]. It mainly includes differentiation of non-enhancing areas of tumor.

This differentiation is important as a considerable amount of complete tumor represents non-enhancing region in gliomas of grade II and III. It is also observed on comparing T1ce and FLAIR sequences.

iii. **Heterogeneity:** The heterogeneous anatomy of tumors causes different tumors component to respond differently. The images formed of these tumors in MRI are difficult to be evaluated. This is because different grade of tumor forms different pixel values that may even get overlapped due to intricate brain structure. Even after the surgery growth is anisotropic and its irregularity also adds to difficulty in assessment of tumor regions.

Recently, there have been great amount of advancement in field of medical image segmentation. It has a great impact on diagnosis, prognosis, patient monitoring and treatment planning of patient. Segmentation techniques primarily identifies abnormal portion that is required for analyzing size, volume, texture and shape of the tumor. It depends on intensity and texture variation of images. Various techniques have been developed by authors over years based on these tissue properties [22]. Broad classification of segmentation techniques is based on various parameter among which some are listed as shown in Figure 1.6 are intensity, clustering, classification and energy based image segmentation techniques.
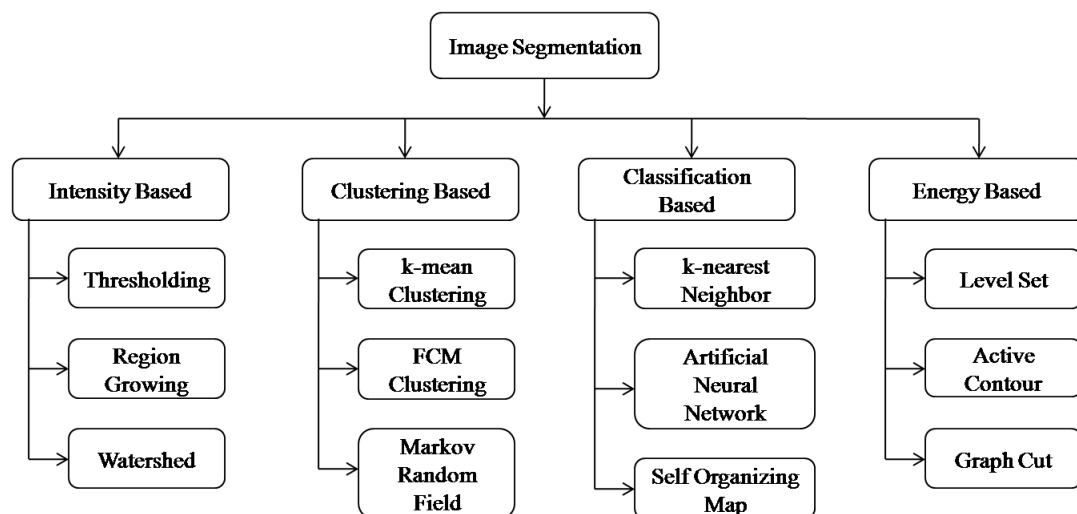
Figure 1. 6 Various image segmentation techniques

A brief description of various segmentation techniques is given in following section.

1.3.1 Intensity based segmentation

In intensity based methods partition is formed on the basis of individual pixel intensity value. MRI brain image mainly comprises WM, GM and CSF region that have independent intensity values. Along with the boundaries between these three region MR Images generally encounter overlap of intensities values between normal and abnormal region of brain. This makes simple demarcation of region difficult. Some of the techniques that come under this category are:

i. **Thresholding:** One of the simplest technique for segmentation of gray image is thresholding. This technique provides binary segmentation by comparing intensity values. An optimum threshold values is evaluated that distributes the entire image in two binary regions. These regions have value 0 (represent black color) and 1 (represent white color). The threshold value is generally obtained by identifying pixel value at valley point in histogram of image [23]. All image pixels that are greater than threshold value are grouped as object region with value 0 and pixels below this value are grouped as background with value 1. Some of commonly used thresholding techniques are: global, local and adaptive [24]. These techniques are commonly used on images that have high contrast region as it become easy to identify the valley point and obtain threshold value. The region partition is done as given in Equation 1.1.

$$I(x,y) = \begin{cases} 1\ ; \text{Object} & I(x,y) \geq T \\ 0;\text{Background} & I(x,y) < T \end{cases} \qquad (1.1)$$

ii. **Region Growing:** Region growing technique has a hierarchical approach and is also called as region merger. It segments well defined boundary regions based on similar intensity values [25]. Region growing require initial seed values in order to execute

complete process. These seed values are primary required that should belong or show high degree of similarity with the object region. Generally, these values are given manually by a user that has high level knowledge of object to be extracted. The region growing algorithm utilizes these values and inspects and groups all neighboring pixels that have similar property. Finally, a connected boundary region is extracted. This process is repeated until no other region is left to be merged with targeted object region.

iii. **Watershed:** Watershed method is based on a metaphorical description of the water behavior in a landscape. It is described with the formation of region with traces on landscape when water drops in different region. All the water is collected at bottom of valley in the regions formed [26]. At maximum peak of water level, the process stops and at final output landscape has different region formation that are split in dams called as water lines or watersheds. Hence an object contour is formed and there is no need of boundary linking. But, this process does lead to the over segmentation of unnecessary regions. The problem of over segmentation is removed by different techniques but generally pre-processing methods are used [27].

The intensity based segmentation techniques are majorly dependent on contrast of the image. So, for images with high contrast difference segmentation is easily performed as boundary pixels are easily identified. But, for images that do not have high contrast variation are not able to be segmented by intensity based segmentation techniques.

1.3.2 Clustering based segmentation

The clustering based techniques are unsupervised techniques that aid in forming different subsets of an images that have similar properties. This technique creates different cluster of pixels hence providing segmentation of a complete image in sub-region form. In its process it performs two important simultaneous steps that calculates the similarity of each tissue type and forms clusters of similar tissue type. The most

commonly used clustering techniques are: k-mean clustering [28], Fuzzy clustering [28] and Markov Random Field (MRF) [29].

i. **k-mean clustering:** One of the most popular clustering technique is k-mean that was given by MacQueen in 1976 [31]. It is an unsupervised clustering method that is also known as hard clustering it is based on iterative process that divides the image into different cluster. The value of k is assumed initially and data points or pixels are grouped in an exclusive way such that if a data point belongs to a certain cluster then it will not belong to any other cluster. This mutual exclusive portioning is done by evaluating the Euclidean distance. All cluster means are computed and similarity is measured of all points in cluster to the mean value. So, all pixels with highest similarity are grouped together. The iteration continues until a convergence is found or cluster mean values do not change.

ii. **Fuzzy clustering:** Zadeh in 1965 [32] introduced fuzzy set theory and used on image segmentation successfully. In 1981 Bezdek [33] proposed Fuzzy c Mean (FCM) algorithm based on fuzzy set theory. This algorithm is simple and widely studied. In FCM clustering clusters of similar pixel is formed by giving membership value to the assigned pixel, these membership values give the degree of similarity. FCM is also called as soft clustering as it does not put any hard constraints on the pixel in forming clusters.

iii. **Markov random field (MRF):** MRF model was pioneered by Geman and Geman [34] for the image processing in their work presented on Bayesian image restoration. This technique provides multi-labelling of image based on the conditional probability. In a binary segmentation the process of labelling has less numerical computation. With the increase in number of region, labels increase and computation is also increased. At higher labels the technique becomes NP-hard and its complexity increases.

The clustering based segmentation technique is able to partition different brain tissue in MRI. These techniques are able provide multi-object segmentation as required by the user. The k-mean and fuzzy clustering method have the limitation of selecting initial value of clusters. It is difficult to know its optimum value at which best accuracy can be obtained. Also, both these techniques are iterative in nature and fuzzy can also lead to over segmentation. The mathematical complexity increase in MRF technique with increase in image size and dimension.

1.3.3   Classification based segmentation

The classification based method segments abnormal region in MR image based on feature space or imaging parameters. These imaging parameter belong to different classes that represent textual, spatial and intensity features. These imaging parameters are first order statistical feature and higher order statistical features. Classification techniques are supervised and unsupervised. In supervised classification manually segmented images are needed for training phase. Depending on training phase the test images are segmented in different regions. In unsupervised classification similarity in dataset is evaluated for performing segmentation. The most commonly used classification techniques are: k-nearest neighbor (KNN), Artificial Neural Network (ANN) and Self-organizing maps (SOM).

i.   **k-Nearest Neighbor:** kNN is primarily a classification technique that was used by Warfield *et al.* [35] for medical image segmentation. kNN classifiers segments the objects by comparing nearest pixels in these regions with features set of training set and k number of data. It is a non-parametric technique that is based on evaluating amount by which pixels agree to a particular feature set. Finally, all pixel with similar feature set are defined in a particular class.

ii.   **Artificial Neural Network:** ANN technique has an adaptive nature as it does not follow any standard set of rules for performing segmentation Buller *et al.* [36]. In this technique training and testing phases are needed. The complete network of

ANN consists input layer, hidden layer and output layer. It works on the analogy of human brain neurons that are able to transfer information from one to another encompassing millions of neuron. ANN network gets trained by learning for which it requires huge dataset. Once the network is trained testing is performed and to increase accuracy better features and good dataset is constructed. ANN performs well on difficult MR Images such as noisy, non-linear and multivariate. It is an application based technique that can be used for tumor segmentation and classification.

iii. **Self-organizing maps (SOM):** SOM is an unsupervised technique that was given by Kohonen [37]. It is a special case of ANN and mostly used for pattern recognition. The goal is to represent all points in the source space by points in a target space, such that distance and proximity relationships are preserved as much as possible. These relationships are related to each point through neighborhood function [38]. All the points are initially trained with randomly selected input samples and get updates according to neighborhood function. Once the training is done a 2D space map is created that consists of typical features that are a topology visualization of input. SOM is particularly used when there is non-linear mapping of the problem.

The classification technique is able to provide segmentation and classification but, they are time consuming and high computation. All the techniques require training and testing phase that require enormous amount of dataset. For a dataset that is small is size is not able to provide segmentation of classification with high accuracy.

1.3.4 Energy based segmentation

i. **Level Set:** Level set technique was given by Osher and Sethian in 1988 [39] that focused on problems related to curves and surface. In this technique Level Set Function (LSF) is evolved in order to set the motion of a contour. The LSF represents an initial contour that is set at level zero. The contour formed at zero

level is actual contour and evolving contour is represented by signed function. It has various advantages like it is able to extract geometric properties of any shape and is able to change with respect to the topology.

ii. **Active contour:** This technique detects the object region even though the boundaries are not defined by any abrupt intensity values. It requires an initial selection of curve that is mostly given through user interaction. Once the curve is obtained it automatically detects the curve from interior contours. Active contours are deformable models also called as snakes for 2D images and active balloon in case of 3D images [40]. This technique is a combination of geometry, approximation theory and physics. All these three components aid in providing the shape, limitations and mechanism of the curve formation.

iii. **Graph cut (GC):** The general theory of graph was given by Wu *et al.* in 1993 [41] and then Boykov [42] introduced this theory to image segmentation. GC provides a very simple representation of an image as a grid. The complete image is divided into subgroups by evaluating the regional and boundary information of image. Labelling of pixels are done based on the minimum energy criteria and cut is formed. This cut partitions complete image in sub regions containing different labels.

In recent time huge work has been done in all these techniques and multiple advancements are achieved in all these techniques. Based on the vast study done on the literature of these techniques, some of advantages and disadvantages are listed in Table 1.4.

Table 1. 4 Advantages and disadvantages of different image segmentation techniques

Segmentation Technique	Advantages	Drawback
Intensity based		
Thresholding	Provides binary segmentation and is easy to implement	High contrast difference is needed so; it cannot be applied to all type of MR images
Region growing	Homogenous regions are segmented easily	Disconnected regions are obtained is noise is high
Watershed	A connected path is formed so less discontinuity is seen	Causes over segmentation
Clustering based		
k-mean	Computation is fast	Value of k should be accurately selected
Fuzzy	Soft clustering and each group has a defined different membership degree	Computational time is very high
MRF	Provides optimal labelling	Not applicable to heterogeneous tissues a higher number of labels may result in a Nondeterministic Polynomial (NP) hard solution.
Classification based		
k-nearest neighbor	Simple in implementation	If the training set is large it may have poor run time performance
Artificial intelligence	It performs very well in non-linear domains especially for images that have high heterogeneity	It is difficult to assemble the dataset for learning phase
Self-organizing map	Provides effective visualization of high dimensional images.	It is computationally expensive as number of regions to be formed have to equal to number of units in competitive layer

Energy based

Level set	Extracts objects with complex shapes and curves.	Numerical computation is high
Active contour	Self-adapting nature; easily track moving object	Gets stuck in local minima state; requires higher computation
GC	Reduced spatial bandwidth is required	Requires appropriate selection of seed values for initialization; forms small regions due to shrinkage problem

After examining merits and demerits of all techniques along with the increased application of GC in field of biomedical segmentation authors chose graph cut technique for performing Glioma extraction from MR brain images. In addition, an exhaustive literature survey is also provided for all these techniques in Chapter 2 that highlights the advantages of GC over the other techniques.

1.4   DETAILS OF DATASET

The publically available standard benchmark for database of MR brain images for the quantitative evaluation as employed by various researcher are given in Table 1.5. Every dataset has images that are relevant for application. Among these datasets MRI brain image dataset used in this research work are: (i) Medical Image Computing and Computer Assisted Intervention (MICCAI) BraTS and (ii) Figshare.

Validation of proposed segmentation algorithm using clinical images is an essential part for measuring the effectiveness. So, in this research work, real time images are also used for validation from the radiology department of Indra Gandhi Medical College (IGMC), Government hospital, Shimla, HP for validation. Based on literature survey it is observed that amount of dataset used of BraTS benchmark is 23% in area of brain tumor segmentation and classification. Figure 1.7 depicts a pie chart that was framed by [45] providing the analysis on basis of dataset used.

Table 1. 5 Publically available MR Images for brain tumor

Database	Image type	Available link
BrainWeb	Three sequences available T1, T2, Proton Density (PD)	http://brainweb.bic.mni.mcgill.ca/brainweb/
Internet Brain Segmentation Repository (IBSR)	MRI available with manually segmented ground truth	https://www.nitrc.org/projects/ibsr
Harvard medical school	MR Images available are of normal brain, cerebrovascular disease, brain tumor	http://www.med.harvard.edu/aanlib/home.html
MICCAI	Multi-contrast MR scans	http://martinos.org/qtim/miccai2013/data.html
The Cancer imaging Archive	Images containing cancer of lungs, brain etc.	http://www.cancerimagingarchive.net/
Figshare	T1ce images of three tumor disease	https://figshare.com/articles/brain_tumor_dataset/1512427
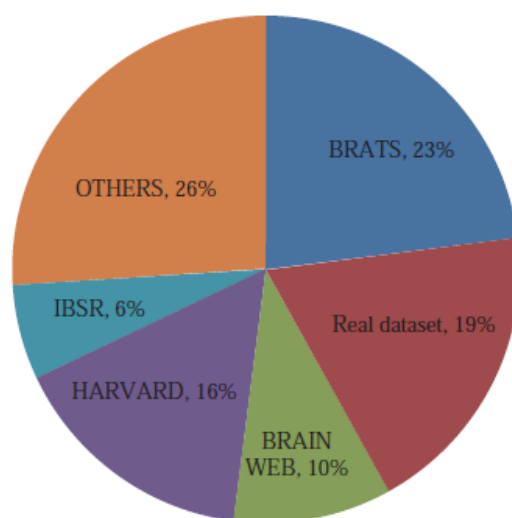
Figure 1. 7 Dataset used by researchers [45]

1.4.1 MICCAI BraTS [43-44]

This dataset is provided by the Parelman School of Medicine; University of Pennsylvania. Section for Biomedical Image Analysis (SBIA), part of the Center of Biomedical Image Computing and Analytics (CBICA), is devoted to the development of computer-based image analysis methods, and their application to a wide variety of clinical research studies. This dataset consists 285 patient images among which 210 are HGG images and 75 are LGG images. Each image has four sequences that are depicted in Figure 1.8 as $I_{Flair}, I_{T1}, I_{T1ce}$ and I_{T2}.

(a) (b) (c) (d) (e)
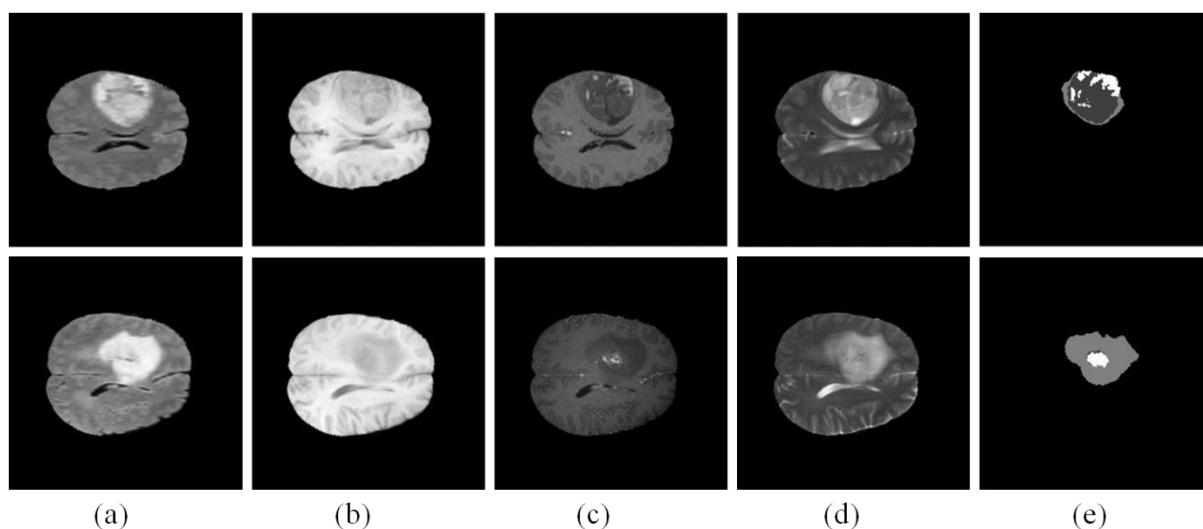
Figure 1. 8 (Left To Right) Different sequences of HGG (row-1) and LGG (row-2) mr images: (a) I_{Flair} Flair, (b) I_{T1} T1 Weighted, (c) I_{T1ce} T1 Weighted contrast enhancement, (d) I_{T2} T2 Weighted and (e) I_{GT} Ground truth

The parameter evaluation of the algorithm is done with respect to ground truth that is also available in dataset represented as I_{GT} in Figure 1.8. The volumetric images are of size 240×240×155 and in this research work we have worked on 90 size as it provided the best visual of glioma in MR image.

1.4.2   Figshare (Cheng *et al.* [46-47])

Another standard database of brain tumor images is Figshare. This dataset consists of 3 types of tumor: Meningioma, Glioma, Pituitary tumor. Researchers share their dataset, research output on this platform as shown in Figure 1.9. The total dataset contains 3064 T1 weighted contrast enhanced MR Images with size of 512×512. The datas*et al.*so provides the ground truth for all three tumors. Different number of slices are provided for each type of tumor.
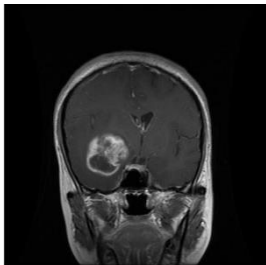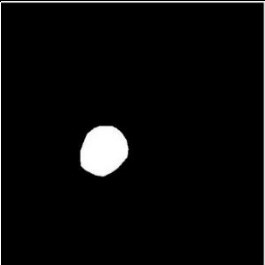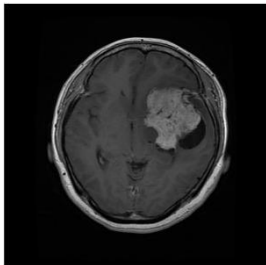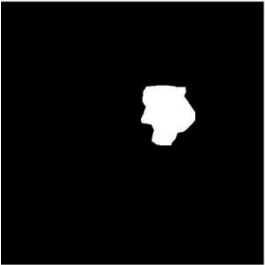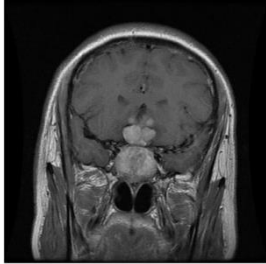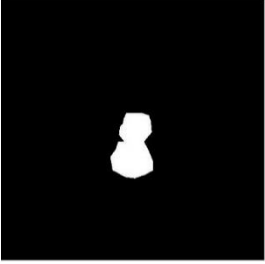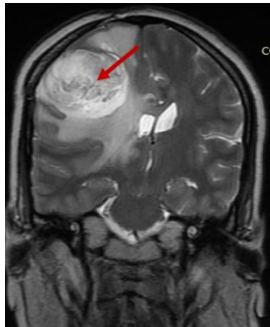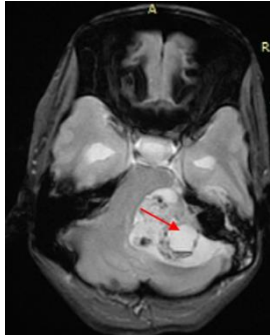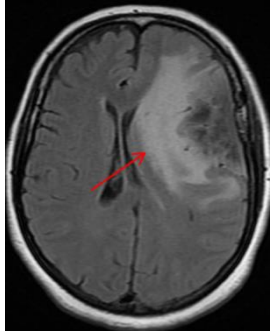
	MR Image	Ground truth	Specification
a			Glioma: (1426 slices)
b			Meningioma (708 slices)
c			Pituitary tumor (930 slices)

Figure 1. 9 Different type of brain MR images with their ground truth

1.4.3   Real patient images

We have also obtained real patient images from the radiology department of Government Hospital, IGMC, Shimla, Himachal Pradesh (HP). These images are shown in Figure 1.10 with tumor marked in red color by the expert radiologist. All four images belong to different patient profile and are diagnosed with different type of tumor.

MR Image	Specification
	• Age: 54 year • Sex: M • Diagnosis: Glioblastoma Multiforme (GBM) • Well defined heterogeneous lesion (red arrow) in right fronto parietal region measuring approximately 5×6.4×4.8cm with surrounding oedema.
	• Age: 35 year • Sex: F • Diagnosis: Cystic Acoustic Schwanoma • Well defined mass in left CP angle showing heterogeneous signal and cystic component extending into left image shows avid heterogeneous enhancement
	• Age: 45 year • Sex: F • Diagnosis: Meningioma • Well defined extra axial soft tissue mass lesion measuring 6×5×2.5cm seen in relation to left fronto-parietal region
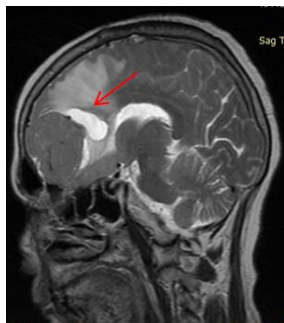
- Age: 45 year
- Sex: F
- Diagnosis: Glioblastoma Multiforme
- Well defined mass lesion(white arrow) of size 5×4.2×3.6cm seen in left frontal lobe invading the corrpus callosum crossing the midline and having oedema with mass effect and midline shift

Figure 1. 10 Real patient images with different patient profile and marked tumor

1.5   PERFORMANCE PARAMETERS

Based on exhaustive literature review of state of art technique in these area of research performance parameters is utilized for evaluation and validation. The comprehensive evaluation of the proposed algorithms in this research work is made by considering the following aspects for accuracy and efficiency of the proposed method. Various parameters used for evaluating results obtained by different objectives are given as follows.

i.   Mean Square Error (MSE): It quantifies error or the difference between segmented tumor and available ground truth.

ii.   Correlation Coefficient (CC): It calculates degree of similarity between two sets of pixels obtained from segmentation and standard ground truth.

iii.   Area: it represents the amount of pixels or pixel population that exist in segmented tumor region.

iv.   Perimeter: It represents the outline or shape of extracted tumor any edges of fine slopes are covered in the evaluation of perimeter.

v.   Major Axis Length (MAL): it is defined as the longest line that passes through object region.

vi. Minor Axis Length (MiAL): it is the length of the longest line that is drawn perpendicular to the major axis length.

vii. Jaccard Index (JI) [48-49]: It is measured amount of similarity between two sample obtained from Ground truth and segmented result.

$$JI = \frac{TP}{TN} \qquad (1.2)$$

viii. Dice Similarity Coefficient (DSC) [48-49]: It measures the overlap or amount of similarity in the pixel between ground truth and affected region obtained after automatic segmentation.

$$DSC = \frac{2TP}{FP+2TP+FN} \qquad (1.3)$$

ix. Positive Predicted Value (PPV) [48-49]: It predicts the amount of segmented region that are over segmented or the pixel region that gets segmented even though it is the part of normal brain tissue region.

$$PPV = \frac{TP}{TP+FP} \qquad (1.4)$$

x. Sensitivity (Sens) [48-49]: This parameter measures number of TP and FN detection which means it calculates the fraction of positives that are correctly detected by the experiment.

$$Sens = \frac{TP}{TP+FN} \qquad (1.5)$$

xi. Specificity (Spec) [48-49]: This parameter calculates the fraction of negatives that are correctly detected. It covers all those pixels that were not be detected and the experiments does not detect them.

$$Spec = \frac{TN}{TN+FP} \qquad (1.6)$$

Table 1. 6 Ideal values attained for analyzing good and bad segmentation

Segmentation	JI	DSC	PPV	Sens	Spec
Good	≈ 1	≈ 1	≈ 1	≈ 1	≈ 1
Bad	≈ 0	≈ 0	≈ 0	≈ 0	≈ 0

Table 1.6 depicts the ideal values that should be attained for good segmentation. All the performance parameters are evaluated in a range between 1 and 0. For a good segmentation the values should be nearer to 1 and for bad segmentation the value is nearer to 0. The variables defining above parameters are: True Positive (TP), True Negative (TN), False Positive (FP) and False Negative (FN) and are described in Figure 1.11.
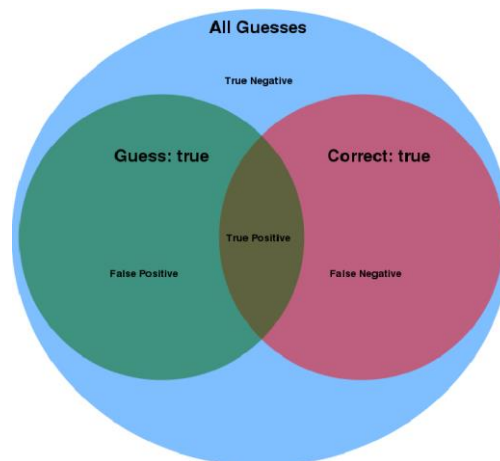
Figure 1. 11 Venn diagram for all the possible outcomes

1.6   MACHINE LEARNING

Classical MR tumor classification involves three major stages; tumor segmentation, feature extraction and tumor MR classification. In supervised machine learning approaches, target classes are also provided along with the input feature vector to obtain better classification outcomes. These machine learning approaches exploits handcrafted feature extraction techniques to extract clinically relevant features from the segmented

tumor region. These features are passes through a specific machine learning classifier for MR tumor classification into HGG and LGG.

The choice of optimal classifier varies with the need of application as well as nature of available dataset. Support Vector Machine (SVM) [50] algorithm is able to predict the testing data by previously constructed hyperplane using labeled training data. This approach is basically applicable for binary classification but its practical applications can be used to solve multi-class pattern recognition problem. K-nearest neighbor (kNN) [51] classifier uses the k- nearest neighbor to identify class of a particular data sample depending upon the Euclidian distance of dataset samples. Euclidean distance between the samples of k- nearest training data points acts as deciding factor for assigning test data to the most frequently occurring class.

1.7   MOTIVATION

As reported by New Philanthropy Capital (NPC) [52] brain tumor has the highest mortality rate in comparison to other cancer diseases. As surveyed by CBTRUS most of the people are diagnosed with brain tumor and it has become a critical issue in medial field for accurate analysis of these tumors. With enormous amount of image data causes delay and non-reproducible results has enhanced the need of Computer Assisted Diagnosis (CAD) tools. These CAD tools assists radiologist to give the final decision with high accuracy. Different types of assistance with the development of efficient CAD tools to medical field are:

   i. Early detection of tumor can help in early treatment by the medical expert.
  ii. Differentiation and segmentation of tumor and non-tumor regions.
 iii. Content based image retrieval system may help the doctors fast forward the treatment of a patient affected with similar tumor.
  iv. Automation of segmentation technique.
   v. Removal of fallacious segmentation by accurate selection of seed values.

vi. Detection of best MRI sequence for providing tumor grading for its characterization.

In the field of medical image analysis segmentation is the first and most important step. It allows the extraction of the conspicuous region with relevant information. But most of these techniques inherent limitations that hinders the path of developing an efficient system, like the selection of seed points. That has been a matter of concern in various segmentation techniques especially graph cut. This selection plays an important role for developing an automatic technique with higher accuracy. Hence, it is critical to develop a highly efficient algorithm that is able to overcome these limitations.

1.8   RESEARCH GAPS

Based on the elaborative literature survey in GC segmentation technique for brain tumor segmentation authors following research gaps are formulated.

Research gap I. *Seed Selection* [53-55]

The basic GC technique has the primary requirement of selecting seed values that initializes the algorithm without any human intervention. These seed point are not only required for this initialization but also performing accurate segmentation.
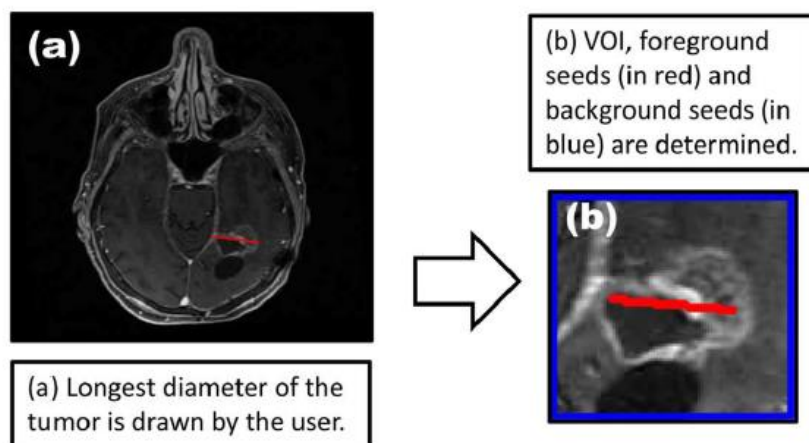
Figure 1. 12 Manual kernel selection from object region provided by Hamamci *et al.* [53]

Previously these values were given manually by a user with high level knowledge of brain anatomy or under expert guidance of a radiologist. Authors in [53-55] have shown manual interaction of user in order to provide seed values. This manual interaction is shown in Figure 1.12 by Hamamci *et al.* by drawing a red line on affected tumor region. All the pixel values on this red line will be taken as the initial seed values.

Research gap II. *Shrinkage problem* [54-55]

The problem of shrinkage was stated by Chen *et al.* in [54] presenting it as an open research issue. This technique evaluates minimum cut due to which small contours are created resulting in fallacious segmentation. These erroneous regions are the unnecessary portion that belong to normal brain region. In this research gap the goal is to develop an automatic framework that eradicates shrinkage problem with accurate tumor segmentation.

Research gap III. *Bias field MR Images* [56-57]

With the technological advancement in the field of MRI acquisition, engineers are able to produce scans at magnetic field above 3T. Recently the MR machines are also able to create images at 7T provide high resolution of full body MRI. But, at high ultra-frequency signal to noise ratio increases and intensity inhomogeneity is created. So, segmentation of these images become difficult but with the advent of time it has become essential. In this research gap a robust framework is developed that is able to accurately segment the tumor regions from such images.

Research gap IV. *Glioma Grading* [58]

Glioma grading is an essential part of medical assessment for a patient having tumor that aids the expert in a second opinion for early treatment. As each patients MRI consists of four sequences so it is important to select the optimal sequence for grading the tumor with highest accuracy. Hence, in this research work a sequence selection

model is proposed that is able to select the best sequence for glioma grading. Statistical analysis and machine learning tools are used in this model for feature selection and binary classification.

1.9   OBJECTIVES OF RESEARCH WORK

Although radiologist and experts are able to provide the diagnosis but development of diagnostic tool are able to provide a second opinion for early treatment of patient. The proposed research work is carried out to develop an efficient and robust framework to provide an application driven system for MR Brain tumor image segmentation and classification. The main objectives framed in this thesis are:

Objective 1: Inception of Seed Selection Techniques for automatizing GC based Segmentation

Objective 2: Addressing Shrinkage problem in Segmentation by developing an Indigenous Technique for its Elimination (open research challenge) [54]

Objective 3: Implementation of Robust Framework for Extracting Tumor Region from Bias field MR images.

Objective 4: To Design an Image Sequence Selection Model for Precise Detection of Glioma Grading.

1.10   ORGANIZATION OF THESIS

The research work includes seven chapter. In Chapter 2, the literature review of all state of art techniques required for image segmentation are detailed. These techniques are categorized under four different groups. The binary classification using machine learning are also detailed.

In Chapter 3, exiting GC technique is explained in detail with its limitations. Three novel techniques are developed for providing automatic and semi-automatic seed selection for initialization of GC. The results include segmented tumor images along quantitative result.

In Chapter 4, the open research issue of shrinkage problem stated in IEEE review on biomedical engineering is addressed. A novel algorithm termed Gradient Based Kernel Selection (GBKS) is developed that eliminates this problem and fully automatizes GC technique providing accurate tumor extraction. The visual and quantitative results are also provided in this chapter.

In Chapter 5, the effectiveness and robustness of proposed GBKS is validated by applying it on bias field images. The impact of bias field on MRI images is shown and difficulty in extracting tumor region from these images is also depicted. The bias field used in this research work are circular and longitudinal. The effectiveness of GBKS GC is also observed by applying it on real patient images that are obtained from Government hospital IGMC.

In Chapter 6, the selection of best MRI sequence is obtained by developing a system model for glioma grading. For this purpose, system model uses extracted tumors obtained from GBKS GC and performs feature extraction and feature selection. Further, machine learning is used for binary classifiers that are kNN and SVM are used.

In Chapter 7 the conclusion and contribution of the entire research work is illustrated. The future research course for glioma segmentation are also mentioned.

CHAPTER 2

REVIEW OF STATE-OF-THE-ART

CHAPTER 2

REVIEW OF STATE-OF-THE-ART

Segmentation and classification of brain tumor is most complex and difficult task. But, it has greatest importance in the clinical routine as it helps radiologist and doctor to get and second opinion. Mostly, brain tumor characterization is done through a biopsy. It is an invasive procedure that requires insertion of some medical devices in the brain. This procedure require a lot of time and patient even go through post-surgical impact. The development of CAD tools helps in stopping all these procedures and provide a more efficient method that is able to provide a second opinion to the clinicians with good diagnostic accuracy. In this literature survey a primary focus has been given to all the state-of-art method for brain tumor segmentation and its classification.

2.1   IMAGE SEGMENTATION

Image segmentation is a vast subject in the field of image processing that involves boundary detection and object extraction of images. It is a fundamental problem in computer vision that partitions an image in different non-overlapping region. This partition is performed in according to some criterion like: homogeneity of a feature space, non-overlapping connected region. Image segmentation is a long studied problem by the researchers like for an instance Muerle *et al.* worked on it in 1968 [59]. Since then many algorithms have been proposed for various application using different mathematical models for better segmentation. Among various research work author Keri [60] suggested necessary points for good segmentation that are given as follows:

i.   With respect to the predefined characteristics such as intensity, texture and color segmented regions must be homogeneous.

ii.   In cases of binary or multi segmentation all the regions should be connected and have no overlapping pixels.

iii. Possibility of merging two distinct region should be minimum.

Image segmentation is a popular core research topic for various computer vision applications especially in medical imaging for developing diagnostic tools, video analysis and cell tracking for biological analysis. It was introduced by Wertheimer [61] in 1938 as Gestalt theory for images. In this theory grouping was performed by considering similarity, continuity and proximity. Most of the segmentation work produced good results but were manually done and depended on symmetry. This ambiguity in symmetry of image posed segmentation as an ill posed problem. Although it is an easier task for human observer but it is difficult process of developing a diagnostic tool that can have a perception of a human being. In segmentation the segmented object region should primarily consist of similar intensity and uniform texture but, it is difficult for any algorithm to cope with various definition of uniformity not only throughout the image but also for any type of images. Thus, there hasn't been any general algorithm that can be used for any type of images [62]. At early time as summarized by Carreira *et al.* [63] no quantitative benchmarks were stated to evaluate the improvement and were unable to provide the effectiveness through comparison.

Gradually better studies and approaches were given in this field by creating annotation benchmarks [64-67] and performance metric [68-69]. Such improvement gave a new understanding to image segmentation that was stuck in nineties. After this the research was mainly focused on two aspects for accurate segmentation: a) extract image information to provide prior knowledge to algorithms and b) incorporate low-level and mid-level information in gestalt theory for image perceptual process. Uijlings *et al.* [70] used image information to generate a bounding box and use the tumor inside it as an evaluation parameter. This bounding box was also used for object detection and localization by Alexe *et al.* [71]. For improving the Gestalt theory Shotten *et al.* [72] used layout, texture and intensity for segmentation. Authors in [73-74] used conditional random field for region based object detection. With the ongoing research and improvement image segmentation has some limitations. Especially with the different imaging modalities providing better resolution and size in the recent time, has led medical image segmentation to be difficult and challenging. The difficulty also arises due to poor spatial resolution, heterogeneity, noise, partial volume effect and ill-defined

boundaries. The heterogeneous structure of brain has an expansive variation in the tumor location, enhancement, size and shape. The current developed diagnostic tools do not withstand these limitations and provide accurate segmentation requiring high level intelligence of validation study.

With the advent of time and enormous work done by researchers in the field of brain tumor MR image segmentation as shown in Figure 2.1 [75]. Based on this enormous research work different type of categorization are given for image segmentation. Depending upon the amount of human intervention involved in the algorithm these techniques are classified as manual, semi-automatic [76-79] and fully automatic algorithm [80-85]. Another type of categorization is done based on the training dataset and Region of Interest (ROI). These techniques are supervised [86-87] and unsupervised [88-90] methods.
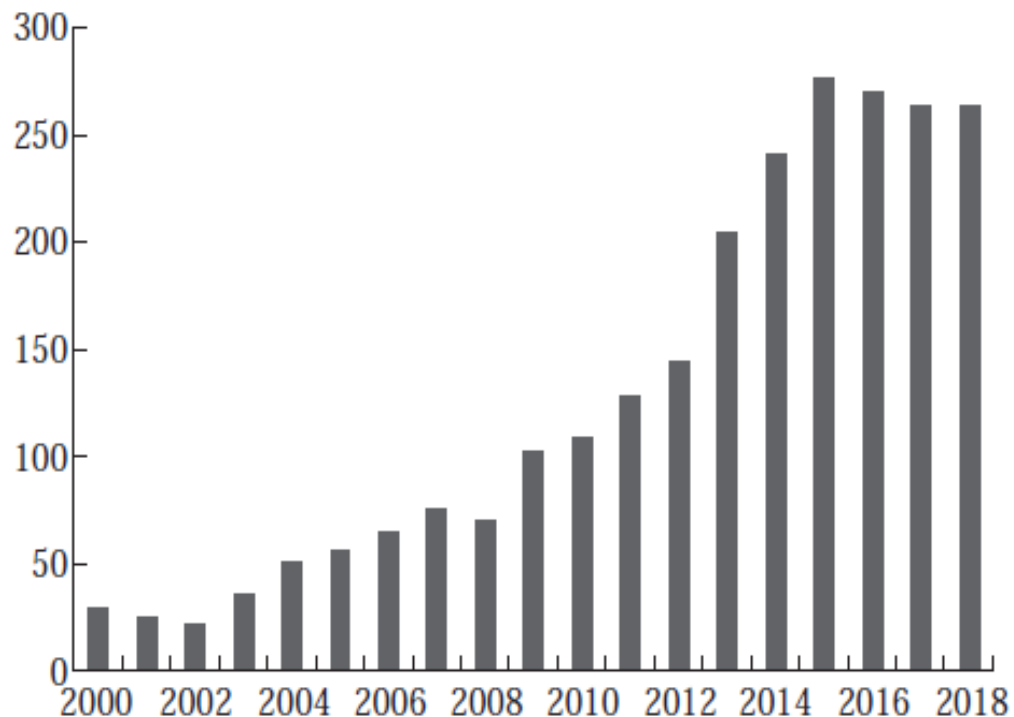
Figure 2. 1 Research work done on tumor extraction from MR images [75]

In this chapter classification of segmentation techniques [91-93] are based on intensity, clustering, classification and energy methods. All the methods included belong to above characterization in some way depending on the application of algorithms. The methods discussed in this chapter are given in Table 2.1 and all these techniques are mostly used for brain tumor MR Image segmentation.

Table 2. 1 Various segmentation techniques studied

Intensity based segmentation	Thresholding
	Region growing
	Watershed
Clustering based segmentation	k-mean clustering
	FCM clustering
	Markov random field
Classification based segmentation	k-nearest neighbor
	Artificial neural network
	Self-organizing map
Energy based segmentation	Level Set
	Active contour
	GC

2.1.1   Intensity based image segmentation

i.   Thresholding: One of the simplest and oldest technique for segmentation is threshold that works on basic principle of converting a given image in binary from. In the binary for the image is divided in two regions that has two values that are 0 and 1. Hence, this division or conversion of a given image is a similar process. The primary requirement for segmentation depends solely on selection of threshold value. Until now enormous work has been done by researcher to obtain the optimum value of threshold. In Otsu's method [94] this value is evaluated assuming a

bimodal histogram and obtained a single value termed as global threshold. But this technique fails if the intensity values are variable and histogram is not bimodal.

Sung *et al.* [95] estimated this value by estimating the prior information and providing it to algorithm for obtaining threshold value. Stadlbauer *et al.* [96] used T2 weighted MR image and obtained the threshold value by using the Gaussian distribution of all data points. Another threshold value is evaluated for boundary region by calculating the mean and standard deviation. Sometimes it is not possible to segment two regions from an image so authors in [97] used both local and dynamic threshold values.

Shanthi *et al.* [98] used man values of local statistical properties of intensity values and authors in [99] used level set evaluated the local threshold. Sujan *et al.* [100] used threshold value obtained by Otsu's method and morphological operator to segment the tumor region from brain MRI. Much more accurate method is proposed by authors in [101] for performing tumor extraction.

ii.   **Region growing:** For an image, the number of pixels contributes for its formation and to define similar intensity regions it always starts with a seed. In this technique the growth of region depends upon the homogeneous neighboring pixels around the seed. The homogeneity criterion depends not only on the problem under consideration, but also on type of image data available. Hence, region growth technique forms the connected region.

Pavlidis, Theodosios *et al.* in [102] have illustrated a new algorithm for image segmentation by integrating the region growing and edge detection. Authors have over segmented the image by using split and merge technique; further eliminated and modified the region boundaries to integrate contrast with boundary smoothness. The segmented output image gives better results for the proposed method than the results when the two techniques are individually applied.

To evaluate parenchymal densities in mammograms Kallergi, *et al.* in [103] have proposed and applied a refined method of local thresholding and region growing. The proposed process is applied on two images i.e. a phantom image and mammograms; the comparisons are hence made. Less than 11% difference is seen on mammograms. Authors have performed image segmentation in three levels: image pre-processing, local thresholding and region growing. Local region growing method is employed in which the resulting image classifies only the seed pixel. This process confers two regions, one is grown region and the other is surrounding region. The average intensities of both the region are compared and the tissue is classified as parenchymal tissue if the grown region average intensities have higher value than the surrounding region.

Region growing method does not give any knowledge about the boundary of the image. Gambotto, Jean-Pierre in [104] have intended to combine region growing and edge detection for the image segmentation. Algorithm is initialized with a gradient image and a patch inside the boundary of region and the adjacent pixels are merged. Region growth is controlled by using the gradient information to detect the optimal region boundary and comparing the image data with region model. This algorithm behaves like snake algorithm to segment closed region having unknown or complex boundaries.

Apart from the conventional region growing which uses homogeneity parameter, SRG employs small number of pixel called seeds in [105]. To seek these initial seeds corresponded to the proposed method in which two ways of using seeded region growing segmentation are mentioned. Proposed ways are: a. Manual seed method, b. Automatic seed method. The initial seeds are manually given in the former method whereas there is an automatic initialization of seed points in the latter method. Author's algorithm produces a robust, rapid and free of tuning parameter image. Algorithm presented is easy to implement.

Zhu, *et al.* in [106] have presented region competition algorithm as a novel, statistical and variational approach to image segmentation. By statistical testing multiple seeds are grown. The proposed method uses MDL criterion which compress the overlapping between regions but the method tries to minimize this criterion. To determine the individual region authors have used region growing, snakes/balloons algorithm. Balloon algorithm tries to fulfill two objectives of maximizing its area while smoothing its boundary contour and also maximizes the intensity gradient along the contour. The authors provided not only theoretical analysis of the proposed method but also have been particular for the following three characteristics for the output image: accuracy of boundary location, criteria for initial conditions, and relationship to edge detection using filters.

Tremeau, Alain and Nathalie Borel in (1997) [107] have illustrated color segmentation algorithm that combines region growing and region merging. Region growing in the proposed algorithm provides the color similarity and spatial proximity. On the basis of color similarity, the image is consequently merged. Region growing is preferred over clustering and thresholding methods as they apply directly on the color space and fit well for the goal of the authors for obtaining a non-portioned segmentation of the image that is being processed.

Fan, Jianping *et al.* in [108] have proposed a method in which automatic image segmentation is done by integrating two methods: edge detection and seeded region growing method. The color edges of the image are detected by the first method and then the centroid between adjacent edges are used as seed points for seeded region growing, hence it becomes automatic as now the initial seed point can be calculated in every step and is initialized for the second method.

This automatic initialization of the seed points overcomes the disadvantages of the region growing method which uses the split and merge technique for the segmentation. In SRG there is a possibility that some of the image regions, because of, different initial seed points are split into different region, so the region

relationship can be further worked upon. The merging method is applied using minimum spanning tree.

Zhao, Yu Qian *et al.* in [109] propose a new method for the retinal vessel segmentation which is significant for the diagnosis procedure of retinopathy. This method is based on two approaches: 1. Region Growing & 2. Level Set. To improve the vessels image initially it is preprocessed by contrast limited adaptive histogram equalization and a 2D Gabor Wavelet. Region growing method and region based active contour model with level set are applied to the preprocessed image. Both the methods are mainly used for the region extraction. The only difference in using the two different methods is that level set is used for wide retinal segmentation and region growing is used for thin retinal vessel segmentation. The main disadvantage of this approach is that for the abnormal retinal images the active contour in the preprocessing will move to pathological region leading to inaccurate image segmentation.

Lu, Xiaoqi in [110] have illustrated an improved region growing method to enhance the accuracy and reduce the effect of selection seed point. Initially the preprocessing is done using non-linear mapping method. Further, Quasi monte carlo method produces low dispersion sequence points in the ROI. Authors have presented a method of calculating the seed points by computing optical seed points. The proposed method produces improved accuracy of liver segmentation and outperforms the traditional region growing method.

For the detection of breast cancer Rouhi, Rahimeh *et al.* in [111] have introduced two automated methods for the detection of suspicious masses in mammograms. First method incorporates region growing whose threshold value is obtained by a trained ANN. Classification of mammograms being benign of malignant is decided by ANN. The intensity contrast in the mammograms is not same so trained ANN is used to determine the threshold for the region growing method to give accurate

result. Cellular neural network (CNN) is used in the second method and the parameters are obtained by genetic algorithm.

iii. **Watershed:** Watershed technique is a metaphor to the geological watershed that creates division in the landscape. This technique denotes intensity value as height of a given point in the landscape and measure the line that runs along ridges. It has a continuous domain and different algorithms provide different type of watershed depending upon the application. The usage of this technique in image is primarily done for segmentation.

The basic process of watershed produces over segmentation which is removed by Wen *et al.* [112] by proposed a hybrid technique that combined watershed segmentation with Competitive Hopfield Clustering Network (CHCN). In this paper the quality of segmentation is improved by using region adjacency graph and the inter region similarity is observed by mapping watershed and CHCN for confirming more accurate segmentation. But, the problem of over segmentation was still observed by Li *et al.* [113] and proposed a novel technique that combined watershed with region based level set method. In this the initial segment is obtained by watershed and this region is used to extract useful information. Region based level set method is then applied for extracting the boundaries of object. This technique is computationally efficient and is able to localize the boundaries due to the edges formed by watershed.

Gies *et al.* [114] prevented the over segmentation by using an independent statistical approach. It involves watershed transformation with the merging of region depending on these statistical data. This type of approach makes the complete process of segmentation more reliable.

Bleau *et al.* [115] provided a novel technique to cope with the formation of tiny regions due to over segmentation. It replicates the process of watershed that happens due to rainfall. The proposed method applies minimum modification in

order to obtain lesser watershed leading to a region that has highest resemblance with the original.

Bhattacharya *et al.* [116] have segmented the ROI by proposing a technique that is based on mathematical morphology employing watershed algorithm. It does not require on any sort of edge linking and decides the complete image in small regions. It provides the initial seed values to initialize and accurately segments the object region through watershed segmentation.

Ratan *et al.* [117] applied the watershed algorithm to 2D and 3D images for detection of the tumor. It is a manual segmentation that used texture, shape and size information for analyzing the MRI and providing a low computational requirement.

2.1.2   Clustering based image segmentation

i.   **k-mean clustering:** Coleman *et al.* (1979) [28] explained the insight view of the basic procedure of k-mean clustering; which is iterative and continues till it converges to local minima. The process iterates on number of clusters and the final clusters of the image are developed based on any parameter. The cluster scatter measure parameter given by the author has been calculated within and between the clusters to present the intrinsic number of clusters in the data. The results of the proposed method are refined and psycho visually pleasing image.

In paper [118] an adaptive k-mean algorithm has been proposed for the segmentation of regions with the smooth varying intensity distribution which is applied on cardiac CT volumetric images. In this paper for the segmentation of 3D images, a novel combination of adaptive k-mean clustering and knowledge based morphological operations has been given. The simulation outcomes show the favorable results when compared with manual outing. The presented algorithm solves the main challenges corresponding to both image and anatomy ambiguities in the 3D segmentation.

The drawbacks in [119] of over-segmentation and sensitivity due to false edges after watershed segmentation process were overcome by using k-mean clustering. To produce a primary segmentation of the image before applying the improved watershed segmentation the k-mean clustering was used. By using the watershed segmentation directly on the image produced large number of partitions. Conventional k-mean sets the number of clusters to be formed in the output image at the initialization of the algorithm. To reduce the number of partitions; the authors have used k-mean at the initial stage of the process. After the primary segmentation is done watershed technique is used. The results showed that with the proposed methodology 92% fewer partitions were produced, hence algorithm was effective.

Fahim (2006) [120] proposed a method to improve the accuracy of the k mean clustering algorithm by assigning the data points to the cluster. The algorithm resulted in the reduction of time complexity, maintaining the accuracy of the clustered output image.

Purohit Pallavi *et al.* in [121] have focused on the main problem of unstable clusters formed by k-mean clustering. The randomly chosen centroid results for the formation of unstable cluster. Also, there is time complexity in the conventional k-mean. Authors proposed algorithm provides a systematic approach for the selection of initial centroids, instead of choosing them in random. In order to improve the accuracy, the authors used heuristic approach to fine tune the clusters. The only difference in the algorithm from conventional is selection of initial centroid, whereas the authors do recalculate the new centroid. To measure the accuracy and efficiency of the proposed algorithm the authors have calculated the mean square error.

Despotovic *et al.* in [122] emphasis on how the pixels or the data points of a k-mean clustered image are forced to exclusively belong to a particular cluster, resulting in

the ambiguity of the pixels at the boundary/edges as they are forced to be a part of a particular cluster. Hence, k-mean also known as hard clustering.

The stability of clustered output image depends on the free parameter i.e. the number of cluster and choice of the value of k. In paper [123] A. Riahi has chosen the free parameter in such a way so as to minimize the energy. Author has used different techniques for the segmentation of MRI image, these are level set, histogram, active contour, region growing. Author has used k mean algorithm several times and every time the results of the images are different. For the simulation value of k=3 and the segmentation is done for the three classes.

Nameirakpam Dhanachandra *et al.* (2015) [124] proposed the use of k mean algorithm and subtractive algorithm for image segmentation. The method includes firstly improvement of the image quality by partial stretching enhancement and secondly finding the initial centroids by using subtractive algorithm. Authors have also calculated the Root Mean Square Error (RMSE) and Peak Signal-To-Noise Ratio (PSNR) to show the better performance of the proposed algorithm. The future work mentioned is for the improvement of the output image by morphological operation and using different type of clustering methods with subtractive algorithm.

The output results of the k-mean clustering depend on the initial values of k. For different values of k, the image is segmented differently and different results are obtained. So, it is inferred that the initial values of k are crucial for efficient result.

ii. **FCM Clustering:** Zadeh in 1965 [32] gave fuzzy set theory and its successful application was done on image segmentation. But the algorithm lacked in the its initialization as the final result depended solely on the input or the initial values. Work was done on these spatial value so that the objective function could be reformulated to obtain accurate clusters.

Clark, Mathew C., et. al. (1994) [125] propose a hybrid method in which the fuzzy clustering is used to detect the tumor and then label the clusters formed. Each slice of the MRI is again processed by FCM into ten classes. The authors provide and automatic segmentation of MR Images. The method lacks in the acquiring absolute accuracy, but relative accuracy is obtained which is acceptable.

Pedrycz *et al.* (1997) [126] proposed a method in which they used the spatial information and applied this information on the optimization procedure.

Iyer *et al.* (2000) [127] proposed a method in which they had designed two classifiers. The first classifier gave the crisp cluster and the second one gave relationship or the membership value. The authors had used an improvised algorithm Gustafson and Kessel. The proposed method was used on mammograms.

Ahmed *et al.* (2002) [128] proposed a method to modify the objective function of the conventional FCM so that the spatial information of the neighborhood pixel could be used for the labeling of neighborhood pixel. But this method was limited as it was applicable to only single feature input.

Keh-Shih Chuang *et al.* (2006) [129] proposed new method called spatial FCM in which the spatial information and the membership value or the weight was changed only after cluster distribution of the neighborhood was considered. By considering the spatial information this proposed method was found to be less sensitive to noise. The proposed method was tested on the MRI images. The less sensitivity to noise found in comparison with the conventional FCM.

Mostly proposed algorithm use Euclidean distance for the measurement of the difference intensity. This is simple but this distance is based on the hypothesis that the data are uncorrelated resulting in same spherical shape of clusters. This drawback was overcome by Mahabolanis distance. Krishnapuram and Kim (1999) [130] concluded that this distance cannot be used directly.

There had been so many lacks in the previous methods so highlighted by Benaichouche *et al.* (2013) [131]. So the authors in their paper provided number of improvements in the FCM algorithm. In addition, they also provided a new post segmentation method based on a new homogeneity criterion to give a finer segmentation. The authors also specify the limitation that some of the pixel were misclassified and proposes a solution to use meta-heuristic optimization algorithm in the post segmentation stage instead of greedy algorithm.

iii. **Markov random field**: MRF is an unsupervised clustering method that considers spatial information unlike other clustering method. The problem of label assignment in image segmentation is reduced by providing probabilistic approach to this assignment through MRF model. Bayesian estimation determines the labelling and prior information is obtained by clique potential.

Wells *et al.* [132] have proposed an adaptive segmentation method for getting more accurate results using intensity inhomogeneity and tissue intensities. The authors have used various type of images that are: axial, coronal and sagittal. High accuracy is observed when the obtained results are compared with the manual segmented regions and supervised multi variate segmentations.

A fully automatic technique using MRF is developed by Held *et al.* [133] for 3D images. The proposed method uses features like intensities of non-parametric tissue distribution, signal inhomogeneities and neighborhood correlations. the authors have also used real MR images and provided good accuracy of segmentation.

Leemput *et al.* [134] have used MRF for model based classification of brain tissues. This model estimates the model parameter that are used for classification. The proposed method is able to segment all MR images, it also corrects the inhomogeneities and contextual information are incorporated by MRF. The prior

information is given to the proposed method by a digital brain atlas that contains all the expectation values.

Capelle *et al.* [135] have proposed an automatic approach that consists two processes. For both the process MRF is employed with anisotropic filtering that is requires for pre segmentation in which brain is extracted from the skull and then the tumor region is segmented. The proposed technique is an unsupervised segmentation hence it is difficult to provide the priori information.

The conventional clustering methods do not need training images but they have an essential requirement of initial parameters. The MRF methods are highly sensitive to the selection of the initial parameters in comparison to the other clustering techniques as described by Pham *et al.* [136].

Gering *et al.* [137] propose a framework that trains algorithm with the image information of normal brain region. The proposed algorithm observes and variation from the normal brain region and a fitness map s computes. The obtained fitness map is used by the conventional segmentation methods for performing the extraction.

Thanh *et al.* [138] have proposed the MRF technique that uses spectral and spatial information for segmentation. Authors have applied this technique not only to MR Images but remote sensing images as well. They have also applied and presented the importance of pre and post processing for the segmentation purpose.

2.1.3   Classification based image segmentation

i.   **k-nearest neighbor:** k-NN is an unsupervised classification technique that classifies complete pixel set into different class in two stages. On comparing similarity of each pixel with the feature of particular class pixels are grouped in different classes. In the initial stage nearest neighbor distance of pixels and features are calculated depending on value of k. Training phase stores feature vector and

class labels of all samples. Finally, all the pixels are classified into their respective classes.

The concept of applying kNN to brain tumor segmentation was given by Warfield *et al.* in 2000 [139]. Authors used statistical classification that is completely MR image intensities. Images with high intensity variation are easily classified but overlapping regions are unable to be segmented. This technique could not be applied to images like skin, ventricles etc.

Cocosco *et al.* [140] developed a fully automatic, robust and adaptive technique for classifying the brain tissues. The training samples are adaptive in this case as it provides robustness against any anatomical variability. Authors have used minimum spanning tree graph theoretic approach for reducing the sample space and removed any features that were not capable to train the system. Finally, kNN classifier is used to classify the entire MR Image without any assumptions for intensity distribution.

Khalid *et al.* [141] have executed five steps for classifying the different region of brain. the training samples are built for different components that are membrane, ventricles, light and dark abnormality. The five steps of classification include assignment of k, calculating distance using objective function, sorting all the pixels with minimum distance, assigning the majority classes and determining the ranking of all the classes.

Steenwijk *et al.* [142] proposed a technique that used spatial Tissue Type Priors (TTPs)by optimizing intensity normalization. In this technique the intensities are normalized by histogram matching and providing a robust range normalization. The training is done by leave-one-out experiment by comparing with a manually reference segmentation. A huge population is used for performing the complete experiment and good segmentation results are obtained.

ii. **Artificial neural network:** Just like the human brain ANN learns and trains in accordance to the behavior of neurons. It consists of multiple layers that processes the input data to the first layer and further transmits it to the multiple hidden layers. The layers are trained through the known characteristics of the data. Final classification is performed through mathematical operations that take place in these layers. Similar to a human being that learns each and every thing through experience, an ANN learns through training and the final classification is performed in the testing phase.

Ozkan *et al.* [143] have proposed ANN that develops an adaptive learning method. To develop a superior ANN the adaptive method reduces the error that occurs due to pixel values that occur in the overlapping of inter slice region. After creating a better learning phase for network segmentation is performed twice. Initially the segmentation is done manually and then it is performed through computer aided method consisting of non-linear characteristics.

Chaplot *et al.* [144] have utilized a hybrid approach that includes training through neural network and classification using Support vector machine. Authors have used wavelets as input to the network for training. A binary classification in normal and abnormal region of entire image is performed using SVM.

A modified region growing is proposed by Kavitha *et al.* [145]. The proposed method utilizes feed forward neural network together with radial basis function. Two types of constraints are included that are orientation of the image and normal pixel intensity.

Damodharan *et al.* [146] presented tumor extraction using Neural Network that includes following steps: pre-processing, segmentation of different pathological tissues, extraction of imaging attributes and classification of tumors using neural network. The extraction of all the pathological tissues provides better accuracy by neural network for detection of tumor.

Wang *et al.* [147] provided classification of normal and abnormal brain region based on Particle Swarm Optimization (PSO) and Artificial Bee Colony (ABC) segmentation of these regions. The proposed method is a hybrid system that further utilized three types of neural network for classification.

Nazir *et al.* [148] utilized ANN for classifying the benign and malignant tumors. Authors developed a method consisting three stages that are pre-processing of the images for reducing effect of noise. Second stage is feature extraction in which author have extracted color moment, phase and mean values. All these features are given to the third stage that is a feed forward neural network. Finally, classification is performed by utilizing ANN.

Sharma *et al.* [149] have presented hybrid technique utilizing k-mean and ANN. In the proposed method mainly Gray Level Co-occurrence Matrix (GLCM) features are extracted. The extracted features aid in developing Fuzzy Inference System for segmentation of brain tumor. Authors have also utilized techniques such as thresholding, morphological operator and watershed.

iii. **Self-organizing map:** Self-organizing map (SOM) are special case of ANN that has recently used for visual pattern recognition. The input training samples are called as map that aids in dimensionality reduction. SOM is different to ANN as it uses competitive learning and preserves the topological property of image by using neighborhood function.

Vijaykumar *et al.* [150] presented a method for performing segmentation and grading of brain tumor. The segmentation is performed by proposing a novel algorithm that is based on SOM. The best matching units are used based on experience for forming the map. This algorithm is able to accurately differentiate between different regions present inside complete tumor region.

Reddick *et al.* [151] proposed a hybrid neural network that is fully automatic and provides segmentation and classification of tumor. The segmentation part is performed by Kohonen self-organizing and a multilayer backpropagation neural network is used for classification.

Murugavalli *et al.* [152] have detected the various tissue regions of brain (WM, GM, CSF and tumor) by implementing a neuro-fuzzy process for segmentation. The classification is provided by hierarchal SOM and fuzzy c mean in the hidden layer.

Tayel *et al.* [153] have provided an automatic extraction of ROI by employing neural network along fuzzy logic. The proposed technique is termed as neuro difference fuzzy that reduces memory space and complexity. It mainly focusses on variation of intensities along the radial lines of MR brain images.

Wells *et al.* [154] have proposed an adaptive segmentation technique to remove the difficulty that occurs due to intra-scan and inter-scan intensity inhomogeneities. The proposed technique uses tissue intensity property as prior knowledge for correcting and segmenting the MR Image.

2.1.4   Energy based image segmentation

i.   **Level set:** Level set method is based on curve evolution theory and its speed depends on speed function. In the traditional level set method due to irregularity of LSF there is instability. A correcting measure is provided by re initializing the LSF whenever required. But, determination of the best LSF is of prime requirement. Li *et al.* in [155] have introduced a distance regularization term that is a potential function aiding in maintaining the shape. In addition, authors in [156] have dealt with the problem of poor convergence by using a hybrid model of fuzzy and level set.

Cobzas *et al.* [157] have proposed variational tumor segmentation to encounter two main challenges that are faced in tumor extraction from MR brain Images. Firstly, the time consumption required due to manual extraction is a prime concern in order to automate the process. Secondly, the usage of prior information in order to define the appearance of normal brain. Authors have used higher dimensional feature set from textures of image for performing tumor segmentation.

Prastawa *et al.* [158] have used expectation maximization technique to perform segmentation of all registered images. An expert prior knowledge is used to develop spatial probabilistic atlas that forms all the contours of tumor. Based on this atlas segmentation is performed and can be modified with respect to subject specific brain.

Ho *et al.* [159] propose region competition method that mainly eliminates certain problem that occur with level set method. Although level set method is better than statistical classification technique but, a careful initialization is needed. This because any contour that has missing edges result in leakage and over segmentation. Probabilities are calculated for tumor and non-tumor region from different contrast images.

Sethian [160] has presented numerical implementation of level set method for forming curve or surface from maps with probabilities with variable topological change.

Gui *et al.* [161] have proposed an efficient method for tumor segmentation from neonatal brain. This method is based on following aspects: high-level brain morphology, structure and tissue location. Level set segmentation aids in forming extraction of brain at global level that consists different hemisphere and tissue level that consists cortical regions.

More research work on segmentation of neonatal brain is given by Wang *et al.* in [162]. The authors have proposed patch based segmentation in which patient specific atlases are formed. From these using the spatial consistency probability

maps are formed based on similarity. Finally, segmentation is performed using these maps and level set technique.

ii. **Active contour:** Another name for active contour is snakes or deformable model for 2D images and surfaces or active balloons for 3D images. In this technique the initial curve can be provided anywhere on the image and final contouring is done depending on the initial curve. These techniques require knowledge of geometry, physics and approximation theory. The only disadvantage with this technique is that it does not perform well images having high topological variations.

Kass *et al.* [163] have used active contour for implementing an interactive interface using well imposed constraints for guiding all the curves used for region extraction. Authors have formed an energy function with a local minimum that is able to provide different solution for high level processes. For providing a good search among these processes interactive approach is used.

The prosed work of Terzopoulos *et al.* [164] focusses on images from real world. To encompass all diverse real world visual, the approach uses dynamic, deformable objects and geometric flexible parameters. Active contours are required to extract various existing shapes of objects.

Cohen *et al.* [165] have presented a 3D generalization of active contours that grows in 3D images in form of surface. Under internal and external forces these surfaces evolve such that they attract the edges of a particular region. The authors have applied proposed technique on MR Images for providing greater stability and faster convergence.

The proposed method by Chan *et al.* in [166] have detected objects that do not have high gradients at the edges. Authors have formulated the problem in such a way that the evolution of active curvature stops only at a desired boundary. The term responsible for the stopping depend only on the extraction of region.

Kichenassamy *et al.* [167] have proposed modification to the existing active contour in such a way that the curves attract the edges more naturally. The gradient flows are modified with respect to new features for Riemannian metric. Authors have applied their technique to 3D images.

Malladi *et al.* [168] propose a new model that focusses on shapes by retaining the existing features in order to eliminate the previous limitations. Authors have applied this method only to complex object and have not used the prior knowledge of any of the object topology.

The model proposed by Caselles *et al.* [169] detects only the boundaries of object with the help of active contours that evolve in time. This evolution of active contours depends on geometric measures of images. A natural merge of region is observed by this model on detection of targeted region. The Riemannian metric is used by authors to the minimal distance calculation.

Li *et al.* [170] have proposed a technique that deals with intensity inhomogeneity. The technique has two stages in which local and global intensity changes of an image are modelled. In the local clustering complete image is considered and in global clustering the intensities of neighborhood pixels are considered. The global intensity criterion aids in forming the level set function and finally removes all biasness.

Huang [171] has proposed an edge based geodesic active contour technique for segmentation. Author has created a novel geometric statistical feature that includes edge geometry and homogeneity of voxels. The technique is robust and applicable to 3D images with automatic segmentation.

Sagiv *et al.* [172] focusses on the textural changes that occur in an image by using local features of Riemannian metric which are extracted through Beltrami

framework. The surface formed by these features provide good indication of all texture changes and better contours are formed.

Mbuyanba *et al.* [173] have presented Localized Active Contour Model (LACM) that improves region based active contour. As the statistical intensity information acquired by this technique have high sensitivity for pixels that are at boundaries. The proposed method reduces attractive forces of active contour towards undesired boundaries especially between object and background region.

iii. **Graph Cut:** The last category in energy based technique is GC. Previously discussed active contour and level set methods require initial curve to be initialized. As both techniques converge at local minimum so it is difficult to obtain a global optimal solution. Also, both these techniques utilize only the boundary information. The energy function constructed in GC include regional and boundary information and is able to achieve a global optimal solution.

The early methods related to graph theory dates back to 1960 that emphasized on gestalt principle based on proximity of pre-defined clusters. Depending on these criterion segmentation of different region is performed with the help of a fixed threshold value. With the technological advancement GC has evolved over decades and in recent times it has played an important role in medical image segmentation. In the Table 2.2, a detailed research work has been listed in the previous years.

Table 2. 2 Detail description of research work done in field of GC segmentation

Author	Year	Description	Application
Wu *et al.* [174]	1993	Interactive nature. Introduced a general approach for practical implementation of data clustering. Construction of adjacency graph to produce better cluster.	Used test images with different geometrical shapes, axial brain MR Image

Boykov *et al.* [175]	1999	Interactive nature. Gave an influential representation of s/t GC algorithm. Developed two algorithms for multi-dimensional energy minimization.	Test image with different geometrical shapes, real image with ground truth.
Boykov *et al.* [176]	2001	Interactive nature. Proposed N-dimensional GC segmentation. Introduced hard and soft constraint for region and boundary information.	Test image with different geometrical shape, real black and white image, bone removal from CT image and video sequence.
Freedman *et al.* [177]	2005	Interactive segmentation using shape priors. Eliminates the problem of segmenting target region in case of diffuse edges and multiple similar object.	CT scan of bladder, MRI of human brain, test images of leaves and fish
Yuri *et al.* [178]	2006	Interactive nature. Improvement over the N-dimensional GC [32] for wide range of application with various contextual information, visual cues and topology.	Cardiac MRI data.
Furnstahl *et al.* [179]	2008	Automatic nature. Uses prior information like intensity, shape of bone and neighboring structure. Proposed a novel energy function.	Segments joints in 3D CT images of bones.
Nhat *et al.* [180]	2008	Interactive nature. Multiple object segmentation using shape priors obtained by shape	Test images of flora and fauna.

		distance given by Chan and Zhu [7-36]. Multi-phase segmentation s proposed to eliminate overlapping of objects.	
Zhou *et al.* [181]	2010	Automatic nature. Uses information like manufacturing environment and geometric shape of work piece.	Segmentation of Industrial images
Wu *et al.* [182]	2011	Interactive nature. Hybrid model using watershed for extraction and GC for energy optimization. Improves efficiency and speed of mass segmentation.	Segmentation of breast masses from mammographic images.
Li *et al.* [183]	2012	Interactive nature. Develops unbalanced bipartite graphs and uses multi-layer super pixels.	Real images with animals.
Mahapatra *et al.* [184]	2013	Fully automatic method. Prostate MRI segmentation using learned semantic knowledge for Random Forest classifier.	MRI image of prostate gland
Ju *et al.* [185]	2015	Integration of PET and CT is done for using superior contrast. Segmentation is implemented by integrating random walk and GC. Random walk is used for providing initial seed values to GC method.	PET and CT scan of lung tumor
Pauchard *et al.* [186]	2016	Interactive nature.	Quantitative computed tomography

		Proposed method develops femur finite element model. GC segmentation is used to generate this model.		(QCT) of hip bone.
Fang *et al.* [187]	2017	Automatic nature. Hybrid framework utilizing convolutional neural network and GC. Segmentation of nine retinal boundaries on OCT images.		Optical coherence tomography(OCT) images.
Gamechi *et al.* [188]	2018	Automatic nature. Used optimal surface GCs. Initial seeds are defined by user.		Axial CT scans of aorta and pulmonary arteries.
Lorza *et al.* [189]	2018	Automatic nature. Optimal surface graph is used to maximize regional properties. Proposed method uses edge and regional information.		MRI of carotid artery
Castano *et al.* [190]	2018	Enhanced GC through a probabilistic approach. Bayesian optimization is used to extract hyper parameters and segment the tumor accurately.		MRI brain images
Song *et al.* [191]	2019	Semi-supervised algorithm. Improved GC using super pixels. Features are extracted from super pixels and neighborhood patches and similarity is evaluated.		US images for evaluating the myocardium.
Reza *et al.* [192]	2019	Combination of k-mean and graph is used for extracting Red Green Blue (RGB) images.		Unmanned Aerial Vehicle (UAV) images of grain

		Predicting the final yield of harvest.	
Zhang *et al.* [193]	2019	Supervised classification.	Brain MR Image
		Classification of multiple sclerosis for disease progression.	
		GC provides maximum a posteriori segmentation.	

Although, all the previously described segmentation techniques have their own pros and cons and improved with the advent of time, GC has following advantages:

i.   Unlike the other segmentation method GC provides a simpler graphical representation and understanding of an image.

ii. It is an efficient tool as it solves segmentation problem in a spatially discrete domain.

iii. Segmentation problem is presented as label assignment. No discretization error occur as combinatorial operators are used.

Once the tumor is accurately identified and extracted by segmentation techniques, its grading allows the radiologist to provide better diagnosis. This aids in an advance treatment planning of the patient with an early detection of tumor. Hence, machine learning can be employed because of ubiquitous use in the field of medical image analysis. The particular machine learning techniques employed in this research work are detailed in the coming section.

2.2   MACHINE LEARNING

The identification of tumor type and its characteristic is a very challenging task. It mostly involves invasive biopsy procedure that are able to identify the exact tumor grade

[194]. But, these procedures are time consuming and have post-surgical impact on patient. By developing a CAD tool for identifying the grade of glioma, is a great help for providing a second opinion to the surgeon. Through these tools a support and understanding of tumor characterization is given. Currently, Support Vector Machine (SVM) and k-nearest neighbor (kNN) techniques of the machine learning techniques are favorably used for providing binary grading of glioma.

Subashni *et al.* [195] have developed a technique that is able to identify low and high grades of astrocytoma tumor. After pre-processing of MR Image tumor extraction from MR Image is performed and extracted tumor is termed ROI. From these ROI imaging attributes Gray Level Co-occurrence Matrix (GLCM) and Principle Component Analysis (PCA) are extracted. Authors have used Support Vector Machine (SVM classifier for grading. Good accuracy value is obtained from all the classifier and the output was approved by a doctor too.

Polly *et al.* [196] proposed binary classification of low and high grade of glioma tumor using SVM. The frame structure consists four stages of pre-processing, segmentation, feature extraction and classification. The authors used 30 images for training and 50 for testing phase of both the grades. A very good value of accuracy is achieved by using SVM and output was evaluated using accuracy, specificity and sensitivity,

Gupta *et al.* [197] presented a method for classifying the input MR Images in four different classes that are Oligodendroglioma, Astrocytoma, Glioblastoma Multiforme, Ependymoma, and normal brain tissue. Adaptive thresholding is used by author for performing the tumor extraction and SVM and kNN classifiers are used for performing the tumor grading.

Arakeri *et al.* [198] classified the malignant and benign tumor using three classifiers that are SVN, kNN and ANN. The decision of these classifier is unified using combination rules like product, sum, mean and median. Image that has largest value for all parameters is given a particular label.

Li *et al.* [199] classified the clinical grade of glioma using linear SVM classifier. This method trained the network using 15 features that included amount of blood supply. These features are estimated by the expert. The classification attains good value of accuracy and other performance parameters.

Alfonse *et al.* [200] presented an automatic classification of glioma tumor using SVM classifier. In this method the author used Fast Fourier Transform (FFT) of features to improve the accuracy. The feature reduction is done by applying Minimal Redundancy Maximal Relevance (MRMR) technique. The authors are able to attain an accuracy value of 98.9% through this technique.

2.3   CONCLUDING REMARKS

This chapter reviews all state-of art methods of brain tumor segmentation and glioma grading. Most of the image segmentation technique are semi-automatic and require high level knowledge of expert to form the priori information for algorithms. In the literature review of GC technique for tumor segmentation it is observed that very less amount of work has been done in automatizing this technique. Also, the major problem of seed selection and shrinkage problem has not been addressed by researchers as per our state of the art review. These challenges of GC and their effect on tumor segmentation has been addressed in this research work.

From the literature survey on glioma grading, its importance has been observed as it possesses the ability to provide assistance in clinical routine. An efficient tool for glioma grading is able to stop the invasive process of biopsy on patient for characterization of tumor. Most of the work done by researches provided in literature survey are computationally expensive and require large amount of dataset. Also MRI scans have four different sequences and it is very difficult to identify the best sequence that could provide glioma grading. An efficient approach for sequence detection is provided that is able to provide accurate glioma grading.

Through an extensive literature review we are able to find the research gaps and frame our objective for this research work.

Research gap I. Seed Selection: The primary and initial requirement in graph cut method is the selection of seed values. These values are of utmost importance as they aid the initialization and accurate tumor extraction. Generally these are given through human intervention in the presence of radiologist.

Research gap II. Shrinkage problem: Shrinkage problem is an inherent limitation of graph cut technique that produces segmentation of ingle connected region. Due to this fallacious segmentation occurs and these unwanted region may conclude bad result. Hence, the eradication of shrinkage problem is necessary.

Research gap III. Bias field MR Images: The bias field images are created at higher magnetic field greater than 3T. Although these images provide high resolution but these also show the problem of intensity inhomogeneity. Due to this the extraction of the tumor region becomes tough.

Research gap IV. Glioma Grading: For better medical assistance the grading of glioma is very important. As each MRI has four sequences so, it is difficult to detect the best sequence that can provide the best glioma grading. Hence a system is required that can provide accurate detection of the sequences for grading glioma.

CHAPTER 3

SEED SELECTION TECHNIQUE FOR AUTOMATION OF BRAIN MRI SEGMENTATION

CHAPTER 3

SEED SELECTION TECHNIQUE FOR AUTOMATION OF BRAIN MRI SEGMENTATION

With the enormous research in the area of segmentation using various advancing techniques, GC emerges as one of the popular technique used especially for medical image segmentation. It provides an easy understanding through a simple graphical representation of image and utilizes a lower spatial bandwidth. The spatial bandwidth includes boundary and regional terms that easily specifies a clear distinction between the object and the foreground regions. Defining these terms require a prior knowledge of seed points that should have high degree of similarity with predefined regions. Hence, expert knowledge of the brain anatomy and described MR images is mandatory for generating accurate seed values. Until now, these values are either given manually under the guidance of the expert radiologist or using shape priors through an empirical selection from multiple seed values as discussed in Chapter 2. The selection of these seeds is critically important for the initialization of the GC method and extraction of the object and background regions.

3.1 PRELIMINARIES OF GRAPH CUT

The graphical representation of a 2D image I is considered to be discrete consisting nodes and edges as shown in Figure 3.1. In the graph $G = \{V, E\}$, all the pixels are represented as nodes/vertices and its complete set is denoted by V, the distance between the any two vertices (x, y) are assumed as the edge $\in E$. The terminal nodes and non-terminal nodes are two sets of nodes. All the vertices of image are called as terminal nodes whereas source S and sink T belong to non-terminal nodes that aid in the maximum flow and minimum cut of the graph. The partition of the graph is formed by a cut $C = (S, T)$ and its cost is summation of edge weight. This cut generate two disjoint sets of the non-terminal nodes S and T as expressed in Equation 3.1.

$$|C| = \sum_{\{(p,q) \in E | p \in S, q \in T\}} c_{pq} \qquad (3.1)$$

For the binary partitions number of cuts are $2^{|V|-2}$ and primary concern for performing the partition is the minimum *st* –cut problem. As portrayed in Figure 3.1 we observe the binary image consisting of foreground and the background region that is partitioned in the two disjoint set belonging to the S and T non-terminal nodes through a cut of minimum cost.
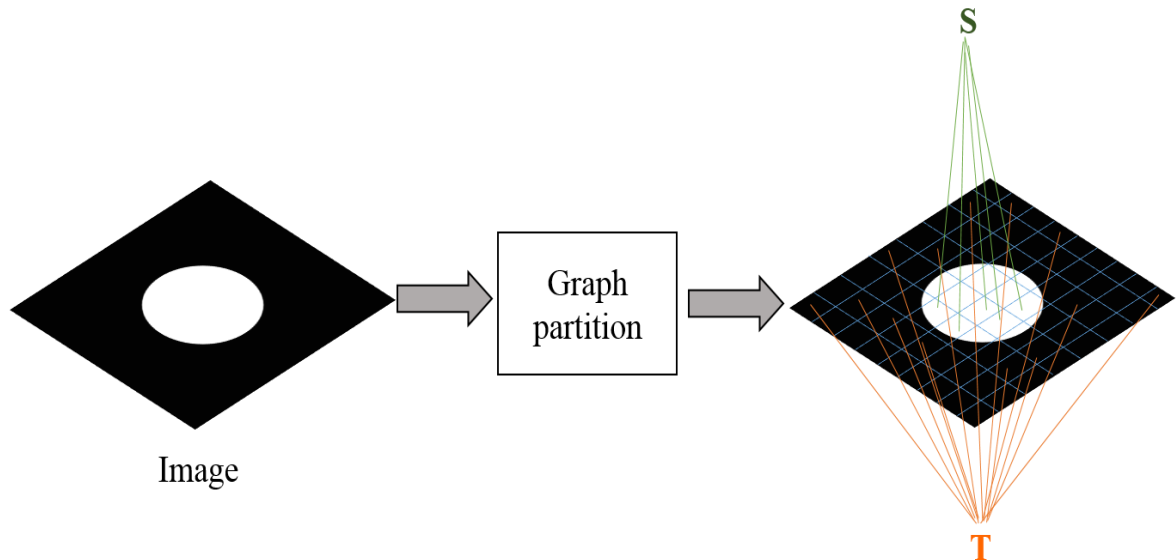

Figure 3. 1 Graphical representation of the images

Hence, we deal solely with the st-cuts that embark the partition in the GC segmentation process. The different parameters that are of prime importance are categorized as following:

i. The edges that connect the source *S* and sink *T* nodes with the vertices of the image are called as terminal links or the *t*-links.

ii. The edges that connect the neighborhood vertices are called as neighborhood links or the *n*-links.

iii. The prior knowledge that provide initial points projecting the highest similarity with the object and back ground region are called as the seed values.

3.2   MINIMUM CUT AND MAXIMUM FLOW

In a combinatorial optimization the minimum cut is formulated by evaluating maximum flow from source terminal to sink terminal [201-202]. The analogy of maximum flow portrays edges as pipes in a graph through which maximum flow should be transmitted from source to sink terminal. The amount of flow is defined as diameter of pipes and it is presented by cost given as c_{pq}. Mathematically, this flow provides a mapping as $f: E \rightarrow R_0^+$ where E is the set of edges between pixels of graph and the flow between these edges are positive presented as f_{pq}. The feasibility of this flow is only possible under condition given as:

$$0 \leq f_{pq} \leq c_{pq} \qquad\qquad \forall (p,q) \in E \qquad\qquad (3.2)$$

$$\sum_{(p,q) \in E} f_{pq} = \sum_{(q,p) \in E} f_{qp} \qquad\qquad \forall_p \in V \setminus \{s,t\} \qquad\qquad (3.3)$$

Equation 3.2 is capacity constraint and Equation 3.3 is flow conservation rule. The capacity constraint represents positive amount of flow that should not exceed edge capacity c_{pq}. Flow conservation rule states that complete amount of flow any direction between any two nodes should be equal. The flow $|f|$ which is a positive value is defined as amount leaving or arriving the source or sink respectively.

$$|f| = \sum_{(s,p) \in E} f_{sp} - \sum_{(p,s) \in E} f_{ps} = \sum_{(i,t) \in E} f_{pt} - \sum_{(t,p) \in E} f_{tp} \qquad (3.4)$$

where f_{sp} is the flow from the source terminal s and node p of the graph and f_{pt} is the vice versa flow. Hence, the maximum flow problem deals with evaluation of maximum feasible flow.

Two different approaches to evaluate the maximum flow in the polynomial time are: Augmenting path [201-202], Push-relabel method [203].

We assume that both the edges (p, q) and $(q, p) \in E$. Each edge in the graph G with flow f, contains the residual capacity r_{pq} of the edge $(p, q) \in E$ that is defined as the maximum additional flow that is sent from vertex p to q using both of the edges. In case the residual capacity is zero it is termed as saturated. The residual capacity is numerically defined as expressed in Equation 3.5.

$$r_{pq} = c_{pq} - f_{pq} - f_{qp} \tag{3.5}$$

The edge weights of the graph reflecting residual capacity are called as residual graph that has a similar structure as that of the image.

3.2.1   Augmenting path

This method of decisive maximum flow was given by Ford Fulkerson [202] with following steps.

i.   Initialize with the edges having zero flow in the residual graph.

ii.   Along the unsaturated sedges new augmented paths are defined.

iii. On the paths with minimum residual capacity allow the flow to pass. Subtract this amount from each of the edges on the path and add it to the opposite flow of the same edge.

iv.   Repeat the step ii to find the new path across the non-terminal nodes s and t.

Although, this method is guarantees integral capacities but has bad time complexity of $O(|E||f|)$ for its convergence. But, non–integral capacities this method diverges as was presented by Edmonds and Karp [204]. He also deduced that for each iteration by selecting shortest augmented path good solution is obtained that has $O(|E||f|)^2$ time complexity. This approach was enhanced by providing a sub-graph that is layered acyclic for all shortest paths using capacity of each edge from sink node. Consequently, a blocking flow is detected that saturates the sub-graph causing the unsaturated paths to be longer for every new iteration.

3.2.2 Push-Relabel method

On the contrary of augmenting method that maintains a feasible flow, in push-relabel [205-206], flow is affirmatively pushed from source terminal to all the vertices indicating them as active. Some heuristic label is given at each node that indicate the lower bound on the flow and admissible pushes are given accordingly. In case no admissible pushes are happening then the relabeling is done by updating the heuristic labels. This is done until the flow across the nodes become zero. At the beginning of the second stage the active nodes do not exist and all the remaining flow is delivered back to the source. In this way push-relabel method violates the flow conservation rule. Nevertheless, at the end of stage one the minimum cut is known. In the recent times this method has found many variants by manipulating the active node selection rule. The time complexity observed for one of these variant method is $O(|V|^3)$ for the first in first out (FIFO) selection method.

Minimum cut: As stated by Ford-Fulkerson [202] the cost for any minimum cut is maximum flow value for weighted graph.

$$|C| = |f| \qquad (3.6)$$

The set S consists of all vertices having unsaturated edges in final residual graph and the set T consists of all the remaining residual graph. We also know that at the end of computation all the edges are saturated and no more flow is possible. Hence, the cost of cut becomes sum of initial weights of saturated edges.

Though we are able to discover the cut set in polynomial time but there are some limitations to it.

i. The finding the maximum cost is NP-hard if the non-terminal nodes k increase.

ii. The minimum multi –way partition is NP-hard

iii. There are no unique solutions for the minimum cut problem as several minimum cuts are possible.

The GC method primarily concerns with the labelling problem and Markov Random Field (MRF) provide the most convenient method to dwell with this problem. It is a highly robust framework that deals with the probabilistic approach for modelling the discrete labelling of the image.

3.3 MARKOV RANDOM FIELDS

Markov Random Field (MRF) model was pioneered by Geman and Geman [207] for the image processing in their work presented on Bayesian image restoration. The initial description the variables used in this method are described as:

i. The sites I describe all the location of pixels in the image.
ii. Labels L describe the region in which a particular site belong.
iii. Neighborhood N is the 4 neighborhood system that is followed in every image graph.

In MRF a configuration is the assignment of label $\{l_1, l_2, l_3, ..\} \in L$ to the sites $\{i_1, i_2, i_3, ..\} \in I$. Finally, X will be the possible set of configuration formed and the neighboring sites will be denoted as N_i. Consider as set of random variable $X = \{X_1, X_2, X_3, ..\}$, hence each random variable acquiring a label is defined as the X_l. X_l is referred as MRF if:

$$Pr(X = X_l) > 0 \qquad \forall X_l \in X \qquad (3.7)$$

$$Pr\left(X_i = X_{l_i|X_{I\setminus\{i\}}}\right) = Pr\left(X_i = X_{l_i|X_{N_i}}\right) \qquad \forall i \in I \qquad (3.8)$$

where, $Pr(X_l)$ is the probability that the random field X acquires the labelling as X_l, $Pr(X_i = X_{l_i|X_{I\setminus\{i\}}})$ is the conditional probability. The first equation presents the technical

aspect of the probability to be less than zero also termed as positivity. The morkovinity property describes the spatial interaction between sites that is presented in second equation depicting the direct dependence of the pixel to their neighborhood. All the image pixels or the sites are dependent on even small changes in the neighborhood.

The MRFs use local conditional distribution that are subject to the non-trivial constraint. So, other approaches used is the Hamersley-Clifford theorem that verifies an equivalence between MRFs and Gibbs random fields (GRFs). As defined in Equation 3.9 GRFs is a joint probability distribution.

$$Pr(x) = \frac{1}{x} exp\left(-\frac{\sum_{c \in C} V_c(x)}{T}\right) \tag{3.9}$$

where, T is the temperature having value 1, C is cliques that is generated in each site by the neighborhood system, $V_c(x)$ is the clique potential that provide the real number to the labels. The energy function given by Equation 3.10 defines sum of $V_c(x)$ potential.

$$\sum_{c \in C} V_c(x) = \sum_{i \in C_1} V_i(x_i) + \sum_{\{i,j\} \in C_2} V_{ij}(x_i, x_j) + \sum_{\{i,j,k\} \in C_3} V_{ijk}(x_i, x_j, x_k) + \cdots \tag{3.10}$$

The theorem provides a joint probability by specifying potential function in such a way that all mandatory priori knowledge and spatial interaction are introduced by the system. The field X is dependent on observation d that is obtained by likelihood function $Pr(d|x)$ that ensures relation to *x*. Maximum a posteriori (MAP) is used to estimate MRFs configuration. It is also called as Bayesian labelling and by using this rule the posterior probability is computed as given in Equation 3.11.

$$Pr(x|d) = \frac{Pr(d|x) Pr(x)}{Pr(d)} \tag{3.11}$$

where $Pr(d)$ defines probability of d (constant value). When $Pr(x|d)$ is maximized the negative logarithm of right hand side is minimized that leads to overall minimization of energy equation and $Pr(d|x)$ is neglected.

Hence, the energy equation of the GC method is a special case of the MRF energy function with two cliques given in Equation 3.12.

$$E(L) = \sum_{i \in I} E_i(l_i) + \sum_{(i,j) \in N} E_{ij}(l_i, l_j) \qquad (3.12)$$

3.3.1   Type of energy minimization

The graph based method provides an abstract data representation and has been applicable to image restoration, extraction, structural analysis etc. But, its complete potential was explored by formulating the energy minimization which was given by Greig *et al.* [208]. The authors showed that in the discrete labelling problems the GC technique are able to find the optimal solution by finding the minimum cut to the graph even though it is slow. Different methods of minimization and approximation are explained as following.

i.   **Approximation method:** Boykov *et al.* [209] developed this method by generalizing Greig's method for more than two labels. With this approximation a multi-way minimum cut problem was created by estimating the maximum a posteriori of the MRFs. The two approximation methods given in 2001 by Boykov *et al.* [42] were α-expansion and α/β-swap. The energy function given in the Equation 3.12 is considered but a finite number of labels were considered. Some restrictions were imposed on the binary energy function in Equation 3.13 and 3.14.

$$E_{pq}(\alpha, \beta) = 0 \leftrightarrow \alpha = \beta \qquad (3.13)$$

$$E_{pq}(\alpha, \beta) = E_{pq}(\beta, \alpha) \qquad (3.14)$$

These restrictions are not given to the data term and it is form of metric that is given to the labels. For label $L > 2$ the minimization still remained NP-hard even though the restrictions are applied. Hence, swap and expansion moves were introduced by Boykov *et al.* to efficiently approximate the minimization of Equation 3.12. Initial labelling is given with α label and with expansion other locations are able to change

or retain original label. The expansion takes place iteratively until the energy for all the attained labels become minimum. The swap move also takes place in the similar manner and in each step any set of the pixel sites are able to change the label from C to β or vice-versa.

With the advent of time this method outperformed many other methods. A comparative study done by Szeliski et al [210] on various vision problem involving loopy belief propagation (LBP), iterated conditional mode (ICM) and other method including the α-expansion algorithm. This study revealed that α-expansion algorithm outperformed all the techniques. Same results were observed in another study of connected graphs done by Kolmogorov and Rother [211]. Various authors have studied the growth and improvement of energy function as depicted in Table 3.1. All these studies show the improvements acquired for different application.

Table 3. 1 Growth and improvement in energy function

	Improvements	**Application**
Kohli *et al.*[212-213]	The energy function is expanded to compute it in polynomial time	Used the energy function for higher order term. (ternary interaction potentials)
Kolmogorov *et al.* [214]	Pseudo-Boolean optimization is used for optimal labelling	Used for non-metric interaction potentials
Komodakis *et al.* [215-216]	Introduces Fast PD that is constructed on the theorem of duality	Used in a wide class of metric and non-metric potentials
Ishikawa [217]	Reduced higher-order optimization to first order problem.	Exploited the fusion move

i. **Exact minimization:** The popular success of α-expansion stimulated its application for discrete labelling problem also. This work was initiated by Ishikawa

[218] for computing the maximum a posteriori of MRFs using convex priors. This work was precisely done by Kolmogorov and Zaibh [219-220] by using the energy function with binary labels. Their study proved that energy function can be presented for graph only if:

$$E_{pq}(0,0) + E_{pq}(1,1) \leq E_{pq}(0,1) + E_{pq}(1,0) \qquad \forall \{p, q\} \in N \qquad (3.15)$$

For computing the exact global minimum of the energy function it is important that the Equation 3.15 is satisfied.

A graph $G = (v, E)$ consists of v nodes and E edges. Nodes are of two type terminal and non-terminal among which all the elements in the graph $i \in I$ are non-terminal nodes. There are two terminal nodes s and t that have label value 0 and 1, respectively. The st cut are able to provide a binary labelling to the complete graph. Any cut that is formed depends on its cost consequently introducing each node with one label. The cost is defined by the minimum cut that means a value representing maximum floe in the graph.

3.4 GRAPH CUT FOR IMAGE SEGMENTATION FRAMEWORK

For any input visual data some hidden parameters h, such as intensity value, site location and their labels are to be inferred. To achieve this information an objective function in the form of an energy called as cost/energy function is designed in Equation 3.16.

$$E: (x, h) \to R \qquad (3.16)$$

where E represents the energy function for the input visual x from which the hidden data h is extracted. This hidden data presents the intrinsic measure on the quality of solution. Depending on the representation of the hidden parameter the energy minimization is done in two groups: continuous and discrete. For continuous case level set framework [221] is used and a solution is obtained through gradient descent method

as defined by partial differential equations (PDEs). In discrete case the energy minimization is posed as a combinatorial problem and depending upon number of classes it is defined as labelling problem.

In a set consisting all the discrete pixel site $I = \{i_1, i_2, i_3, \dots\}$ with the size of $r \times c$ (r is number of row in the image; c is number of column in the image) are to be labelled as per the set $L = \{l_1, l_2, l_3, \dots l_k\}$ having k different labels. In this process of labelling the energy function is to be determined in such a way that lowest amount of energy define the label assignment. This is called as the discrete labelling problem. Generally, a neighborhood system is specified in order to derive an energy relationship among the pixel sites. This because all the pixel sites are not independent and the spatial interaction is introduced in the model.

In the computer vision each pixel site correspond to a hidden quantity on the basis of which the label assignment is done. For different desired output the hidden quantity derived from these sites vary and so does the label assignment. For example, in an environment where image restoration is the objective each pixel site will provide the intensity value and the labels produced will specify the restored intensity value. Likewise, in stereo matching the label represents the set of values that provide pixel disparity. In binary segmentation process 0 and 1 labels are provided and each label defines object and background region providing object categorization.

Finally, the type of energy function used in the image segmentation process is expressed by equation 3.17.

$$E(L) = \sum_{i \in I} E_i(l_i) + \sum_{(i,j) \in N} E_{ij}(l_i, l_j) \qquad (3.17)$$

An unknown labelling assignment is to be done of each pixel site $I = \{i_1, i_2, i_3, \dots\}$ to the labels $L = \{l_1, l_2, l_3, \dots l_k\}$. This relationship is defined by the neighboring values of the unordered pair (i, j). The unary function in Equation 3.17 E_i is the regional term that describes the label penalty for the wrong assignment of the labels. The binary function

E_{ij} describes the boundary contextual information between neighboring sites. Both these function correspond to the data and prior terms, respectively composing complete from called as MRF. It is laborious and difficult to perform the label assignment for a vast state space that has many local minima in energy functions. By numerical methods this become computationally infeasible. In recent advancing years there have been profound discoveries of deterministic algorithm in image processing for the problem of discrete labelling. The most prominent work has been done in developing various method for exploiting existing GC.

For the binary segmentation consider $p(i)$ the pixel intensities that are to be partitioned in two discrete group with the labels; $L = \{0,1\}$, where, 0 defines the background region and 1 defines the object region. Boykov and Jolly [176] used objective function for solving the problem of binary segmentation in GC as shown in Equation 3.18. The unary function in this equation determines the conditional probability of the intensity distribution for particular class of segmentation and is defined in the term of negative log-likelihood.

$$E_i = -logPr(p(i)|l) \qquad i \in I, l \in L \qquad (3.18)$$

It is observed that for a higher probability value a particular label is assigned as it generates the minimum energy penalty. The binary term in Equation 3.19 describes the boundary condition on the selection of the interaction potentials.

$$E_{ij} = \begin{cases} \lambda. B_{ij} & l_1 \neq l_2 \\ 0 & otherwise \end{cases} \qquad (3.19)$$

where, $\lambda \geq 0$ is the relative factor, if for a particular pixel the labels are not equal a penalty term is assigned described as B_{ij} and for equal label 0 value is assigned.

$$B_{ij} \propto exp\left(-\frac{(p(i)-p(j))^2}{2\sigma^2}\right).\frac{1}{dist(i,j)} \qquad (3.20)$$

where, σ is the standard deviation, B_{ij} penalty value is assigned when any two neighboring pixels have a very small intensity difference and this value gives the contrast sensitive criterion. For a difference value zero the value 1 is assigned and otherwise this value declines to zero if the contrast reaches infinity.

The E_i and E_{ij} term combine to form the energy equation and the ideal segmentation is framed. It is a linear combination that considers both the data term and piecewise term to frame an optimal labelling with smallest energy. The data term labels all the pixels according to their existing intensity but the discontinuity in the labelling arises at the boundary region. At the edges high contrasts are observed that face this discontinuity and the segmentation boundary tends to follow the edges. Hence, a balancing parameter λ is required that controls the amount contrast that will be perceived as an edge. The different edge weights formed are given in Equation 3.21, 3.22 and 3.23:

$$w_{sp} = E_i(1) \tag{3.21}$$
$$w_{pt} = E_i(0) \tag{3.22}$$
$$w_{pq} = w_{qp} = \lambda. B_{pq} \tag{3.23}$$

where, w_{sp} and w_{pt} is the weight assigned to the pixel belong to the object and the background region respectively; w_{pq} is the weight assigned to the pixels at the edges or the boundary. Regardless of the soft constraints that are given to the energy terms, some hard constraints also aid in the segmentation framework. If we choose the weight of $E_i(1)$ as infinity it forces a minimum cut to form and the pixel i will belong to the background region as the energy will become infinity. Similarly, this procedure can be done for the pixels belonging to the object region or label 1.

An a priori classification of some manually selected pixels is provided to the graph. This introduces the concept of interactive segmentation where the user can some initial seed points from the object and the background region by using the brush tool and color

coding each of the separate class pixel. But this manual of the interactive procedure requires the precise knowledge of the anatomy of the organ that is to be segmented.

3.5   MRI SEGMENTATION

The methodology used for performing the partition is explained stepwise in the Algorithm 3.1. Although GC can provide a multi object segmentation with extraction of more than two regions but, in the presented work we have performed binary segmentation. The presented methodology generates two regions that are: object (tumor) and background regions. The following constraints are considered in the algorithm:

Constraint 1: A binary segmentation is performed on input 2D MR images. The labels defined are $L = \{B, O\}$ with the following binary assignment:

$$r_k = \begin{cases} 0 & O;\ Object \\ 1 & B;\ Background \end{cases} \tag{3.24}$$

where, r_k is the defined regions, B represent the background and O is the object region.

Constraint 2: The initialization is done by using the seed values defined as m_O is the average object seed value and m_B is the average background seed value.

Algorithm 3.1

BEGIN

Step 1: Calculate background and foreground mean as given.

$$m_O = \frac{f_{o1}o_1 + f_{o2}o_2 + f_{o3}o_3 + \dots}{f_{o1} + f_{o2} + f_{o3} + \dots}$$

$$m_B = \frac{f_{b1}b_1 + f_{b2}b_2 + f_{b3}b_3 + \dots}{f_{b1} + f_{b2} + f_{b3} + \dots}$$

where, $\{f_{o1}, f_{o2}, f_{o3}, \dots \dots\}, \{f_{b1}, f_{b2}, f_{b3}, \dots \dots\}$ are the frequently occurring pixel intensity and $\{o_1, o_2, o_3, \dots\}$, $\{b_1, b_2, b_3, \dots\}$ are pixel values belonging to the foreground and background region.

Step 2: Calculate weights of the pixels are calculated with reference to the mean values.

$$w_O^p = 1 - U_p(B)$$
$$w_B^p = 1 - U_p(O)$$

where, $U_R(P)$ is the regional term described as:

$$U_p(B) = \frac{\sigma_B^p}{PV} = \frac{\sqrt{(I_p - m_B)^2}}{PV}$$

$$U_p(O) = \frac{\sigma_O^p}{PV} = \frac{\sqrt{(I_p - m_O)^2}}{PV}$$

σ_B^p, σ_O^p are the difference between pixel intensity (I_p) and mean values of object and background, and PV is the highest pixel value.

Step 3: By comparing the weights the labelling is performed to partition one complete MRI brain image into a segmented image. Label the pixel according to the condition given:

$$r_k = \begin{cases} 0 & Object \\ 1 & Background \end{cases}$$

Step 4: The tumor region is partitioned from the background.

END

The Algorithm 3.1 details all the steps required for tumor segmentation by existing graph cut technique. It consists of four steps that are: i) calculation of seed values, ii) weight calculation for evaluating the regional term of each pixel, iii) labelling of pixels by comparing regional term of object and background pixels, iv) tumor extraction.

3.6 PROPOSED WORK FOR SEED SELECTION USING GRAPH CUT

The selection of the priors is mainly done to remove any human interaction and provides m_O and m_B seed values to the GC algorithm. Many researchers have developed Computer-aided design (CAD) for avoiding this problem and provided an automatic seed selection as discussed in Chapter 2. Many hurdles have been presented by the researchers for the selection of initial seed. These represent values that show high similarity to the target or the tumor region. Selection of these values have remained a hurdle for many researchers [222-223]. In this section we have propose three novel techniques: Centroid Based Seed Selection (CBSS), k mean seed selection (KMSS) and Fuzzy Seed Selection, for the selection of the seed points that provide effective tumor segmentation. The proposed methodology is shown in Figure 3.2 that illustrates all the steps involved in the process of the proposed methodology. The block diagram mainly focusses on the selection the seed point that is achieved by the proposed methods and are given to the GC method for performing the segmentation.
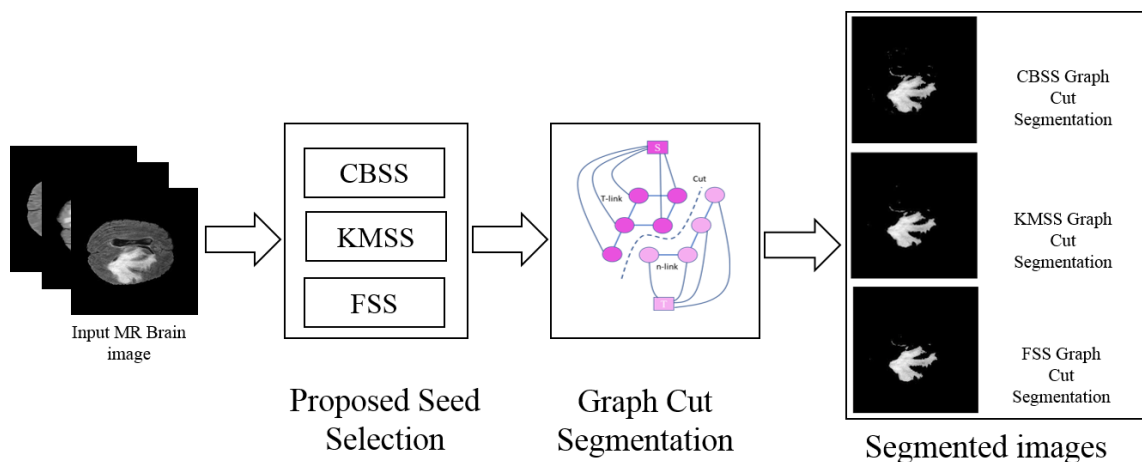
Figure 3. 2 Block diagram for the proposed algorithm of seed selection using GC technique

The proposed work is performed on the brain MR images from the standard BraTS database [43-44] and from Figshare [46-47]. The Brats dataset consists HGG and LGG images. Each image is of size 255×255×155 and has four sequences T1, T1ce, T2, Flair. In our proposed work we have used the 90 slice of HGG and LGG Flair images. The dataset obtained from Figshare consists of images of size 180×218 with a single Flair sequence.

The seed points obtained from both the proposed seed selection techniques are used for the initialization of the GC segmentation. The GC method sets costs to all the edges by using the max-flow/min-cut algorithm. Edges with minimum energy are broken and these edges are the boundary location with the highest difference between the tumor and background region.

3.6.1 Centroid Based Seed Selection (CBSS) image segmentation

In the proposed CBSS GC technique this symmetrical nature of the brain is exploited as presented in Figure 3.3. Any abnormal portion of the brain differs in the intensity values that provides the seed point required to initialize the GC algorithm. These difference value also indicate the presence of tumor region present in the brain.
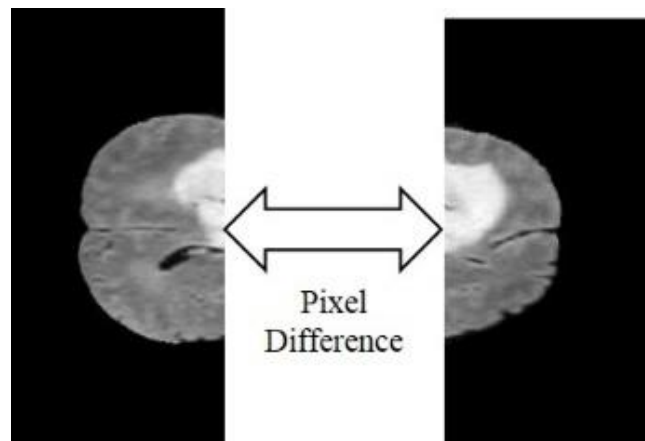
Figure 3. 3 Pixel intensity variation between vertical half of the brain image

3.6.1.1   **Methodology:** The proposed CBSS method is an automatic approach for generating seed values. As tumor region has hyper intense region so pixels adjacent in this region have highest difference value to the pixels in its symmetrical half. All these values are potential seeds of the object region, and remaining pixels as evaluated in Equation 3.27 belong to non-tumor region. In Equation 3.25 and 3.26; C_O and C_B provide complete set of seeds in tumor and non-tumor region. In the proposed method these values are termed as centroid that are given to GC method for performing the partition.

$$C_O = [d - \alpha, d + \alpha]; \ \{o_1, o_2, o_3, \dots\} \tag{3.25}$$

$$C_B = [d_1 - \alpha, d_1 + \alpha]; \ \{b_1, b_2, b_3, \dots\} \tag{3.26}$$

$$d_1 = 255 - d \tag{3.27}$$

where, α is taken 10 for proposed method it provides range below and above maximum value, d_1 represent value with maximum intensity in non-tumor region. The proposed method is described in a flow diagram in Figure 3.4 and its methodology is explained in Algorithm 3.2.
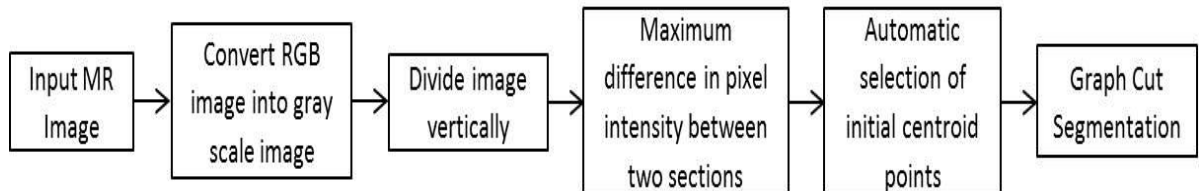
Figure 3. 4 Flow chart of CBSS GC segmentation

Initially, MR image is converted into gray scale and divided in sub images of vertical section. For a healthy or normal brain MR image both vertical section will contain similar values but, unhealthy of brain having tumor dissimilar will be found in the tumorous region. The potential seed also known as centroid are evaluated in two stages. In the first stage maximum intensity difference is calculated.

This value is given to second stage in which the range of all centroids is are calculated as per Equation 3.25 and 3.26 in the step 4 of Algorithm 3.2. Finally, according to step 5 of Algorithm 3.2 tumor extraction is performed.

Algorithm 3.2.

BEGIN

Step 1: Horizontal division of the MRI image is done.

Step 2: The highest difference obtained represent the location tumor region.

Step 3: Identify the pixel location where maximum difference is obtained as this location serves as the seed point.

Step 4: A small range α is taken above and below this seed point to include all the potential seed points.

Obtain the object pixel range and background pixel range as expressed in Equation 3.25 and Equation 3.27.

Step 5: required seed values for tumor region extraction from the complete MRI brain image are obtained.

END

The obtained values the potential seed points C_O, C_B that are given to the GC Algorithm 3.1 for performing the segmentation.

Results: Figure 3.5 presents the input MR brain image from the dataset [46-47] that is given to the algorithm and the obtained results. Figure 3.6 and Figure 3.7 present the original MR images and their segmented output from the Brats dataset. These images contain the tumor region that have different intensity values. In the CBSS method the pixels with highest difference are located accurately. From Figures 3.5, 3.6 and 3.7 the tumor can be visually easily identified. Therefore, it is inferred that CBSS algorithm has successfully extracted initial seed points for all images. Although, presence of extra region that are a part of normal brain is also observed.

(a)   (b)   (c)

(d)   (e)   (f)
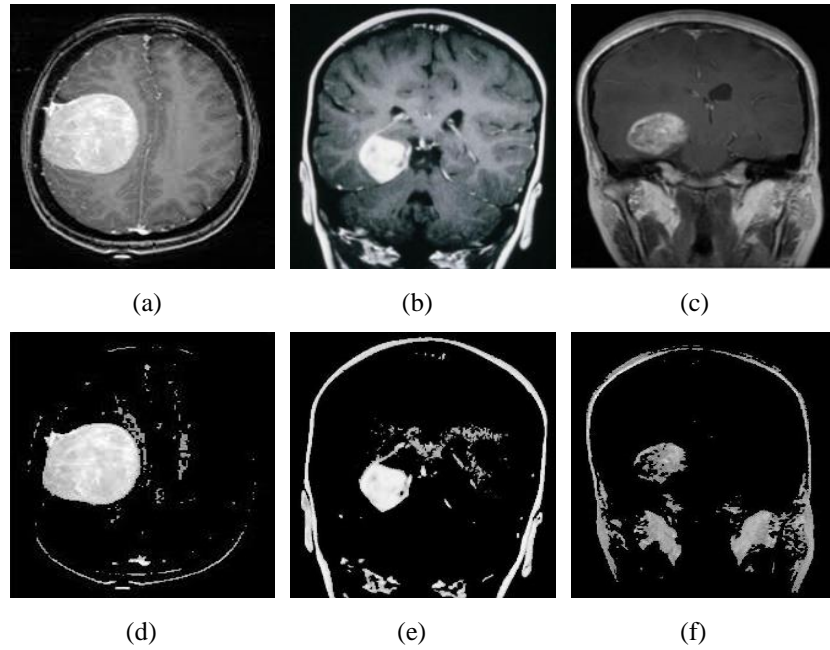
Figure 3. 5 (a, b and c): Original MR brain images from dataset [46-47]; (d, e and f): segmented output of the respective images using CBSS GC

(a)   (b)   (c)

(d)   (e)   (f)
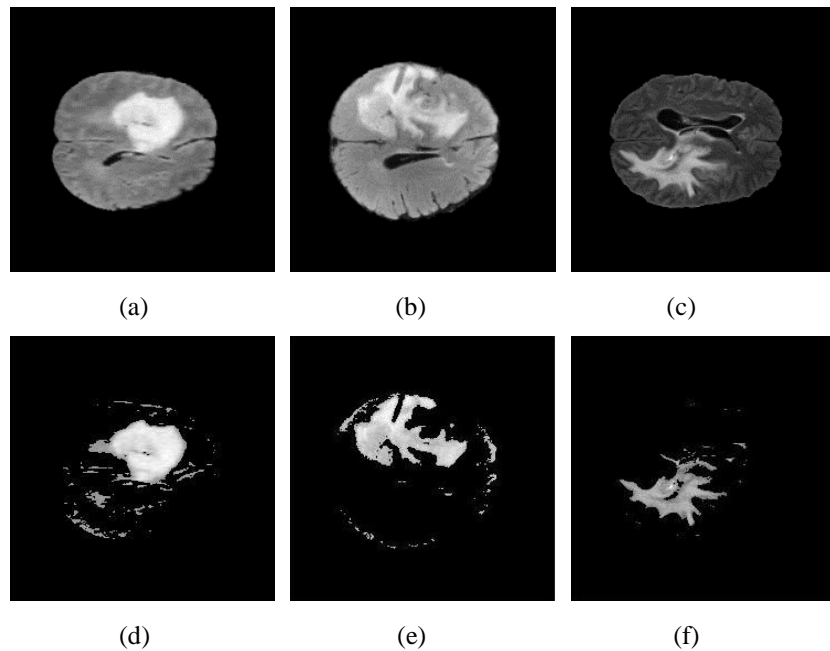
Figure 3. 6 (a, b and c): Original HGG MR brain images from dataset [43-44]; (d, e and f): segmented output of the respective HGG images using CBSS GC

(a) (b) (c)

(d) (e) (f)
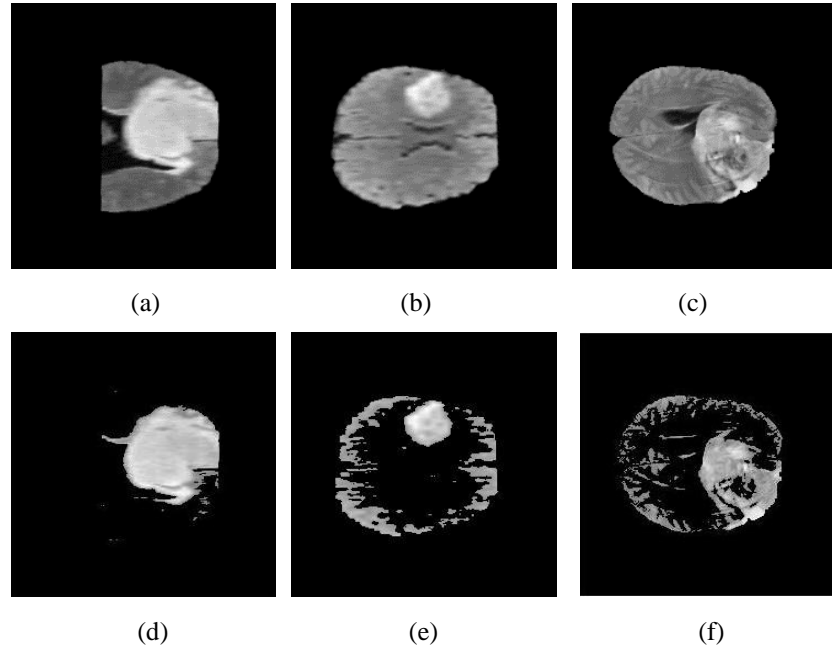
Figure 3. 7 (a, b and c): Original LGG MR brain images from dataset [43-44]; (d, e and f): segmented output of the respective LGG images using CBSS GC

The validation of the extracted tumors is done by evaluating the performance metric that is provided in Chapter 1. From Table 3.2 it is observed that values of DSC and JI are closer to 1 for most of the images. Some images show the lower values for both the parameter, this is due to extra erroneous pixels present in the output. PPV values for HGG images are higher and for LGG images it is lower. As the seeds are automatically selected but there is a possibility of selection of less effective seeds as higher difference level can observed in other normal brain region also. A higher computation time is observed as the mean time elapsed for BraTS_LGG is 9.04 sec and for BRATS_HGG is 8.29 sec.

Table 3. 2 Performance metric for the proposed CBSS GC technique

Technique		Images	DSC	JI	PPV	Time Elapsed (sec)
CBSS GC	LGG	1	0.94	0.89	0.91	7.47
		2	0.57	0.40	0.41	7.57
		3	0.88	0.79	0.80	7.65
		4	0.54	0.37	0.37	6.44
		5	0.41	0.26	0.26	8.34
		6	0.71	0.56	0.56	7.40
		7	0.96	0.93	0.94	9.69
		8	0.75	0.57	0.54	7.20
		9	0.80	0.60	0.56	10.5
		10	0.81	0.68	0.80	10.1
		11	0.88	0.79	0.91	14.47
		12	0.79	0.66	0.99	10.4
		13	0.91	0.84	0.99	9.11
		14	0.88	0.79	0.99	10.28
	HGG	1	0.84	0.81	0.94	7.55
		2	0.88	0.72	0.99	7.52
		3	0.78	0.79	0.87	6.54
		4	0.76	0.64	0.99	7.08
		5	0.88	0.62	0.99	8.63
		6	0.88	0.79	0.91	6.96
		7	0.95	0.74	0.93	7.67
		8	0.91	0.91	0.97	9.16
		9	0.74	0.78	0.98	6.27
		10	0.90	0.60	0.94	8.25
		11	0.89	0.81	0.99	10.58
		12	0.92	0.86	0.95	9.84
		13	0.85	0.74	0.90	11.05
		14	0.86	0.75	0.97	8.99
		15	0.90	0.82	0.96	7.69
		16	0.77	0.63	0.99	8.95

Table 3. 3 Range of performance metric observed

	DSC	JI	PPV
Highest	0.96	0.93	0.99
Lowest	0.41	0.26	0.26

3.6.1.2   Challenges: The proposed CBSS GC technique is able to successfully select the seed points and provide tumor segmentation. This process is completely automatic as human interaction is completely eliminated and seed selection is provided by the process of the algorithm. But, some limitations are still observed which are given as:

i.   The proposed CBSS technique depends on the contrast difference of the symmetrical regions of the brain. So, if this difference is observed in the normal region it causes fallacious segmentation.

ii.   High contrast difference is needed in the tumor region else it is unable to recognize the abrupt changes.

iii.   As the algorithm calculates the higher population of the difference pixel so, for a tumor with small size does not gets segmented.

iv.   From the Table 3.3 it is observed that a highest value of 0.96, 0.93 and 0.99 for DSC, JI, PPV respectively is obtained. But, for some images the range has lowered to a values of 0.41, 0.26 and 0.26 for DSC, JI and PPV respectively.

To overcome these limitations of CBSS technique a new technique is proposed namely k Mean Seed Selection (KMSS) GC.

3.6.2 k-Mean Seed Selection (KMSS) image segmentation

The MR brain images are constituted with different pixel intensity distribution that are clustered by employing the KMSS technique. These clusters constitute the complete distribution of the image that show different variation to each other. Hence, one of these clusters show highest resemblance with the associated tumor infected region in the brain MR image.

3.6.2.1   Methodology: The methodology of proposed technique is shown in Figure 3.8. The input MR Image is converted into gray scale image. The value of k is assumed as, $k>2$ and for our proposed method it is taken as $k=10$. This is due to the fact that increase k results in more clusters and consequently aids in including micro centroid points. Through k-mean clustering groups are formed and mean value of each cluster are potential seed value.
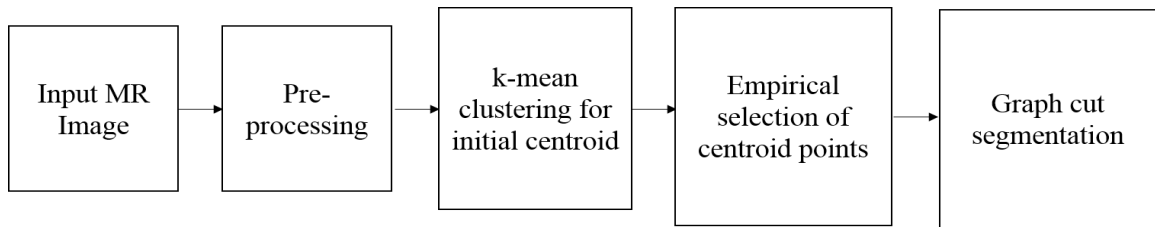
Figure 3. 8 Methodology of KMSS GC segmentation

Due to user interaction involved initially in the selection of the most appropriate seed point, this technique is semi-automatic. GC segmentation is initialized using the empirically selected seed values and tumor extraction is performed. For obtaining the particular cluster that shows the highest resemblance with the tumor region Algorithm 3.3 is executed.

Algorithm 3.3

BEGIN

Step 1: k number of clusters are initialized.

Step 2: The Euclidean distance is calculated for entire images with each centroid point.

Step 3: Clusters of MR Images are created when the iteration converges from step 2.

Step 4: Calculate object mean C_O and background mean C_O.

Step 5: Calculate weights of the pixels given in step 2 of Algorithm 3.1.

Step 6: Label the pixel according to the condition given step 3 in Algorithm 3.1.

Step 7: Tumor portion is precisely segmented from the background.

END

The selected seed points by using the Algorithm 3.3 are provided to the GC technique and the extraction of tumor is performed.

3.6.2.2   Results: The visual depiction for the tumor segmentation by using KMSS GC technique are shown in Figure 3.9 for the dataset from Figshare, Figure 3.10 and 3.11 for the dataset from BraTS MICCAI 2017.

(a)	(b)	(c)
(d)	(e)	(f)
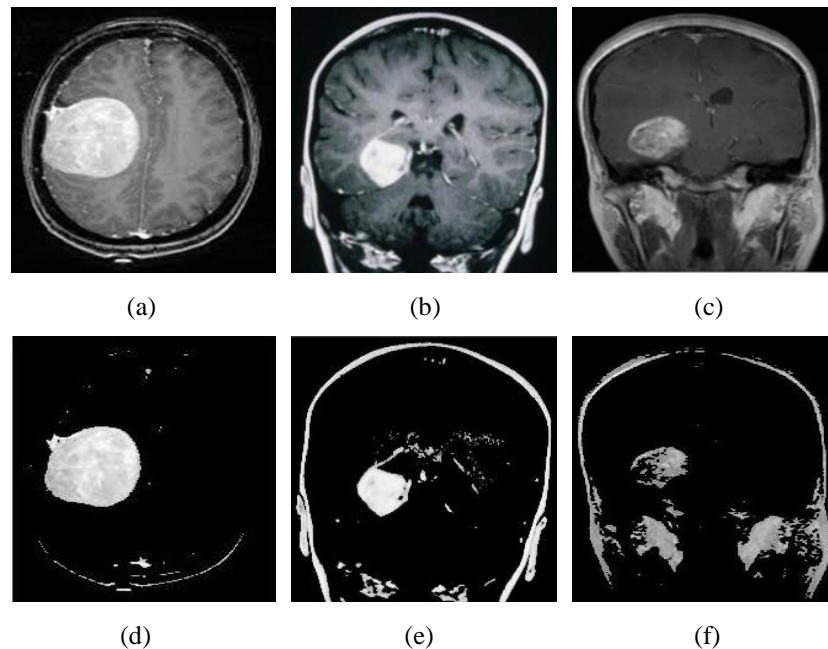
Figure 3. 9 (a, b and c): Original MR brain images from dataset [46-47]; (d, e and f): segmented output of the respective images using KMSS GC

In all the obtained results a clearer visualization of the tumor is observed in comparison to the CBSS GC technique. This is due to better and much accurate selection of the seed points by the proposed KMSS technique. Along with the tumor region a small amount of the erroneous regions can also be observed.

(a)   (b)   (c)

(d)   (e)   (f)
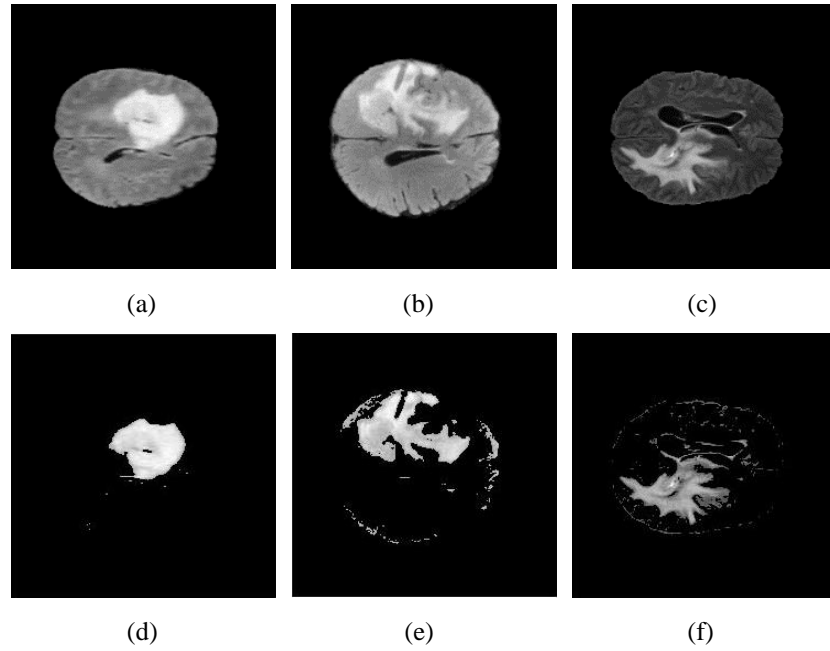
Figure 3. 10 (a, b and c): Original HGG MR brain images from dataset [43-44]; (d, e and f): segmented output of the respective HGG images using KMSS GC

(a)   (b)   (c)

(d)   (e)   (f)
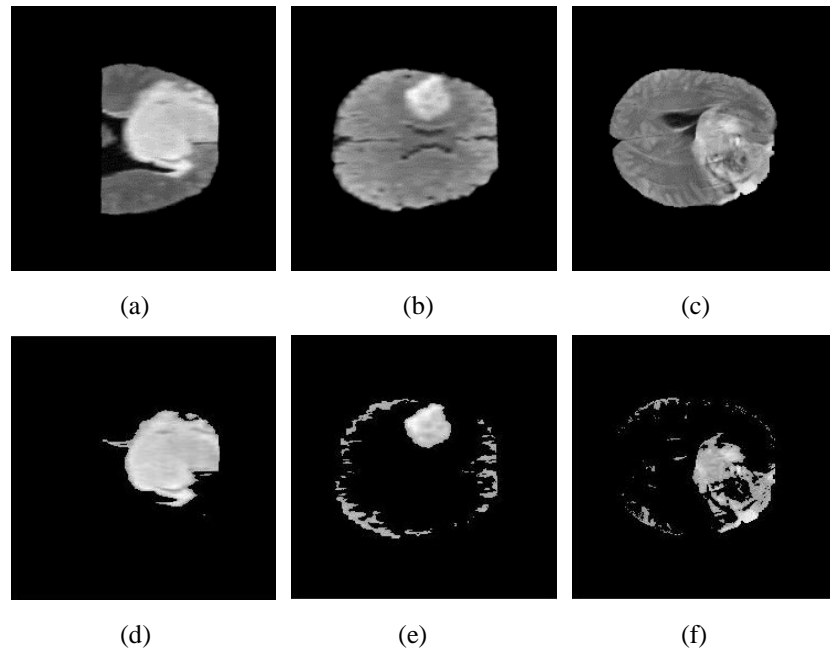
Figure 3. 11 (a, b and c): Original LGG MR brain images from dataset [43-44]; (d, e and f): segmented output of the respective LGG images using KMSS GC

Table 3. 4 Performance metric evaluated using proposed KMSS GC technique

Technique		Images	DSC	JI	PPV	Time Elapsed (sec)
KMSS GC	LGG	1	0.95	0.89	0.94	3.70
		2	0.85	0.73	0.77	3.15
		3	0.89	0.80	0.82	3.18
		4	0.86	0.75	0.77	3.16
		5	0.86	0.75	0.77	3.33
		6	0.89	0.81	0.90	3.56
		7	0.69	0.53	0.95	4.06
		8	0.96	0.92	0.99	3.59
		9	0.89	0.80	0.90	3.53
		10	0.91	0.84	0.98	4.24
		11	0.68	0.51	0.54	3.52
		12	0.78	0.64	0.99	3.69
		13	0.94	0.90	0.93	6.74
		14	0.84	0.73	0.99	4.11
	HGG	1	0.93	0.86	0.88	3.18
		2	0.96	0.92	0.98	3.33
		3	0.88	0.79	0.85	2.77
		4	0.88	0.79	0.98	3.40
		5	0.94	0.88	0.95	3.16
		6	0.86	0.83	0.91	3.37
		7	0.86	0.75	0.77	3.08
		8	0.85	0.75	0.75	3.15
		9	0.93	0.86	0.95	2.88
		10	0.87	0.76	0.94	3.68
		11	0.89	0.81	0.99	6.93
		12	0.92	0.85	0.89	4.3
		13	0.89	0.81	0.82	3.92
		14	0.89	0.81	0.95	3.28

In Table 3.4, DSC and JI values are illustrated for all the images. Maximum DSC for BraTS_LGG is 0.94 and BraTS_HGG is 0.96. Maximum JI for BraTS_LGG is 0.92 and BraTS_HGG is 0.92. The higher values of DSC and JI imply a better similarity between the ground truth and the segmented output image. The highest PPV value for BraTS_LGG and BraTS_HGG are 0.99 and 0.99 respectively. Higher values of PPV indicates a lesser amount of over-segmentation. Meantime elapsed observed for both the images are 3.83 sec and 3.67 sec. In comparison to the time elapsed for conventional GC technique, this technique signifies lesser time consumed and better result. All the parameters incline towards an accurate segmentation of the tumor region.

Table 3. 5 Range of performance metric for entire dataset observed for proposed KMSS GC technique

	DSC	JI	PPV
Highest	0.96	0.92	0.99
Lowest	0.85	0.53	0.75

From the Table 3.5, it is observed that a highest value of 0.96, 0.92 and 0.99 for DSC, JI, PPV respectively is obtained. The lower range of theses parameters are 0.85, 0.53 and 0.76 for DSC, JI and PPV respectively.

3.6.2.3 Limitations: The proposed KMSS GC technique provides efficient tumor extraction but there are some challenges that are encountered.

i. It is difficult to assign the value of k.

ii. The selection of the initial seeds is empirical.

iii. The presence of erroneous region is still observed.

iv. The performance metrics evaluated for extracted tumor are lower for some images.

3.6.3 Fuzzy seed selection image segmentation

Contrary to the k-mean clustering, fuzzy provides better membership functions and the pixels are less prone to be misclassified from their clusters. In this technique a pixel may belong to several groups with varying degree of membership. These memberships contain more information for making the final decision of grouping the pixels in comparison to the k-mean clustering. It also removes the ambiguity in classifying the pixels that have higher overlapping regions. All of these advantages provide a strong point for employing fuzzy clustering in the selection of seed points.

Fuzzy kernel selection includes fuzzifier that determines the level of cluster fuzziness. All the intensities of pixels $P_I = \{p_1, p_2, \dots\}$ are partitioned into group of c clusters. A partition matrix is formed which contains the weights $W = w_{ij} \epsilon [0,1]$ that are calculated in the iteration for $i = 1,2,3 \dots n$ and $j = 1,2,3 \dots c$. The w_{ij} is the degree of belongingness between pixels P_I and cluster C_j. For every cluster the objective function should be minimized.

$$\underset{c}{\arg\min} \sum_{i=1}^{n} \sum_{j=1}^{c} w_{ij}^m \left\| p_{ij} - c_j \right\|^2 \tag{3.28}$$

where; the degree of similarity is iteratively calculated as $w_{ij} = \dfrac{1}{\sum_{k=1}^{c}(\frac{\|p_i - c_j\|}{\|p_i - c_k\|})^{\frac{2}{m-1}}}$, c_j are the pixel intensity in the jth cluster, c_k are the pixel intensity in the kth cluster. The final cluster mean values are obtained which is a vector with length of number of cluster. In this vector the maximum and minimum of the first and second half of the complete sets are computed as:

$$\mu_T : S_{TF}^{\Omega T} = \max \left(C_{\frac{Mk}{2}} \right) \tag{3.29}$$

$$\mu_{NT} : S_{NTF}^{\Omega NT} = \min \left(C_{\frac{Mk}{2}} \right) \tag{3.30}$$

3.6.3.1   Methodology: The proposed methodology provides a hybrid approach for the seed selection and segmentation by GC technique. The block diagram for this methodology is depicted in Figure 3.12 that consists five stages. In the first stage the gray brain MR Image infected with tumor is given as the input. Intensity normalization is done at the pre-processing stage for reducing the memory space. At the third stage potential seed points are calculated by applying fuzzy clustering. These seed values encompass the complete range of the pixels that are present in the image. From these selected seed values an empirical selection of the most appropriate seeds is done at the fourth stage. The final seed values are given to the GC technique for initializing the algorithm and perform the tumor extraction. The algorithm for obtaining the seed values for GC technique is given in Algorithm 3.4.
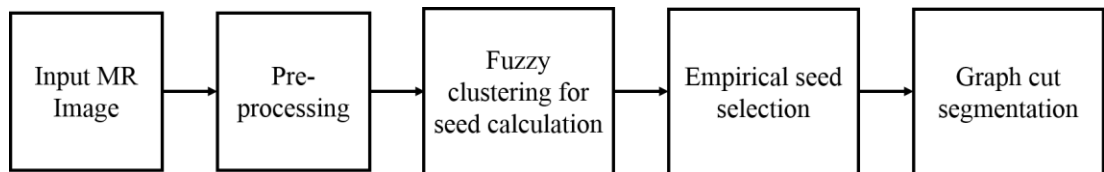
Figure 3. 12 Block diagram for the methodology of fuzzy seed selection GC technique

Algorithm 3.4

BEGIN

Step 1: Set the number of cluster c.

Step 2: Randomly assign the initial average seed values c_k.

Step 3: Compute the Euclidean distance.

Step 4: Update fuzzy partition matrix U^s.

Step 5: Calculate the minimum distance $\left|U^{(s+1)} - U^{(s)}\right| \leq \varepsilon$.

Step 6: Goto step 2 if step 5 is true else goto step 7.

Step 7: Calculate the average of the cluster points c_k.

Step 8: c_k are the seed values are that are given to the GC technique.

END

The potential kernel values obtained are empirically selected by dividing the complete set of the seed values as described in Equation 3.31 and Equation 3.32.

$$\mu_O : S_{TF}^{\Omega T} = \max\left(C_{\frac{Mk}{2}} \right) \tag{3.31}$$

$$\mu_B : S_{NTF}^{\Omega NT} = \min\left(C_{\frac{Mk}{2}} \right) \tag{3.32}$$

where, μ_O, μ_B are the final selected seed for the object and background regions that are provided to the GC algorithm.

3.6.3.2 **Results:** After the seeds are evaluated GC segmentation is performed for extracting the tumor region. The results obtained for both the dataset that encompass various form of tumor are shown in Figure 3.13, 3.14 and 3.15. It is observed from the obtained segmented image that the tumor region is present along with very low amount erroneous regions. On comparing these results with the KMSS and CBSS technique a better segmentation of the object region is identified that infers better selection of the seed points. Even the presence of erroneous region is lower in comparison to KMSS and CBSS technique.

(a)	(b)	(c)
(d)	(e)	(f)
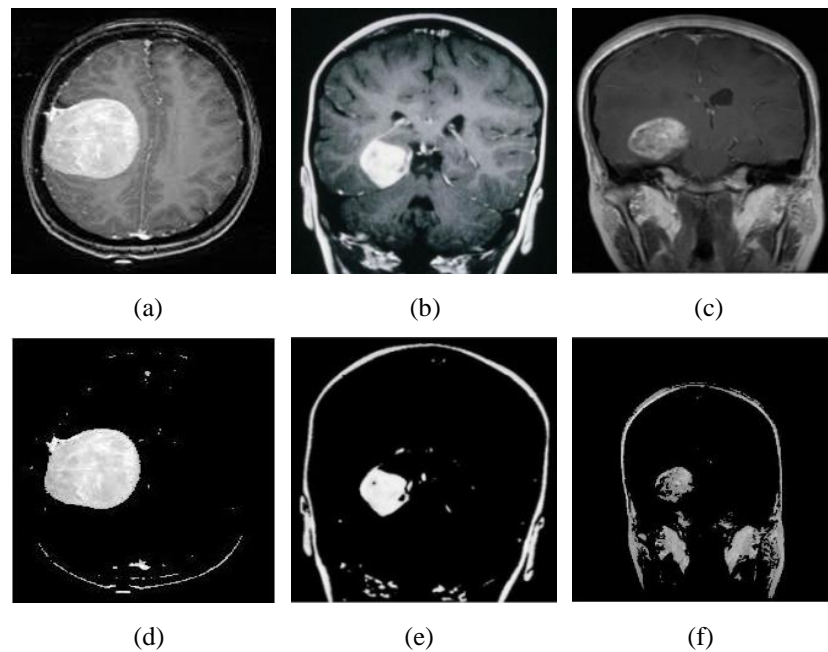
Figure 3. 13 (a, b and c): Original MR brain images from dataset [46-47]; (d, e and f): segmented output of the respective images using Fuzzy GC
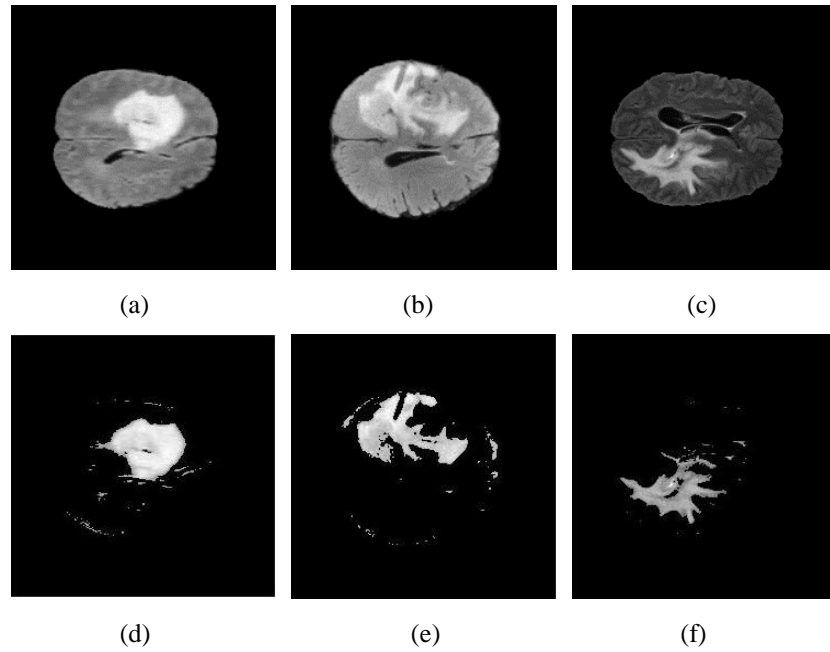
Figure 3. 14 (a, b and c): Original HGG MR brain images from dataset [43-44]; (d, e and f): segmented output of the respective HGG images using Fuzzy GC
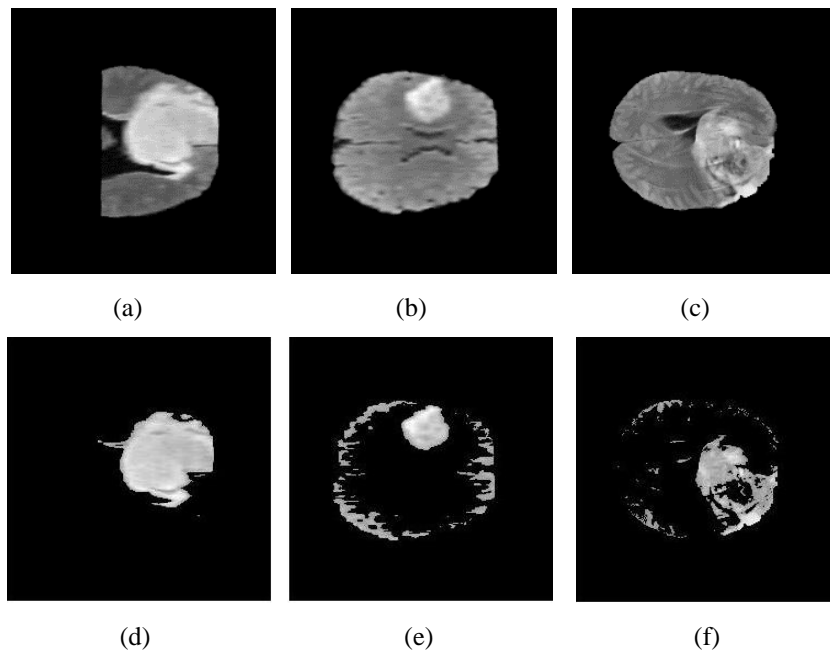
Figure 3. 15 (a, b and c): Original LGG MR brain images from dataset [43-44]; (d, e and f): segmented output of the respective LGG images using FUZZY GC

For providing a better insight of the extracted images a quantitative analysis is provided by evaluating the performance metric as tabulated in Table 3.6. In this table

it is observed that good segmentation of tumor region is obtained as the highest value obtained for DSC, JI and PPV is 0.97, 0.94 and 0.99 respectively among the LGG and HGG MR Images.

Table 3. 6 Performance metric evaluated using proposed Fuzzy GC technique

Technique		Images	DSC	JI	PPV	Time Elapsed (sec)
Fuzzy GC	**LGG**	1	0.94	0.89	0.95	9.33
		2	0.84	0.73	0.99	9.82
		3	0.89	0.80	0.58	9.75
		4	0.74	0.58	0.95	9.91
		5	0.85	0.74	0.74	9.74
		6	0.85	0.73	0.85	10.09
		7	0.78	0.63	0.36	9.85
		8	0.97	0.94	0.98	10.82
		9	0.75	0.60	0.91	10.81
		10	0.84	0.72	0.97	12.98
		11	0.84	0.73	0.88	19.84
		12	0.89	0.80	0.95	11.29
		13	0.89	0.81	0.81	10.5
		14	0.95	0.91	0.93	12.1
	HGG	1	0.93	0.86	0.91	9.38
		2	0.96	0.91	0.96	9.83
		3	0.88	0.79	0.87	11.37
		4	0.92	0.84	0.95	9.731
		5	0.90	0.82	0.83	10.18
		6	0.87	0.77	0.77	10.31
		7	0.84	0.72	0.73	9.88
		8	0.93	0.86	0.87	9.48
		9	0.93	0.86	0.91	9.39
		10	0.87	0.71	0.96	10.03
		11	0.86	0.76	0.99	13.30
		12	0.93	0.87	0.91	14.23
		13	0.85	0.74	0.90	15.80
		14	0.85	0.71	0.97	9.69

It is also observed that a high computation time is required by the proposed Fuzzy selection technique due to its inherent iterative nature. Good segmentation of tumor region is obtained as highest values are obtained for DSC, JI and PPV is 0.97, 0.94 and 0.99 respectively among the LGG and HGG MR Images. It is also observed that a high computation time is required by the proposed Fuzzy selection technique due to its inherent iterative nature.

Table 3. 7 Range Of performance metric observed for proposed Fuzzy GC technique

	DSC	JI	PPV
Highest	0.97	0.94	0.99
Lowest	0.78	0.71	0.73

3.6.3.3   Limitation: Even with the accurate segmentation obtained by the proposed technique there are some challenges. The proposed KMSS GC technique provides efficient tumor extraction but there are some challenges that are encountered.

i.   It is difficult to assign the number of cluster c.
ii. The selection of the initial seeds is empirical.
iii. Due to the iterative nature computation time is highest among the CBSS and KMSS techniques.
iv. From the range of performance metric shown in Table 3.7 a higher range of DSC, JI and PPV is observed. Also, the lower range of these metrics is closer to one that implies good segmentation for all the images.

3.7 DISCUSSION

We implemented the proposed algorithms on database [46-47] images with different types of tumor. Also, the proposed algorithm is implemented on images from the database [43-44] and the performance parameters are evaluated. Our technique is

simulated on all images, due to space constrain we have shown three images with their outputs for both the techniques. The MRI images and their segmented results obtained by applying all the proposed technique from the complete database [43-44, 46-47] are depicted in Figure 3.16 and 3.17.
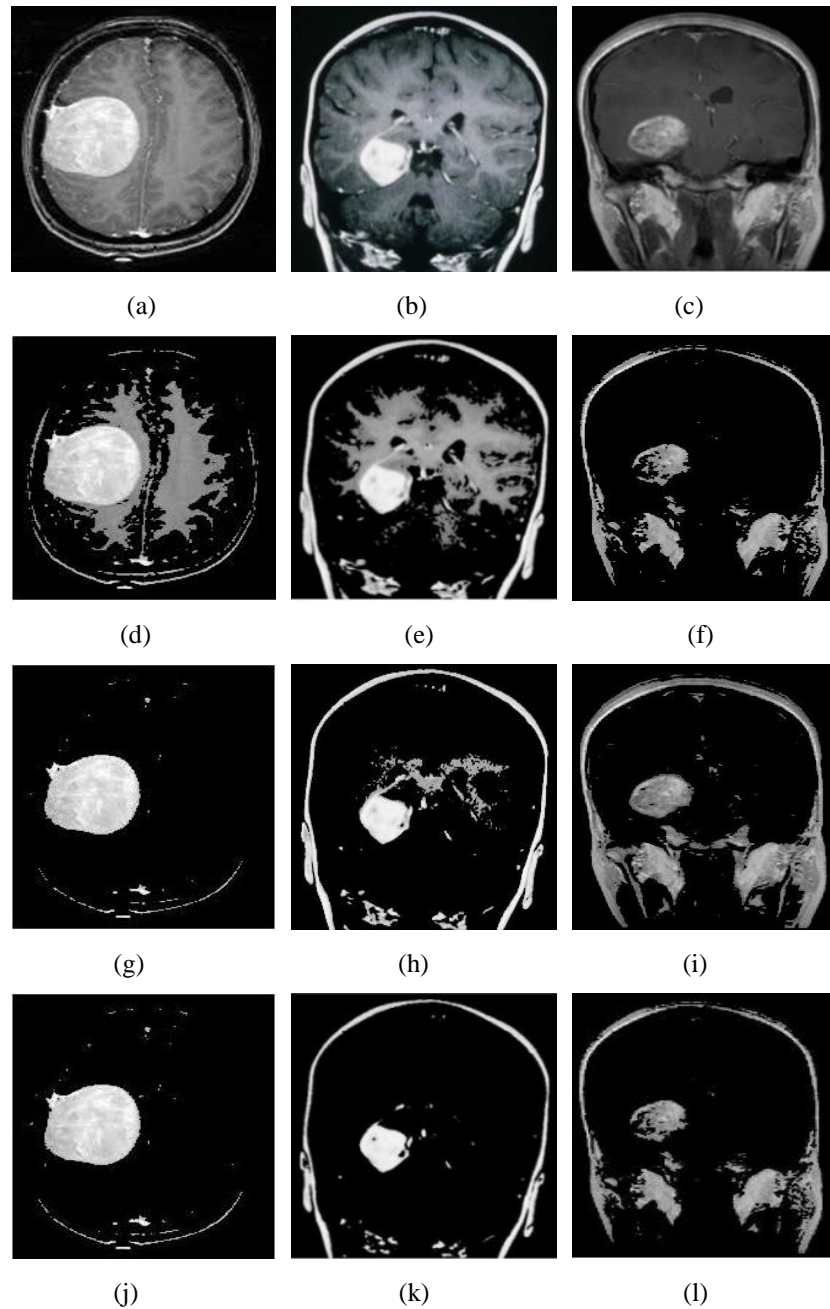
Figure 3. 16 (left to right) (a, b, c): MRI brain image obtained from Figshare dataset; (d, e, f): segmented output images by proposed CBSS GC segmentation technique; (g, h, i): Segmented output images by proposed KMSS GC segmentation; (i, j, k): Segmented output images by proposed Fuzzy GC segmentation

Results of the CBSS GC method shown in Figure 3.16 (d), (e) and (f) depict presence of unnecessary region that get included with foreground region. Hence, the desired tumor region is not accurately segmented. The results obtained by KMSS GC technique in Figure 3.16 (g), (h) and (i) illustrate that tumor regions are completely extracted.
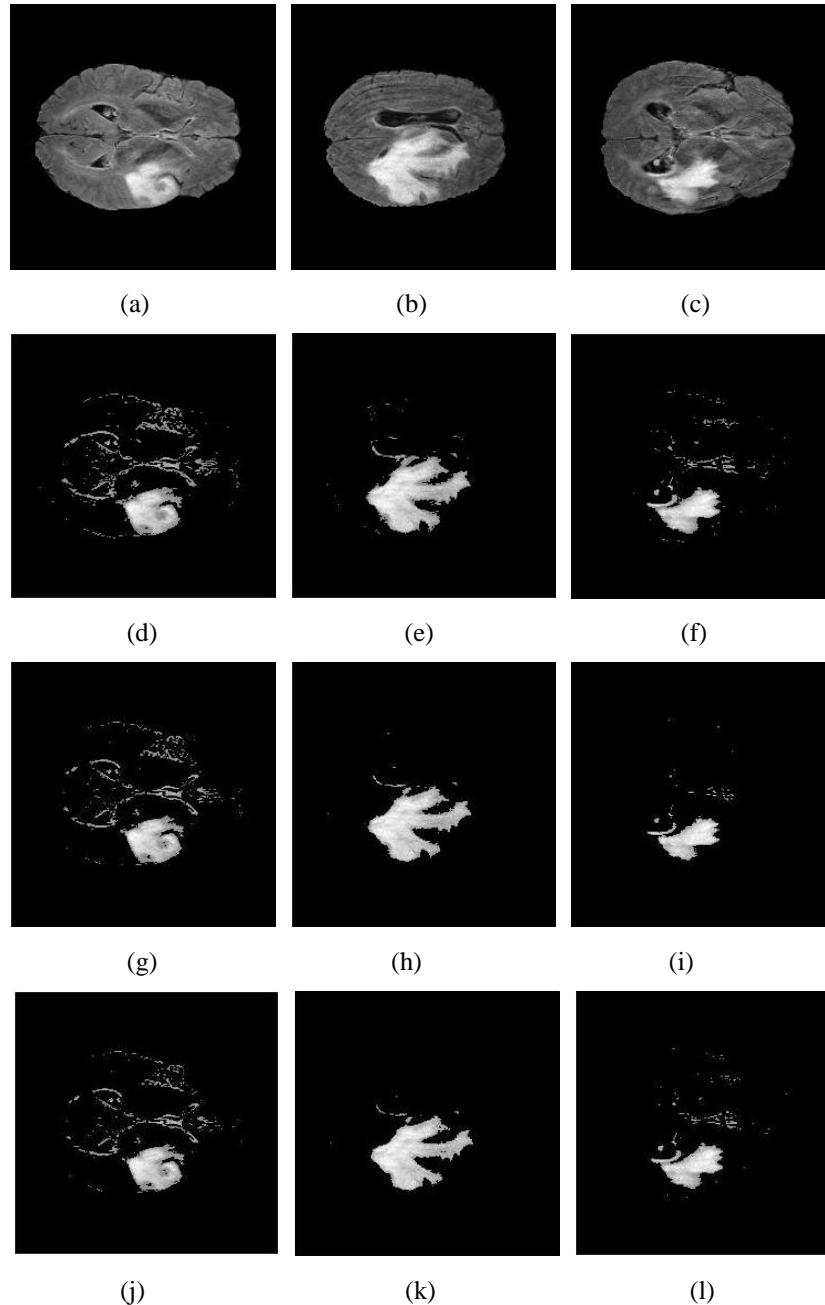
Figure 3. 17 (left to right) (a, b, c): MRI Flair modality brain image obtained from MICCAI dataset; (d, e, f): Segmented output images by proposed CBSS GC segmentation technique; (g, h, i): Segmented output images by proposed KMSS GC segmentation; (i, j, k): Segmented output images by proposed FUZZY GC segmentation

But, in comparison to both these techniques a much better segmentation is observed from the proposed Fuzzy GC technique as an accurate tumor extraction is done with very less erroneous regions occurrence. Results are depicted in Figure 3.16 (i), (j) and (k). The original MRI images from the database [43-44] and their segmented results obtained from both the proposed technique are visually depicted in Figure 3.17. The Figure 3.17 (a), (b) and (c) represent the original flair modality MRI brain image.

These images depict the complete tumor region which serves as the input for the algorithm. The Figure 3.17 (d), (e) and (f) represent the segmented output image obtained by CBSS GC segmentation. These results depict the presence of extra erroneous region which is outside the tumor region by observing the histogram. In Figure 3.17 (g), (h) and (i) illustrates the results obtained by applying KMSS GC segmentation technique. Also the extracted tumor regions obtained by the proposed Fuzzy GC is shown in Figure 3.17 (i), (j) and (k).

By comparing the images obtained by all three the techniques following observations are concluded: (a) there is the lesser amount of erroneous pixel present in the Fuzzy GC technique; (b) a lower amount of over-segmentation is obtained in the Fuzzy GC technique; (c) adjacent regions to the tumor are completely disjoint.

The mean DSC and JI values are calculated for images and the images used in the presented work. These evaluated parameters are tabulated in Table 3.8. The results obtained for the database [43-44] are encouraging when compares with the existing techniques.

Table 3. 8 Results obtained using proposed technique

Proposed	Figshare [46-47]			MICCAI BraTS [43-44]		
	CBSS	KMSS	Fuzzy	CBSS	KMSS	Fuzzy
DSC	0.72	0.84	**0.90**	0.79	0.89	**0.90**
JI	0.65	0.81	**0.89**	0.68	0.83	**0.85**

To validate the accuracy of the above observations, these results are compared with the existing techniques as well provided in Table 3.9. It is observed from the tabulated values that proposed Fuzzy GC has acquired highest value for both DSC and JI values. The existing technique proposed by Jiang *et al.* [49] is a semi-supervised approach that required high level information for performing the GC segmentation. In the paper [49*] the author has used population set that comprises all the patient specific feature in order to provide the initial seed values. Boykov *et al.* [120] proposed the general GC technique that require manual interaction for the seeds. Grady *et al.* [224] has proposed random walk method that is a graph based method but has high time complexity. In this approach decision are made at each step and the location jumps to another site according to the probability distribution.

Table 3. 9 Comparison of the performance metric with the existing techniques

	DSC	JI
Jiang *et al.* [49]	0.85	0.74
Jiang *et al.* [49]*	0.76	0.62
Y. Boykov *et al.* [120]	0.69	0.53
Grady *et al.* [224]	0.74	0.60
Kwon *et al.*[225]	0.88	-
Pereira *et al.* [48]	0.88	-
Proposed Fuzzy GC	**0.90**	**0.85**

The framework proposed by Kwon et. al. [225] performs joint segmentation and registration that uses multiple seed values using shape priors. These shape prior information are given by random walk into the framework through an empirical selection. Pereira *et al.* [48] has proposed a deep CNN architecture that uses small convolutional kernels for segmentation. This technique requires a large amount of dataset and data augmentation which is a tedious and laborious process. All the

experiments conducted by the existing technique are performed on the standard dataset of BraTS.

3.8 CONCLUSION

The purpose of the research stood to acquire the precise seed values that provide efficient brain tumor segmentation. These seed values are the key element that aids in the initialization and the accurate segmentation. The results incline better performance as compared to the existing methods. These selected seed points obtained from the proposed methods are applied on real time images providing good segmentation of the tumor region. Higher computation time and laborious data evaluation is required for the existing method. Whereas, for the proposed techniques no training is required so the proposed method does not deal with the enormous processing time required to train the system. We have obtained a semi-automatic method for performing accurate segmentation of the tumor region from MRI brain image.

Some limitation is observed with the fully automatic CBSS GC segmentation method. Even with the fully automatic method, the selection of the seed points is not quite accurate. Whereas, for KMSS GC segmentation the technique is semi-automatic and the results obtained are much more accurate with presence of erroneous regions. To reduce these erroneous regions Fuzzy GC technique is proposed that could provide better clustering of the overlapping pixels. The results depict that Fuzzy GC approach not only outperforms the previous two techniques but also the existing techniques. The erroneous regions have regions have reduced by a large mount. The main challenges that stays are the complete elimination of the erroneous region and automatic initialization. These regions occur due to the shrinkage problem that is caused due to the formation of small cuts resulting. Hence, the intensity similarity between the tumor pixels and other brain regions the erroneous regions are not eliminated completely. In the Chapter 4 both these challenges are addressed and a novel technique is proposed that conquers these difficulties simultaneously.

CHAPTER 4

AUTOMATED FRAMEWORK DESIGN FOR REMOVAL OF FALLACIOUS SEGMENTTAION

CHAPTER 4

AUTOMATED FRAMEWORK DESIGN FOR REMOVAL OF FALLACIOUS SEGMENTTAION

The perception of seed selection and its critical importance for tumor extraction has been dealt with in Chapter 3. The selected seeds that are given to GC technique for segmentation of tumor region faces certain limitations. One of the limitation is **Shrinkage problem** that is an open research issue stated by Chen *et al.* [54] in IEEE Reviews in Biomedical Engineering, causes fallacious segmentation. To overcome this limitation, the developed algorithm should generate accurate seed values, a single connected region and an automatic process. Such kind of automatic algorithm requires high level knowledge of brain anatomy and MR Images. An efficient novel Gradient Based Kernel Selection Graph Cut (GBKS GC) technique is proposed in this chapter to address this research challenge. Focus is laid on the abrupt changes of pixels at boundary regions of tumor and symmetrical composition of brain anatomy.

4.1   GRAPH CUT SEGMENTATION

Image graph structure comprise two elements nodes and edges. The complete set of node v has variety of pixel intensity and distance between the neighboring nodes is called as edge. The primary role in GC segmentation is formation of partition in two subgroups. These are exclusive groups (i.e. object and background region) that resemble non-terminal nodes s and t with highest similarity.

The familiarity with formation of minimum cut and role of energy equation is established in Chapter 3. But, the ambiguity in initialization of algorithm remains most difficult step due to intricate structure of brain.

Initialization of GC technique mainly faces following problems:

i.   What are the intensity values that comprise object and background region?

ii.   What will be nature of kernel values?

iii. How to obtain kernel values?

iv. How accurate these kernel values are?

v. Avoiding manual interaction.

The cumulative effect of these problems leads to unwanted fallacious segmentation. Other than these problems GC produces small cuts causing formation of small groups of unwanted pixels known as leakage. This complete problem is called as the Shrinkage Bias in GC image segmentation that is an open research challenge [54] and has been tried to be addressed by many researchers.

In some or the other way, whether it is selection of kernel values or shrinkage problem, tumor segmentation is directly affected. Hence, selection of kernels that can produce accurate results with no shrinkage problem remains the ultimate goal. In this chapter this challenge is addressed by considering a few connectivity Constraints. We define the graph to be undirected with defined connectivity between the nodes.

Constraint 1: The two subgroups $x \epsilon \{x_O, x_B\}$, must be connected to the non-terminal nodes s and t individually with highest resemblance.

The selected kernels should belong to the individual group in such a way that it does not hinder the generation of the two group and is able to initialize the GC algorithm. The resemblance provides a formation of a path consisting all the pixels belonging to the individual group of the non-terminal nodes. It is possible through user interaction that provides all potential kernels to the algorithm. But this way of human interaction requires predefine knowledge of the brain construction in the MR images.

Constraint 2: Producing closed target region from the original image that comprises the complete object region with pixel set x_o (Removal of shrinkage problem).

In binary segmentation two labels are assigned with data points in the set formed by object region that are labelled as 1 i.e. $x_O = \{x_O \epsilon x | x_O = 1 \}$ and set with background region are labelled as 0 i.e. $x_B = \{x_B \epsilon x | x_B = 0 \}$. But due to the leakage or formation

of small cuts a challenging situation of shrinkage problem arises. It also takes place due to interactive segmentation as inaccurate prior information may provide false kernel as a result of which structures are incorrectly segmented. Hence, Constraint 2 lays emphasis on the segmentation of single connected region as the small cuts may create fallacious segmentation with regions belonging to the background region.

In Figure 4.1 the problem of shrinkage problem is depicted and the unwanted extra regions are observed that do not belong to the targeted object region. As existing GC technique depends on intensity so, these extra regions get partitioned due to similar intensity values.

Unnecessary pixel regions extracted due to shrinkage problem
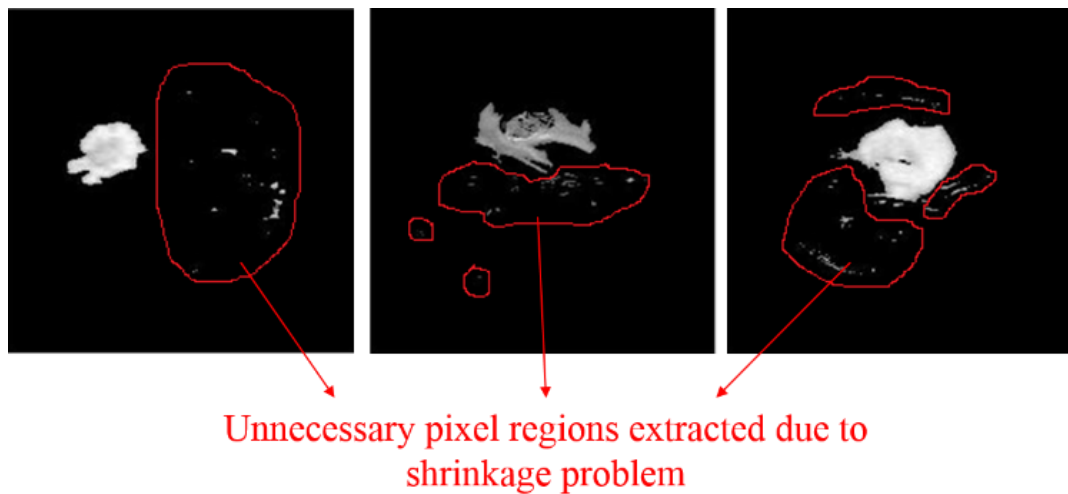
Figure 4. 1 Unwanted extra regions extracted by GC method due to shrinkage problem

Vicente *et al.* [55] in the Figure 4.2 depict the limitation of GC segmentation. It is observed from the image in Figure 4.2 (a) that a manual selection of the kernel values for the object and background region is done by the authors (manually using a brush tool). By applying the GC technique, it is observed that the object is still not segmented completely as the thin elongated parts of the object did not get segmented as shown in Figure 4.2 (b).

In Figure 4.2 (c) the problem of shrinkage bias is observed with extra region segmented that belong to the background. To obtain a single connected region the kernels are again

given manually as depicted in Figure 4.2 (d). Finally, the complete object is segmented by two-time manual selection of the kernel values as shown in Figure 4.2 (e).

| (a) | (b) | (c) | (d) | (e) |
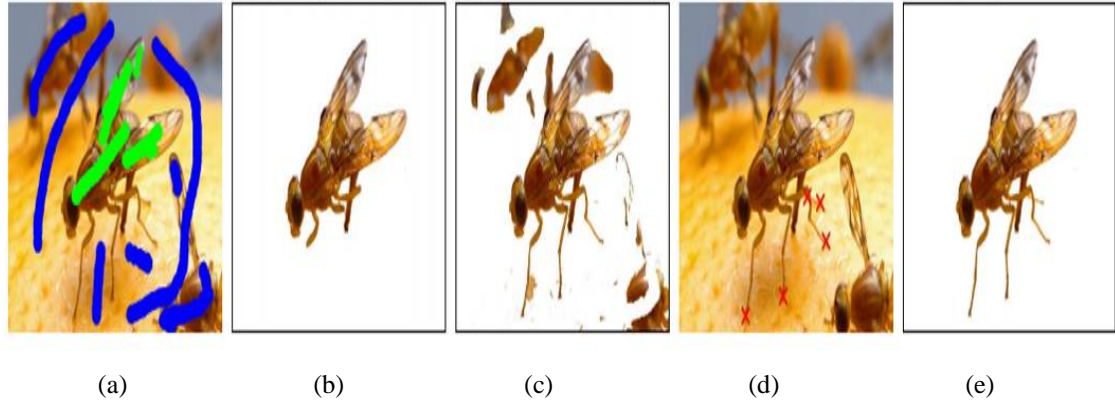
Figure 4. 2 [55] (a) the initial kernels of object and background region are given through manual selection using brush tool; (b) Incomplete segmentation of object region; (c) Segmentation of object region with erroneous region (due to shrinkage bias); (d) Additional kernels values given manually and (e) Final manual segmentation of a single connected region

4.1.1 Shrinkage problem

For accurate kernel selection by eliminating the limitation of shrinkage problem for the GC segmentation. The selected kernels satisfy the following multi objectives:

i.   Automatic initialization.

ii. Object segmentation

iii. Removal of shrinkage problem

Vicente *et al.* and Hamamci *et al.* [53, 55] have provided the kernel points manually as depicted in the Figure 4.3 (a) and (b) for the GC segmentation. Hence, the primary goal of proposed algorithm is the automatic and accurate selection of the kernel values and secondary goal is the extraction of a single connected region with no erroneous region (removal of shrinkage bias).

(a) (b)
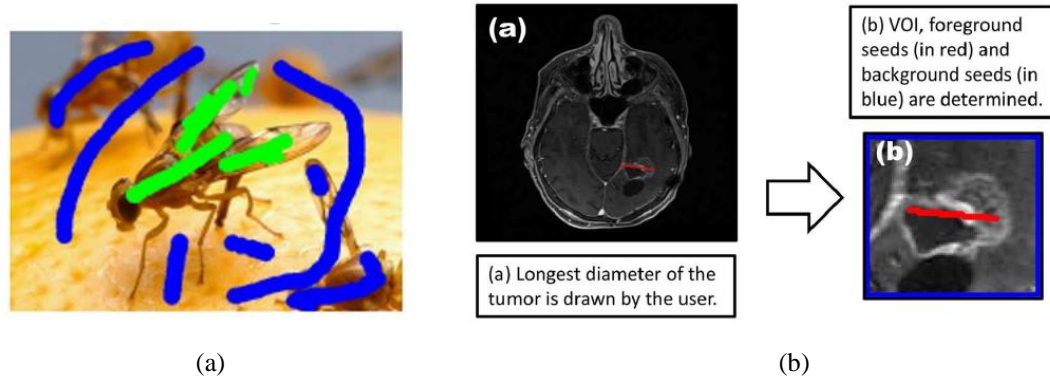
Figure 4. 3 Manual kernel selection from object and background region provided by (a) Vicente *et al.* [55] (b) Hamamci *et al.* [53]

These values act as the priori information for the execution of the algorithm and provide an automatic initialization and accurate extraction of the tumor.

4.2 PROPOSED GRADIENT BASED KERNEL SELECTION (GBKS) TECHNIQUE

Proposed GBKS depends on the intensity of the images and mainly deals with the abrupt changes of the pixel intensity. All the pixel with high intensity variation are identified as potential kernel values. The following conditions are assumed for the proposed algorithm:

i. Flair sequence is considered as the abnormal tumor region has lighter intensity as compared to the normal brain region.

ii. The symmetric nature of the brain is exploited for the proposed technique.

Some of the kernel selection techniques applied by researchers are; use of Distance transform operator by Rosenfled *et al.* [226] and Ultimate Erosion for Convex Sets (UECS) method by Park *et al.* [227]. The Distance transform [226] method is only used when some single local maxima exists in each of the target region. The UECS [227] overlapped the regions and used an iterative morphological method.

In the proposed technique abrupt changes that are termed as Gradients are evaluated. These gradients reflect positive and negative slope between intensity scales of two

symmetrical halves of MRI. They represent all the abrupt changes that are occurring in the image at regions lying on the symmetrical halves. The visual depiction of the process of proposed method is shown in Figure 4.4. Proposed GBKS method comprises a 2 level division of the images and at each level the gradients are calculated with respect to the previous level. All the gradients calculated at each level provide the positive and negative slope. In our method we consider positive slope with no intensity changes and negative slopes as the pixel scale where the highest abrupt changes occur. Hence, all the negative slopes are taken under consideration and the region responsible for these slopes are further divided for the next level. This process takes place till level 2 and at the last level a quarter part of the region is obtained that is converted into the binary form. From this image we retrieve 2 most important parameters: (a) kernel values and (b) location of these values.
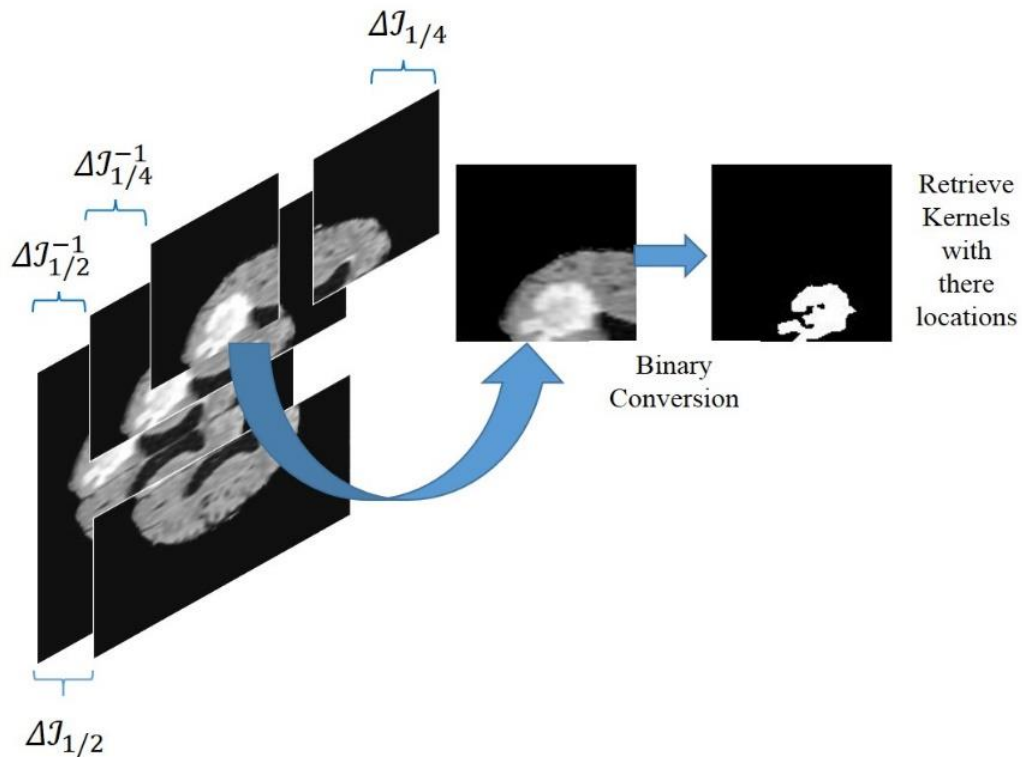
Figure 4. 4 Process Gradient Based Kernel Selection (GBKS) method

In the initial level input flair image is distributed in equally $Im: \{Im_{11}, Im_{12}\}$ and the weighted mean μ_{Im_K}, $\mu_{Im_{11K}}$, $\mu_{Im_{12K}}$ of the intensities present for all three sub images

Im, Im_{11}, Im_{12}. The weighted average for the image Im are calculated as given in Equation 4.1.

$$\mu_{Im_K(current)} = \left(f_r * \widehat{H}_l(A(x,y))\right)\big/\widehat{H}_l(A(x,y)) \tag{4.1}$$

where, r is the set of all pixel intensities excluding the black intensity value, f_r is the set of pixels that are containing the value r, $\widehat{H}_l(A(x,y))$ is vector consisting pixel values at site $A(x,y)$. In the similar manner the weighted averages $\mu_{Im_{11K}}$ & $\mu_{Im_{12K}}$ for the two half of the images are also calculated. In our methodology we have represented these divided images as Im_{11} & Im_{12}^{-1}. The inverse is indicated to a particular half that contains the tumor region. This is because eventually the process of proposed method will lead to a divided image that will contain the major region of the tumor at the end of each level.

Any difference present in the intensity distribution in the symmetric halves of brain will solely indicate the presence of abnormal tissues or tumor region. If there is no difference in the intensity distribution in both of the symmetric halves, then absence of any abnormal region is indicates. To calculate these abrupt changes, gradients are calculated between the weighted average means of intensity values of all the three sub images at the first level.

The gradients at the first level also depicted in Figure 4.4 are calculated as given in Equation 4.2 and Equation 4.3.

$$\varDelta\mathcal{I}_{1/2} = \varDelta\left(\mu_{Im_K} \sim \mu_{Im_{11K}}\right) \tag{4.2}$$

$$\varDelta\mathcal{I}_{1/2}^{-1} = \varDelta\left(\mu_{Im_K} \sim \mu_{Im_{12K}}\right) \tag{4.3}$$

where, $\varDelta\mathcal{I}_{1/2}$, $\varDelta\mathcal{I}_{1/2}^{-1}$ are the gradients computing the positive and negative slopes respectively that also indicates the inclination between the two pixel intensity scales. The negative slopes are important as they will indicate the large difference value for

abnormal region. So, we calculate the negative slopes for both the divided images as given in Equation 4.4 and Equation 4.5.

$$S_N = \sum \left(negative \left(\Delta \mathcal{I}_{\frac{1}{2}} \right) \right) \tag{4.4}$$

$$S_N{}^{-1} = \sum \left(negative \left(\Delta \mathcal{I}_{\frac{1}{2}}^{-1} \right) \right) \tag{4.5}$$

In these equation the inverse represent the negative slopes obtained for the image containing the tumor or abnormal region. Proceeding to the second step, again Im_{12}^{-1} image is divided for gradient calculation. This process is repeated until a confined tumor region is approached. The initialization kernel values obtained from the final image through the process of proposed GBKS technique are given in Equation 4.6 and the site of these kernels are given in Equation 4.7.

$$O = \{o_1, o_2, o_3, \dots\} \tag{4.6}$$

$$X = \{X_{o_1}, X_{o_2}, X_{o_3}, \dots\}; Y = \{Y_{o_1}, Y_{o_2}, Y_{o_3}, \dots\} \tag{4.7}$$

These values can be present in any part of brain and proposed method has ability to locate the tumor in such an ambiguous environment. Consider a case when tumor may lie in center of brain. In this case that portion of image will get selected that has highest amount of negative gradient. Finally, the values shown in Equation 4.6 and 4.7 are extracted from this portion of image. These values are prior information for GC algorithm and their location provide information on location of tumor. The proposed flow chart for kernel selection is elaborated in Figure 4.5.
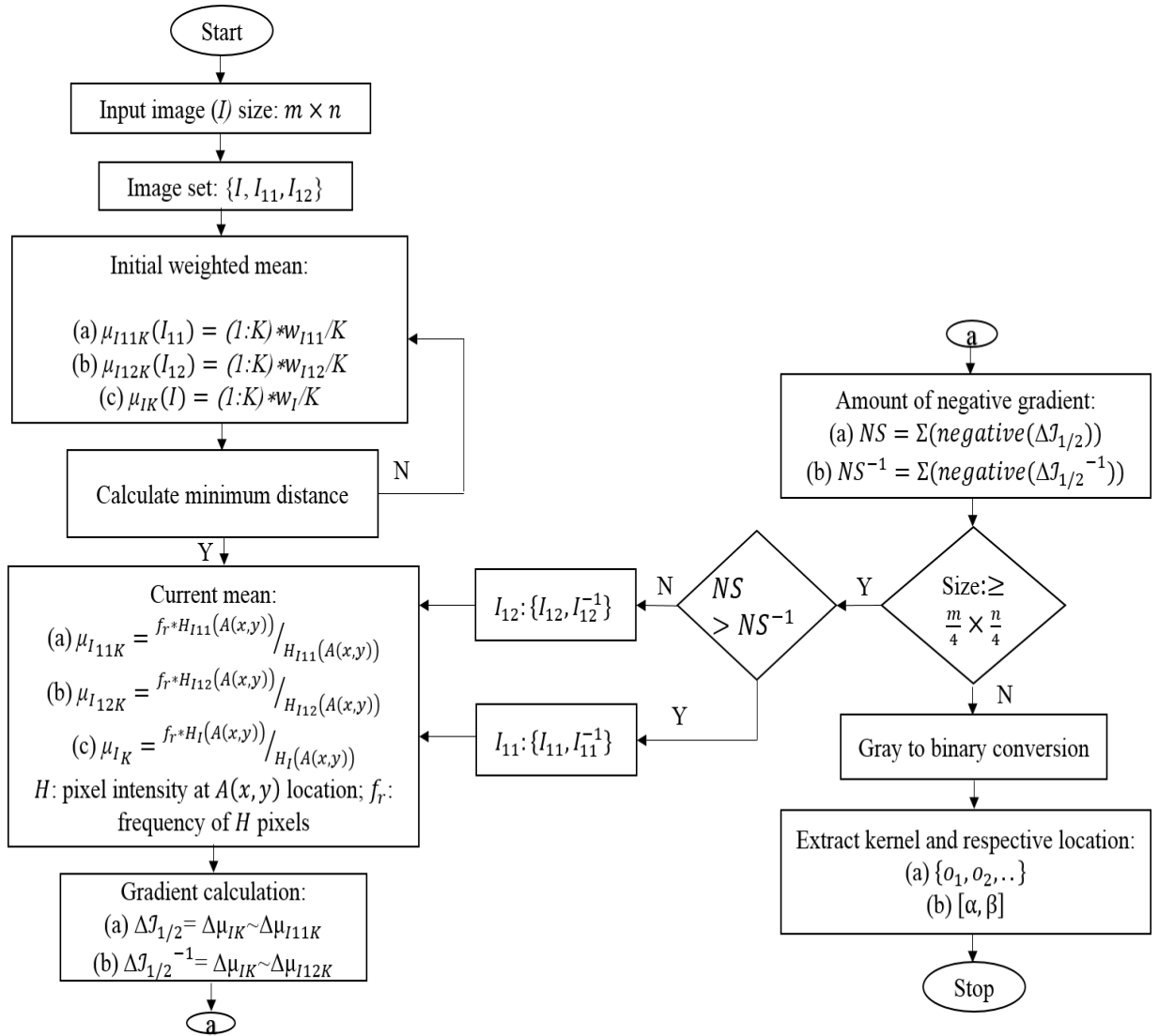
Figure 4. 5 Proposed GBKS method for kernel selection

Once the segmentation takes place using GC the background and the foreground region are completely separated as explained in Chapter 3. But, due to some small cuts or the shrinkage behavior the erroneous regions also get segmented. To avoid the occurrence of these regions the site extracted for the respective kernel values are extracted and a single confined region is acquired as explained in flowchart given in Figure 4.6.
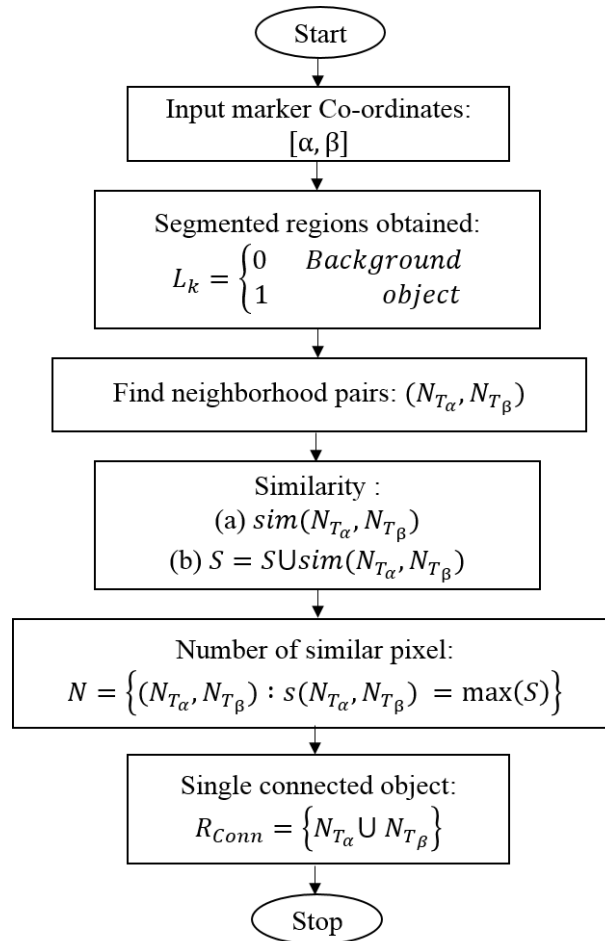
Figure 4. 6 Proposed GBKS method for extraction of single connected component

Both the flowchart provides prior information of potential kernels with their co-ordinate that are further given to the GC algorithm. These are the key requirements for constructing an accurate framework for tumor extraction from MR Images.

4.3   FRAMEWORK FOR PROPOSED GBKS GC TECHNIQUE

For each MR image that has a range of pixel intensity from 0-255, the kernel value is calculated individually that are provided to the GC technique for performing the segmentation. But, to avoid the shrinkage problem the kernel value is extracted with its location in the image. These locations are able to produce a single connected region and final single segmented region is obtained. The complete methodology for the proposed

novel GBKS GC segmentation technique is depicted in Figure 4.7. This methodology consists of following steps: Pre-processing, kernel selection, tumor extraction and evaluation of performance parameter for validation.
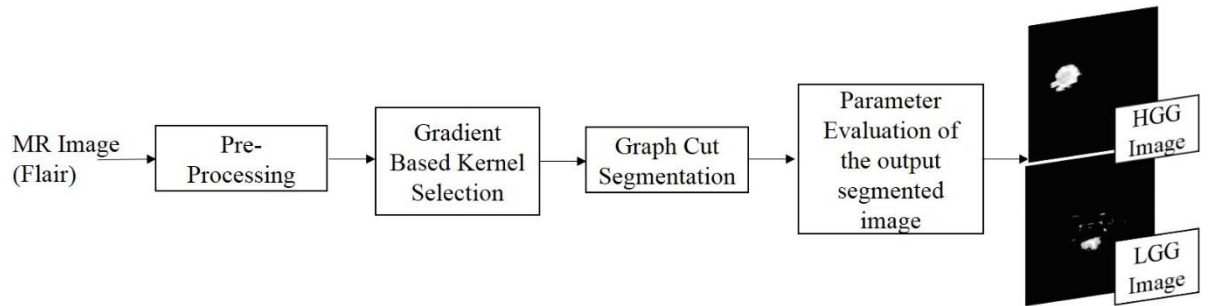
Figure 4. 7 Block diagram for proposed GBKS GC technique

The experiment is carried out on dataset as described in Chapter 1. This dataset is a gold standard adapted by many researchers and is obtained from challenges organized by MICCAI (BRATS) [43-44] of University of Pennsylvania. In our experiment we have worked on Flair images that consists both grades of Glioma tumor that is HGG and LGG. Selection of Flair image is considered because it comprises hyper intense pixels in tumor region [228]. Details of proposed technique are covered in following section.

4.3.1 Image Pre-processing

Image pre-processing technique is performed to get an enhanced image or extracting some useful information as depicted in Figure 4.8. MR images may be altered by noises or uneven distribution of the tissue intensity. One of the process in image pre-processing is the process of normalization that is also called as contrast stretching or histogram stretching. This process changes the range of the pixel intensities and is mostly referred as dynamic range expansion [54]. The brain MR images have high dynamic range of the intensity values that may imply a bad estimation of mean and variance values. This is because, the tumor region contains the lighter intensity values in comparison to the normal brain region. These intensity value provide significant abrupt changes at the boundary regions and a different group of intensity value is assigned to the normal and abnormal region of the brain. The original MR images

contain the intensity pixels in the range 0 to 65025 that increases the memory space for each image of the entire dataset of flair images.

(a)   (b)
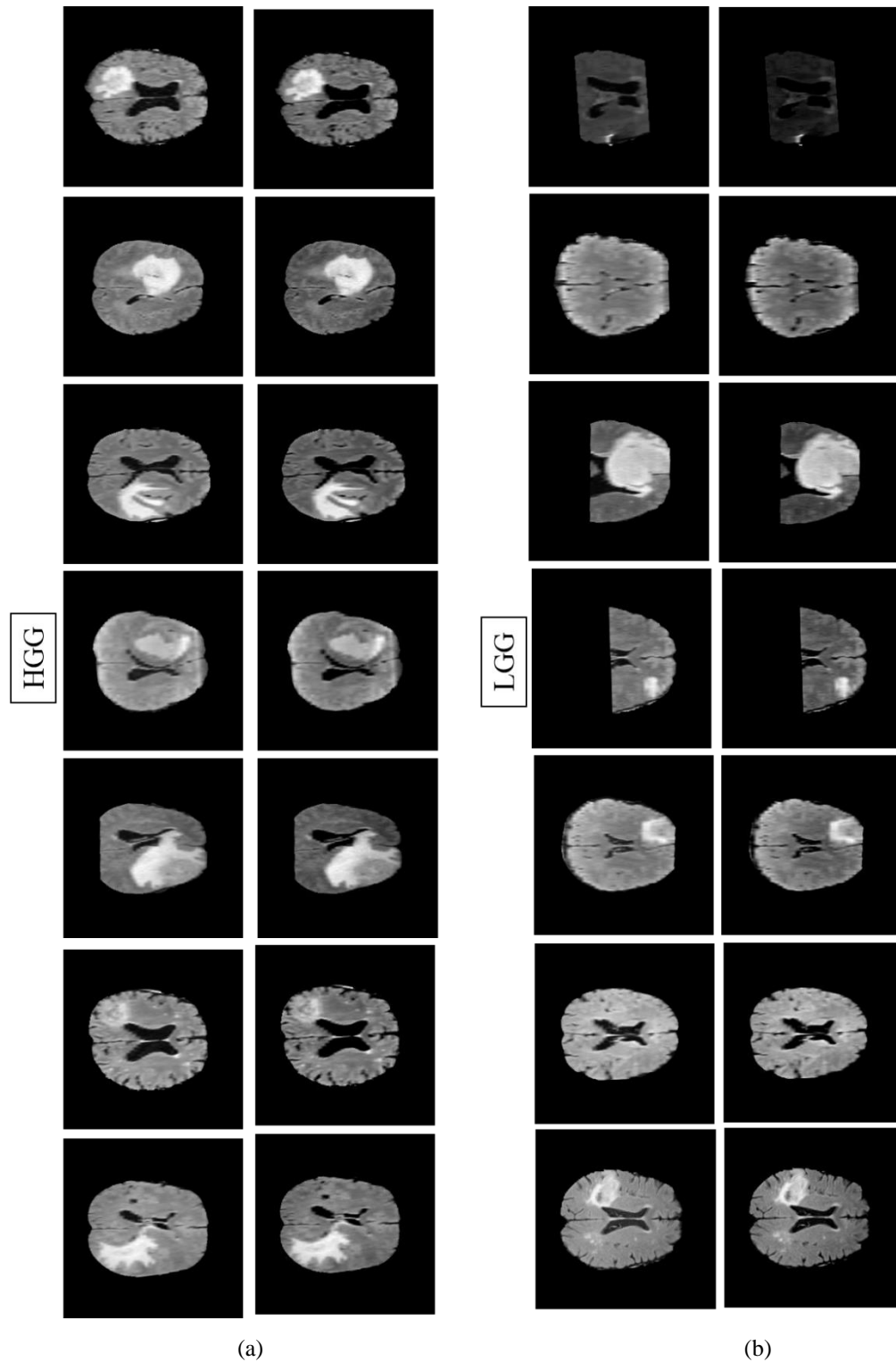
Figure 4. 8 (a) Original HGG Flair MR Images and their respective intensity normalized images; (b) original LGG Flair MR Images and their respective intensity normalized images

Hence, we need to employ intensity normalization for reducing the memory space and provide even intensity distribution as applied by other authors like Nyul *et. al.* [229]. Throughout the process of intensity normalization, an explicit or implicit assumption of uniform distribution is made [230] in segmentation methods. It is ensured that the intensity distribution of particular tissue type is in the same intensity scale across different subjects for the same MR image sequence. By applying intensity normalization, a reduction from 16 bit to 8 bit is done in order to scale the complete intensity range from 0-255. This is done by applying Equation 4.8 on the complete set of the pixel intensities $P = \{p_{i_1}, p_{i_2}, p_{i_3}, \dots.\}$ of the flair images.

$$P_N = (P - \min(P)) \frac{255}{\max(P) - \min(p)} \tag{4.8}$$

After intensity normalization, images in the intensity scale of 0-255 is obtained. The Figure 8 demonstrates effect of pre-processing on both grades of glioma flair images. Through this process memory space is reduced as input image is converted into size of 8-bit.

4.3.2 Gradient Based Kernel Selection (GBKS)

A two-level division of MR image is done according to Algorithm 1 and further the quarter image key elements are extracted. As depicted in Figure 4.9 following observation are found in the final quarter image:

i.   It contains the major part of the tumor region so the location of the tumor in the entire image is found.

ii. This image consists the potential kernel values that are the primary requirement.

iii. The site of these kernels are also known.

In accordance to the flow chart detailed in Figure 4.5 tumor extraction is performed as final quarter image provides key requirement to GC algorithm. This segmentation is explained in next section.
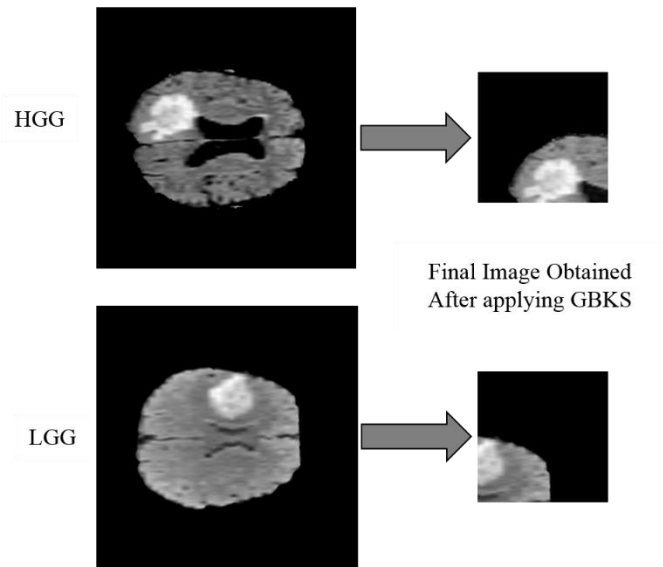
Figure 4. 9 Final quadrant image with tumor location obtained by proposed GBKS technique for both grades of glioma MR Image

4.3.3　Graph Cut Segmentation

The GC technique is employed for obtaining partition of abnormal and normal region of original MR image. Its initialization depends on accurate selection of the kernel points. In Section 4.2.2 were able generate these kernel values accurately via proposed GBKS technique. The key element retrieved are kernels and their respective location. Both of these parameters aid in GC initialization and avoiding shrinkage problem. Based on kernel values object and background mean values are calculated and respective binary labelling is done. Execution of GC is explained in detail in Chapter 3 for segmentation of tumor region and its corresponding experimental results are depicted in framework developed by Dogra *et al.* [231]. Using flow chart given in Figure 4.6 shrinkage problem is removed providing a resultant single connected object. The Figure 4.10 illustrates appearance of erroneous region that occurs due to shrinkage bias for HGG and LGG images. By accurate selection of kernels and their site of location we are able to remove shrinkage problem from all images. It is observed from Figure 4.10 that amount of enormous region is different for all HGG and LGG MR Images. Hence occurrence of shrinkage is independent of shape and size of tumor

region. This is due to the fact that small cuts are formed that partition all those regions having similar intensity value as that of object region.

`
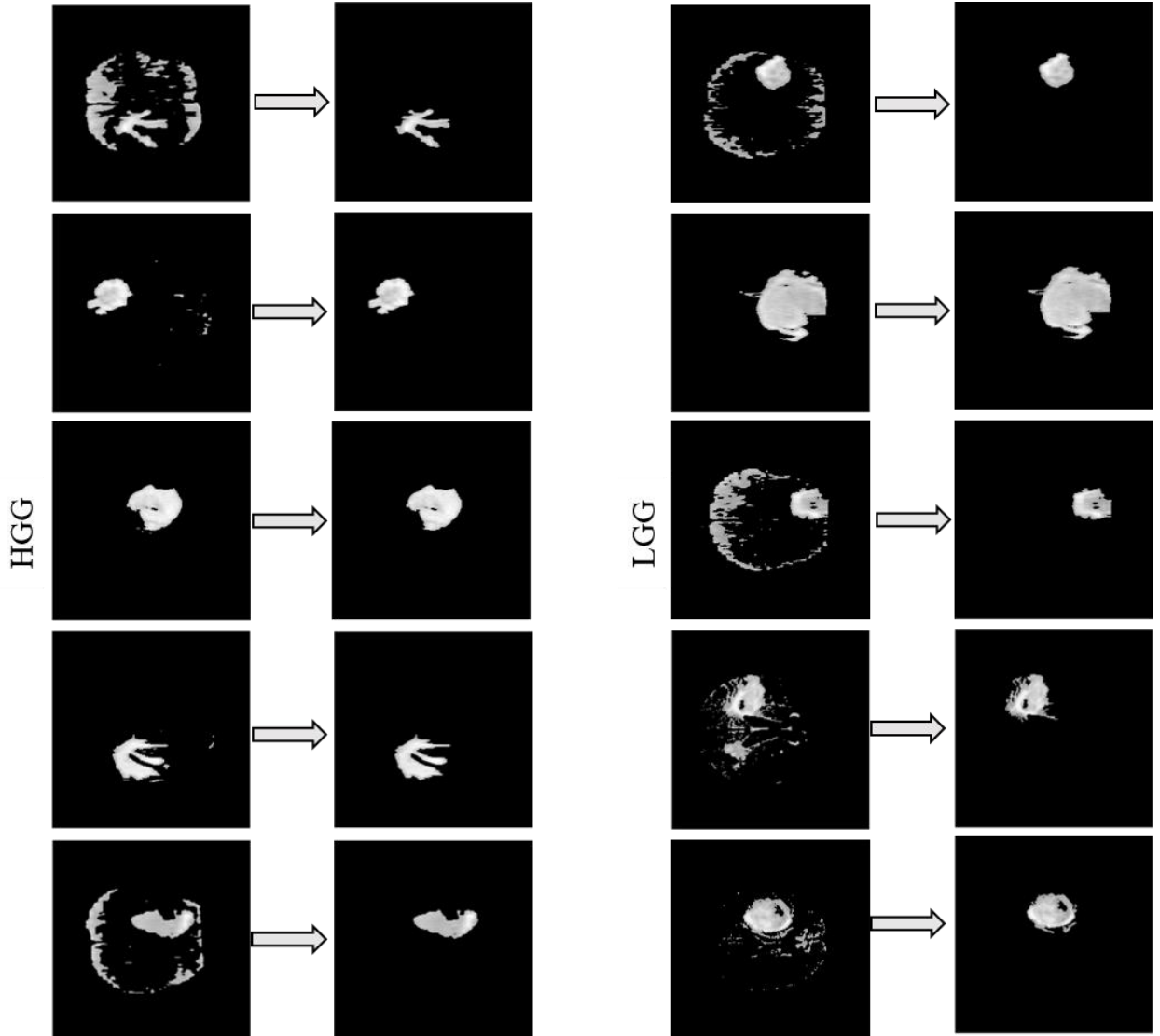
Figure 4. 10 Removal of shrinkage problem for HGG and LGG MR Images

4.3.4   Parameter Evaluation

A quantitative analysis is provided of extracted tumor region for following cases and the detail of performance parameters evaluated for each case are discussed in Chapter 1.

i. Accuracy of selected kernel

ii. Validation of extracted mask

iii. Quantification of the performance of proposed technique

4.4 RESULTS AND DISCUSSION

In this section the results obtained after conducting various experiments on datasets used are detailed.

4.4.1 Results for accuracy of selected kernel

One of the critical requirement fulfilled by the GBKS GC method is accurate selection of kernels and automatic initialization of GC technique. Extracted kernel values are validated by measuring Mean Square Error (MSE) and Correlation Coefficient (CC) values between extracted tumors from proposed GBKS GC with its ground truth and existing GC with its ground truth.

Table 4. 1 Performance metrics obtained for 10 HGG and 10 LGG MR Images for comparison of GBKS GC and existing GC technique

MSE (HGG)		CC (HGG)		MSE (LGG)		CC (LGG)	
GBKS GC	GC	GBKS GC	GC	GBKS GC	GC	GBKS GC	GC
0.014	0.014	0.903	0.904	0.011	0.014	0.935	0.92
0.007	0.011	0.923	0.879	0.002	0.005	0.889	0.752
0.002	0.009	0.950	0.841	0.004	0.056	0.904	0.484
0.001	0.003	0.890	0.796	0.008	0.025	0.899	0.726
0.005	0.012	0.936	0.875	0.001	0.008	0.958	0.749
0.011	0.021	0.904	0.829	0.002	0.005	0.949	0.874
0.008	0.007	0.905	0.911	0.008	0.017	0.849	0.732
0.007	0.011	0.844	0.715	0.009	0.016	0.903	0.839
0.005	0.005	0.950	0.939	0.002	0.002	0.888	0.894
0.005	0.009	0.930	0.842	0.002	0.004	0.959	0.924

The complete experiment is conducted on all HGG and LGG images and in Table 4.1 results are shown for 10 HGG and LGG images respectively.

Among these results the lowest MSE value obtained by applying proposed GBKS GC for HGG and LGG images is 0.001. The lowest MSE value obtained by applying existing GC for HGG and LGG images is 0.003 and 0.001 respectively. Similarly, on comparing the highest values of MSE it is inferred that tumor obtained by proposed technique has less error.

The highest value of CC for HGG and LGG images is 0.95 and 0.958 respectively by proposed GBKS GC technique. The highest values value obtained by existing GC technique for HGG and LGG images is 0.939 and 0.924 respectively. Form these values it is inferred that proposed GBKS GC is able to extract tumor region from MR Image with higher similarity in comparison to existing GC.

The average MSE and CC values for all images are depicted in Table 4.2. On comparing the mean MSE values between proposed GBKS GC and existing GC it is observed the MSE value for proposed method is 0.008 and 0.006 for HGG and LGG images respectively. High MSE value of existing GC method in comparison to GBKS GC. Similarly, average CC value obtained for HGG and LGG images is 0.899 and 0.919 respectively by proposed technique and 0.852 and 0.778 respectively by existing GC technique. These values of CC infer that tumor extracted by proposed technique has higher similarity. The high CC value and low MSE value present good selection of kernel values as tumor extraction solely depends on it.

Table 4. 2 Comparison of proposed GBKS GC and existing GC technique

	MSE(mean ± std)		CC(mean ± std)	
	GBKS GC	GC	GBKS GC	GC
HGG	0.008 ± 0.004	0.011 ± 0.005	0.899 ± 0.031	0.852 ±0.063
LGG	0.006 ± 0.005	0.017 ± 0.014	0.919 ± 0.044	0.778 ± 0.132

The segmented tumor images are depicted in Figure 4.11 for both grades of glioma respectively. From the Figure 4.11 presence of extra pixels is observed that appear with tumor by existing GC method. The resulting fallacious segmentation is cause for high MSE and low CC values given in Table 4.2. But, this fallacious segmentation does not occur by proposed GBKS GC technique. The effectiveness of the GBKS GC is even proved by quantitative values given in Table 4.2 and an effective kernel selection for segmentation of the tumor is confirmed.

(a)   (b)   (c)

(d)   (e)   (f)
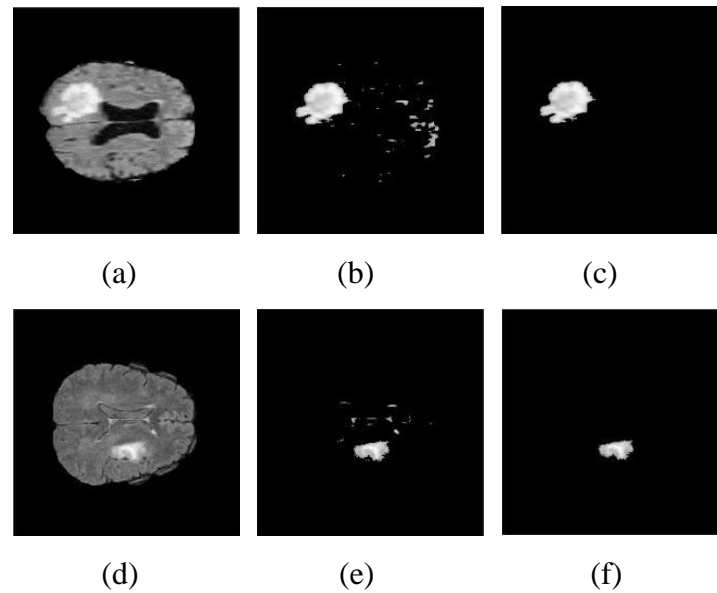
Figure 4. 11 (a) Original HGG MR image, (b) Extracted tumor by existing GC, (c) Extracted tumor by proposed GBKS GC method, (d) Original LGG MR image, (e) Extracted tumor by existing GC, (f) Extracted tumor by proposed GBKS GC method

The MSE and CC evaluation is based on number of pixel value extracted in the tumor region. These values do not provide any knowledge about shape of extracted tumor. More effective study is provided by validating shape of tumor.

4.4.2 Mask evaluation

The user always remain at blind side as there is an ambiguity for extraction of tumor. So, in order to validate the shape and location of the tumor region from the extracted image mask evaluation is performed. Regional properties are extracted from obtained

tumor and the available ground truth mask. The error values obtained between the two mask for the regional properties are tabulated in the Table 4.3 for 10 HGG and LGG images respectively.

Table 4. 3 Error calculation for validation of tumor shape obtained from GBKS GC method for reference 10 HGG and 10 LGG MR Images

HGG (mean)				LGG (mean)			
Area	Perimeter	MAL	MiAL	Area	Perimeter	MAL	MiAL
0.07	0.06	0.05	0.09	0.04	0.07	0.03	0.01
0.02	0.08	0.03	0.03	0.05	0.16	0.07	0.09
0.08	0.04	0.03	0.03	0.08	0.13	0.04	0.10
0.01	0.03	0.02	0.03	0.01	0.12	0.09	0.01
0.01	0.11	0.01	0.05	0.01	0.01	0.01	0.02
0.12	0.16	0.01	0.01	0.01	0.11	0.01	0.03
0.06	0.08	0.02	0.01	0.04	0.14	0.03	0.09
0.06	0.07	0.03	0.02	0.02	0.12	0.04	0.05
0.07	0.02	0.01	0.04	0.12	0.09	0.01	0.09
0.09	0.10	0.09	0.05	0.01	0.09	0.01	0.02

* MAL Major axis length; MiAL Minor axis length.

Table 4. 4 Mean error calculation for the shape of the tumor (mean ± std)

	Area	Perimeter	MAL	MiAL
HGG	0.10±0.06	0.10±0.06	0.04±0.03	0.05±0.03
LGG	0.02±0.02	0.01±0.01	0.02±0.02	0.05±0.06

Also, mean values for the complete dataset are evaluated and tabulated in Table 4.4. From the Table 4.4 it is observed that the percentage error is very low for all the parameters. Though, a little higher error value is observed for the perimeter, this is because some rough edges are formed in extracted tumor in comparison to ground truth mask. An overall, percentage error for all the parameters is 4-10% for HGG images and 1-5% error obtained for LGG images respectively.

Large error implies high shape difference between extracted and ground truth mask. As, the evaluated results show small error values so, this signified that proposed method has conserved tumor shape.

4.4.3 GBKS GC technique validation with respect to tumor location

In this section the quantitative analysis of proposed technique is provided in terms performance score. Further, validation of extracted tumor region is provided by overlapping the extracted tumor mask on all sequences of MR images. In Figure 4.12 location of extracted tumor validated and its mask overlap is shown.

Figure 4.12 (a, b, c and d) depict all the sequences of the original MR image modality; Figure 4.12 (e) represent the extracted tumor mask by GBKS GC method and Figure 4.12 (f) is the mask of ground truth obtained; Figure 4.12 (g, h, i and j) represent the extracted tumor mask and the ground truth tumor mask overlapped on all the sequences of the MR images. This overlapping validated the shape and the location of the extracted tumor region. Further, it is also perceived that a single confined tumor is obtained and erroneous pixels remain absent. Similar results are obtained for LGG images and are presented in Figure 4.13.

(a) (b) (c) (d)

(e) (f)

(g) (h) (i) (j)
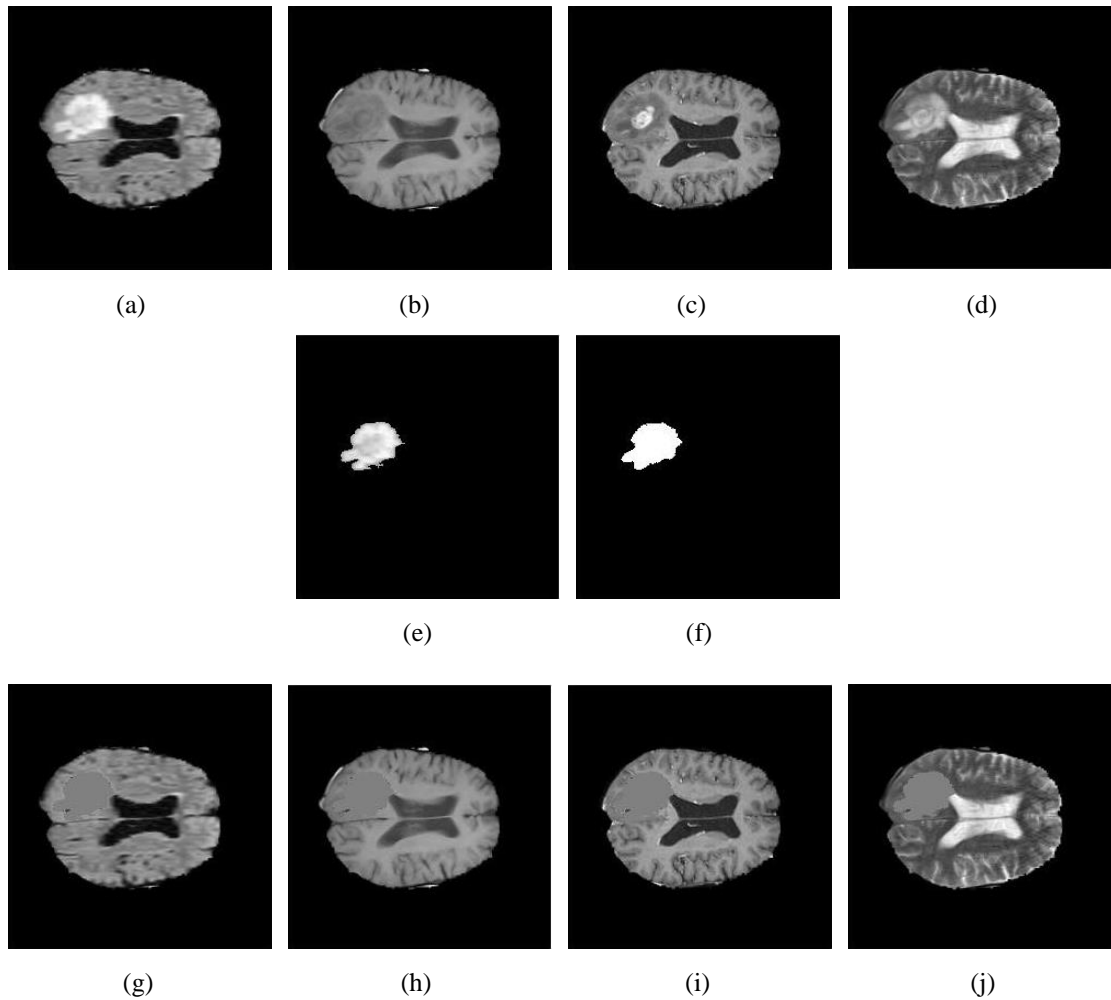
Figure 4. 12 (left to right: HGG MRI sequnces) a: Flair, b: T1, c: T1ce and d: T2; (e and f): Tumor extracted by GBKS GC and ground truth respectively; (g-j) Overlap of extracted and ground truth mask over all the available sequnce

The images depict complete overlapping of the tumor mask with small amount underlying of pixels that did not get segmented. Nevertheless, major area of the tumor region is well extracted from the original image. For clarity performance metric of 10 images of each grade are tabulated in Table 4.5. The average mean of performance metric for all images in dataset are given in Table 4.6. All the values are evaluated between extracted tumor and ground truth available.
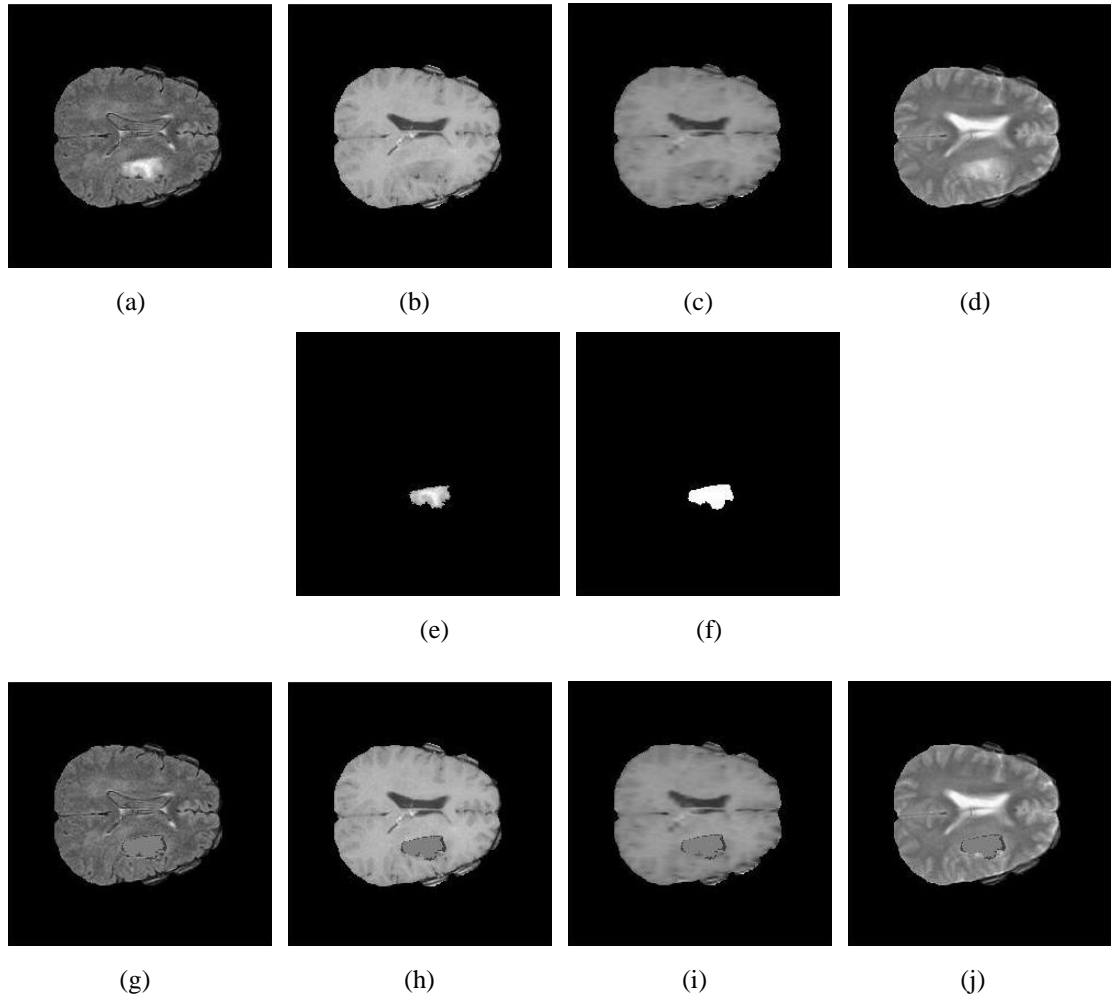
Figure 4. 13 (left to right: LGG MRI sequnces) (a) Flair, (b) T1, (c) T1ce and (d) T2; (e and f): Tumor extracted by GBKS GC and ground truth respectively; (g-j) Overlap of extracted and ground truth mask over all the available sequences

All the parameters are evaluated on scale of 0-1, values closer to 1 are perceived as good segmentation and the opposite is true for poor segmentation. The highest values of JI, DSC, PPV, Sens., and Spec. obtained by proposed GBKS GC method are 0.95, 0.91, 0.96, 0.99 and 0.99 respectively for HGG and 0.95, 0.96, 0.95, 0.99 and 0.99 respectively for LGG images. From these values it is perceived that good segmentation of tumor region is obtained.

Table 4. 5 Performance metric obtained by GBKS GC method for 10 HGG and LGG images

HGG					LGG				
JI	DSC	PPV	Sens.	Spec.	JI	DSC	PPV	Sens.	Spec.
0.91	0.83	0.83	0.99	0.99	0.88	0.94	0.92	0.98	0.91
0.93	0.86	0.92	0.99	0.93	0.89	0.79	0.93	0.99	0.85
0.95	0.91	0.98	0.99	0.91	0.82	0.89	0.94	0.99	0.87
0.89	0.80	0.86	0.99	0.92	0.88	0.94	0.94	0.99	0.99
0.94	0.88	0.93	0.95	0.94	0.95	0.92	0.95	0.99	0.95
0.91	0.83	0.85	0.94	0.97	0.95	0.91	0.95	0.99	0.95
0.91	0.83	0.83	0.89	0.99	0.84	0.91	0.91	0.98	0.95
0.84	0.72	0.73	0.91	0.97	0.89	0.94	0.95	0.95	0.98
0.95	0.91	0.99	0.92	0.91	0.87	0.93	0.87	0.96	0.99
0.90	0.82	0.96	0.91	0.85	0.93	0.96	0.95	0.98	0.97

The values depicted in Table 4.6 for JI, DSC, PPV, Sensitivity and Specificity is high, emphasizing better segmentation. The lower PPV value signifies the amount of over segmentation, which means the output contains extra pixel region that are not a part of tumor region. It is also observed from the Table 4.4 that a high sensitivity value is obtained for both the LGG and HGG images which correspond that all positives in the original image are correctly detected by the proposed algorithm. Same is true for specificity where all the negatives of the original pixels are also correctly detected.

Table 4. 6 Performance metrics obtained by GBKS GC method for 300 HGG and LGG images

	JI	DSC	PPV	Sens	Spec
HGG *(mean ± std)*	0.87 ± 0.06	0.87 ± 0.06	0.89 ± 0.07	0.99 ± 0.03	0.91 ± 0.05
LGG *mean ± std)*	0.89 ± 0.05	0.92 ± 0.04	0.93 ± 0.03	0.99 ± 0.03	0.95 ± 0.04

The evaluated results from Table 4.5 and Table 4.6 infer that the extracted tumor region from proposed technique complies with the ground truth.

Different tumor validation provided in this section imply highly effective extraction of tumor with respect to its shape, location and similarity. All the results are compared with available ground truth and images of extracted tumors are also shown.

4.5   COMPARISON WITH EXISTING TECHNIQUES

The results obtained by proposed algorithm are compared with the existing segmentation techniques employing GC on the same dataset available in literature and the results are shown in Table 4.7. Jiang *et al.* in [49] constructed a graph with the help of priori information that is obtained from the feature sets of the multimodal magnetic resonance of population and patient specific. Although the segmentation is done by using GC technique, but, the seeds are manually selected. Hence this method involves user interaction compelling it to be prone to human error. The proposed technique is also compared with the conventional GC method [120] and Random Walk (RW) technique [224].

Table 4. 7 Comparison of GBKS GC with the existing techniques (mean ± std)

	JI	DSC	Sens	Spec
Jiang *et al.* [49] with population	0.74 ± 0.14	0.84 ± 0.09	0.87 ± 0.07	0.83 ± 0.14
Jiang *et al.*[49] without population	0.61 ± 0.08	0.75 ± 0.06	0.92 ± 0.06	0.64 ± 0.07
Boykov *et al.*[120]	0.69 ± 0.12	0.53 ± 0.15	0.87 ± 0.09	0.59 ± 0.20
Grady *et al.*[224]	0.60 ± 0.18	0.73 ± 0.16	0.75 ± 0.26	0.75 ± 0.07
HGG (Proposed GBKS GC)	0.87 ± 0.06	0.87 ± 0.06	0.99 ± 0.03	0.91 ± 0.05
LGG (Proposed GBKS GC)	0.89 ± 0.05	0.92 ± 0.04	0.99 ± 0.03	0.95 ± 0.04

The GC technique is entirely pixel intensity dependent and there is no knowledge acquired regarding features for region or boundary. The RW technique is also a graph based technique wherein, decisions are made based on the probability distribution in the graph. Hence, both these techniques are entirely involved with human interactions. The RW has high computation complexity indifferent to the GC technique. Due to leakage or shrinkage problem both these techniques pose lower value of the presented parameter. Also, the number of initial seed points in these techniques is limited. The graphical representation of the comparative results is shown in Figure 4.14.

Figure 4.14 presents percentage improvement of proposed technique over existing state-of-art method that are depicted in Table 4.7. It is observed that a highest improvement of 64% and 54% is obtained for DSC and Spec. respectively over existing GC presented by Boykov *et al.* [120], and an improvement of 45% and 32% is obtained for JI and Sens. respectively on comparing with proposed technique of Grady *et al.* [224].
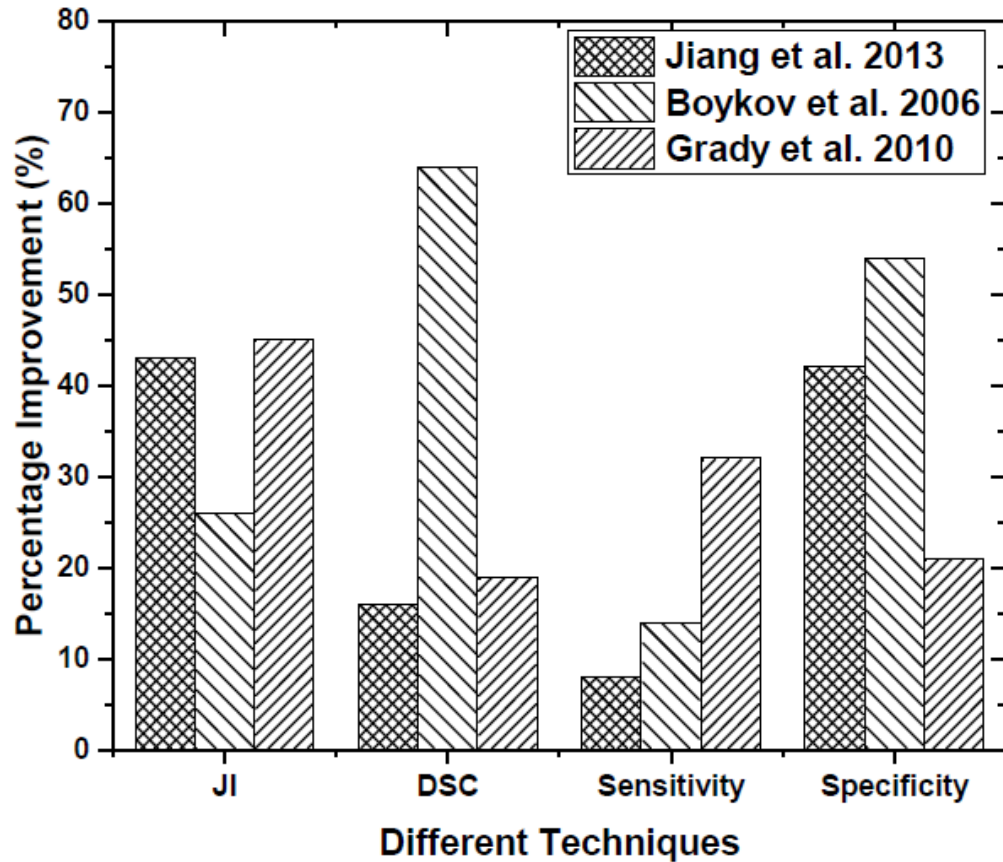
Figure 4. 14 Percentage improvement of the performance metrics for segmentation of glioma images.

On comparing the percentage improvement with Jiang *et al.* [49] a significant is improvement is observed for all the performance parameters.

4.6   CONCLUSION

The open research problem of "Shrinkage Bias" stated by Chen *et al.* [54] is the biggest limitation of GC technique. It causes fallacious segmentation causing hindrance in providing tumor characterization. Besides this automatic initialization of GC is also mandatory to develop an effective diagnosis system. The proposed GBKS GC technique is able to remove all limitations and majorly solves problem of 'Shrinkage Bias' in GC technique. The effectiveness and accuracy of proposed technique is provided by an elaborative quantitative analysis of extracted tumor by validating the shape, location of

tumor and evaluating the accuracy of selected kernels. Proposed algorithm is compared with state of art and existing techniques that infer outperformance of this technique.

Here, the effect of noise is not considered although in real time applications images are mostly corrupted with noise. In Chapter 5 we validate the robustness of proposed GBKS GC technique for its efficient working in real time applications. As our proposed technique is intensity dependent so, in case of intensity inhomogeneity its versatility is assessed. The type of noisy environment considered is the impact of bias fields that are caused at magnetic field >3T. This cause huge effect on intensity values and tumor extraction becomes difficult as it effects boundary and object pixels. It also causes difficulty in selection of kernels and calculation of gradients.

CHAPTER 5

ROBUST DESIGN FOR BIAS FIELD EFFECTED MR IMAGE FOR GLIOMA SEGMENTATION

CHAPTER 5

ROBUST DESIGN FOR BIAS FIELD EFFECTED MR IMAGE FOR GLIOMA SEGMENTATION

One of the challenge of MRI machine is bias field that causes Intensity Inhomogeneity (IIH) problem in the images. It causes low frequency variation of brightness throughout the image that affects the quantitative analysis of MR images. The bias field is caused due to the electric and magnetic interaction of the fields that corrupts the image directly when magnetic field is greater than 3T. Although at greater magnetic field good spatial resolution is created but at higher magnetic field the signal received from human body are also increased that cause different artifacts. These artifacts depend from patient to patient and cause high variation of in the intensity values of MRI. The IIH causes a string effect on the intensity values of the MR image.

5.1   ACQUISITION OF MRI IMAGES

The MR images are formed directly from the object and based on the nuclear magnetic resonance principle. On the contrary to the other imaging techniques like Positron Emission Tomography (PET) and Single Photon Emission Computed Tomography (SPECT), MRI doesn't employ any sort of injection of radioactive isotopes [232]. In addition, this technique provides images that are rich in quality and is very safe for human body as none of the rays of any radioactive isotopes pass the internal tissue. The appearance of pixels totally depends on the intrinsic parameters that provide examination of human anatomy in form of different sequences. The effect of these parameter can be manipulated by parameters called as operator selectable that changes the echo time, flip angle and repetition time [233]. Hence, imaging of a single anatomical structure provides different images depending on how the data or image is acquired.

Signal Generation and Detection: In MRI powerful magnets are used that align all the protons to the strong magnetic field produced from these magnets [234]. This magnetic field is directly proportional to the resonant frequency. The orthogonal perturbing electromagnetic field provides the response that is used to produce high resolution spectra image. In Figure 5.1 the modules used for MR system to acquire images are illustrated.

```
                    ┌─────────┐
                    │   MRI   │
                    └─────────┘
        ┌───────────────┼───────────────┐
        ▼               ▼               ▼
 ┌─────────────┐ ┌─────────────┐ ┌──────────────────┐
 │ Main Magnet │ │Gradient System│ │ Radio Frequency  │
 │             │ │              │ │     System       │
 └─────────────┘ └─────────────┘ └──────────────────┘
```
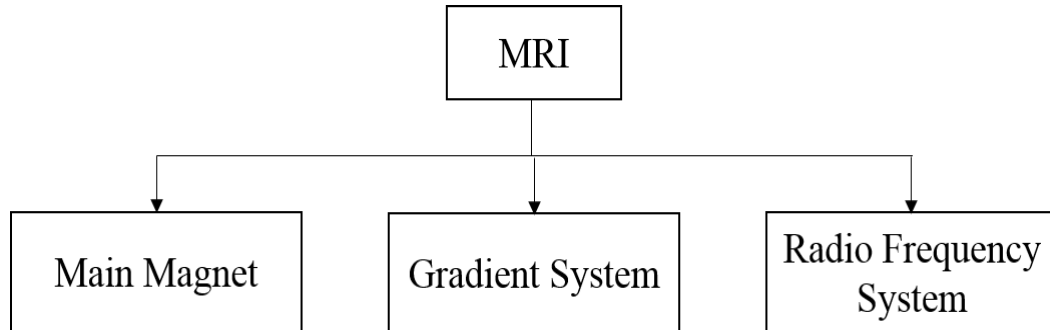
Figure 5.1 Main modules of MR system

The modules in MRI machine that are main magnet, gradient system and radio frequency system are depicted in Figure 5.1 explained as follows:

i. **Main Magnet:** The main magnet is the primary source of external magnetic field to the system and is denoted as $\vec{B_o}$. A uniform and strong magnetic field is produced that gets aligned with the spin of the protons [235]. The strength of the magnetic field is directly proportional to the signal to noise ratio. If field is high, it produces better signal to noise ration. Hence, a perfect intensity uniformity is produced by the magnet. On increasing the field like 3T, 7T or 14T this intensity uniformity is disturbed and it is difficult to ensure a reliable MR image.

ii. **Gradient system:** Three gradient coils forming a gradient system provides signal localization. This system develops a time varying magnetic field in a controlled spatial non-uniformity. Two critical specification of the system is maximum strength and rate of gradient. There is no significant noise introduced by this system.

Some other criteria are that the lower limit for gradient strength is at the point at which the gradient file is more than the main field and rise time is defined as gradient strength to reach its maximum value [236]. Shorter the rise time better is the gradient system, conventionally it is 1.0 ms. But, for fast imaging system the rise is much shorter.

iii. **Radio frequency system:** The signal acquisition is done by the radio frequency system that consists of transmitter coil and receiver coil. The transmitter coil generates rotating magnetic field that is converted into electrical signal by the receiver coil. For obtaining different acquisition characteristics various types of shapes and sizes of coil are employed [237]. These coils allow the system to capture the complete image or a particular target region. For capturing the complete region volume coils are required and for a specific region surface coils are required. These components provide high detection sensitivity, uniform rotating magnetic field with different characteristics.

5.2   MR IMAGES WITH BIAS EFFECT

The MR images have played a vital role in the vast application of the medical field for the diagnosis and detection [238]. Even with such a profound use of this technique it has some insufficiencies caused due to the intensity inhomogeneity, partial volume effect and noise interferences. These limitations cause huge problem in the accuracy of the segmented results. In most of the method of segmentation an assumption of uniform intensity distribution is made to present a noise free segmentation. The main cause of intensity inhomogeneity is bias fields of the magnetic field in MR machine. It occurs due to the eddy currents and poor uniformity of the radio frequency coil. These noises interfere severely that affect the accuracy of image segmentation. Hence, it is difficult to follow any conventional method of segmentation.

Bias field is a smooth low frequency signal that degrades the MR image quality due to presence of inhomogeneity of the pixel values [239]. This field causes blurring of the

image resulting in reduction in the high frequency components and provides undesirable smoothening of the edges and contours. It also causes variation in the intensity value of the pixels that disturbs the intensity distribution of same tissue region [240]. If these low frequency signal have lower variation, then it doesn't cause great impact but at the higher magnetic fields these signals can cause higher degradation of the performance of various algorithms like segmentation and grading.

Authors in [241] have shown the presence of intensity inhomogeneity caused due to the bias field in the MR image of brain. The effect of IIH is illustrated in Figure 5.2 (a) on the brain MR image. In Figure 5.2 (b) the bias field has been estimated that can be further used for generating the correct image. As discussed before the bias filed is described as the low frequency disturbance affecting the gray levels of the MR image. This low frequency modulation of the bias field is shown in Figure 5.2 (c) that depicts the field in a form of surface.
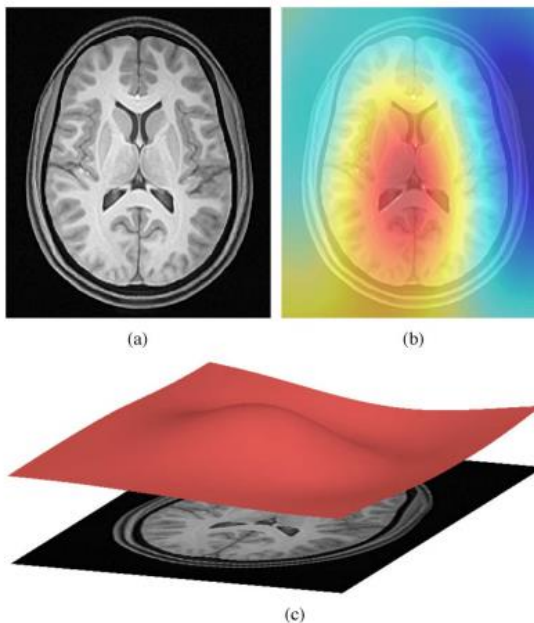
Figure 5.2 [241] (a) T1-weighted MR image exhibiting bias, (b) Estimation of the bias field which can then be used to correct the image, (c) Viewed as a surface, the low frequency modulation of the bias field.

The bias field are mainly caused due to the magnetic field and are entirely dependent on its strength. Images that are scanned at 0.5T have negligible bias effect and is completely ignored. But, on increasing the magnetic field strength like 1.5T and 3T the scanned MR images cause a significant effect on the intensity values of the MR images. Even the trained medical experts can visually analyze the images up to a certain limit of intensity inhomogeneity (i.e. 10%-30%) [242]. In this research we have worked with two types of the bias field that are in circular and longitudinal shapes. The bias field in circular shape is presented in Figure 5.3 of size 192×56.

Figure 5.3 Bias field of circular shape

The longitudinal bias fields as discussed by authors in [241] are depicted in the Figure 4 of the size 128×80×31. As observed from Figure 5.3 and 5.4 it is inferred that both bias fields illustrate a smooth variation in the intensity values. At such a high magnetic field strength these bias fields due to their multiplicative nature affect the performance of segmentation process that conventionally assume intensity homogeneity in all the tissue regions.
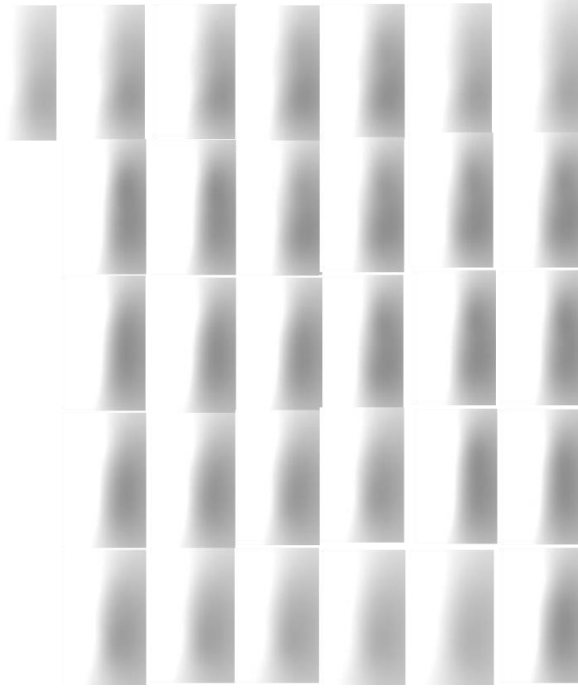
Figure 5.4 Longitudinal bias field of size 128×80×31presenting a smooth variation of the gray values

The typical mathematical model of bias field is expressed as a low frequency multiplicative model. For volumetric image $I(x, y, z)$; where x, y are the row and column values of value R and C respectively; z is the slice number with length D. The complete volumetric image is presented in a column vector as $\vec{\imath} = \{i_1, i_2, .., i_m\}$; where $m = R \times C \times D$; that presents each image element. The mathematical presentation of the image degradation caused by the bias field is expressed as:

$$i_l = i'_l b_l; \qquad l = 1,2, \dots . m \tag{5.1}$$

where i_l is the original image and i'_l is the degraded or corrupted image; b_l is the smoothly varying intensity values in the bias field. Once the bias field factor b_l defined in Equation 5.1 is completely estimated it is easily eliminated from the degraded image. This is done by transforming the multiplicative factor into additive bias filed by taking the logarithm as shown in Equation 5.2.

$$\log i_l = \log i'_l + \log b_l \tag{5.2}$$

Most of the existing bias correction method [243-245] used this simplified model for eliminating the bias fields. Though this elimination may sound easy but it is difficult due to certain limitations. It is difficult to measure the relationship between the true and calculated values of the intensities. This is because of difference between induced currents and spatial excitation field that are inhomogeneous. The spatial excitation field depends on subject's electromagnetic properties and its geometry.

5.2.1 Effect of bias field

To get a better understanding of the bias effect on the MR Images the histogram behavior is studied. The visual analysis of the bias fields is depicted in Figure 5.5 and Figure 5.6 that are used in our experiment. Two types of bias fields are used: a) circular, b) longitudinal. These bias field are superimposed on the original images for analyzing the bias field on the MR images

HGG   Bias Field   Bias Field HGG

LGG   Bias Field LGG
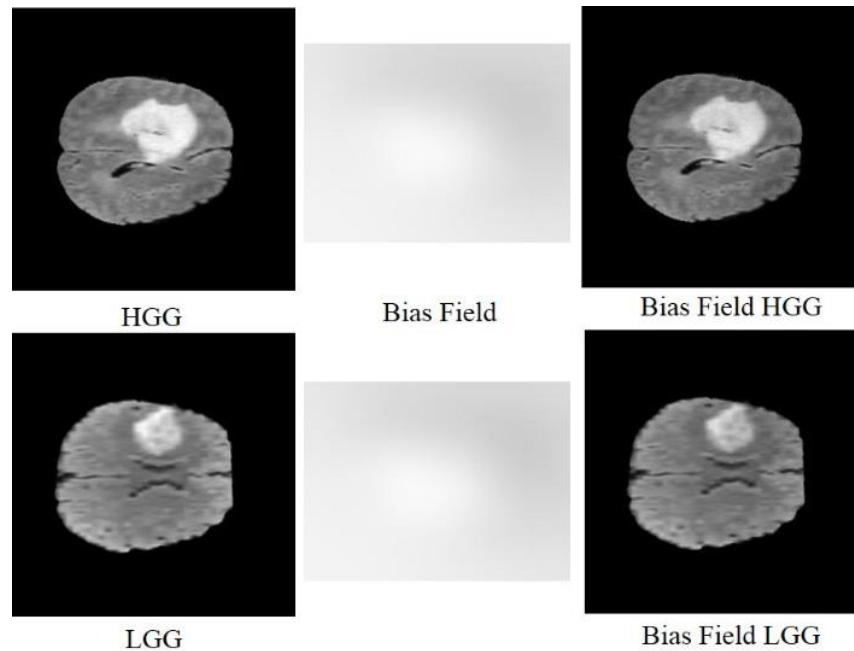
Figure 5. 5 Superimposition of circular bias field on the HGG and LGG MR Images respectively
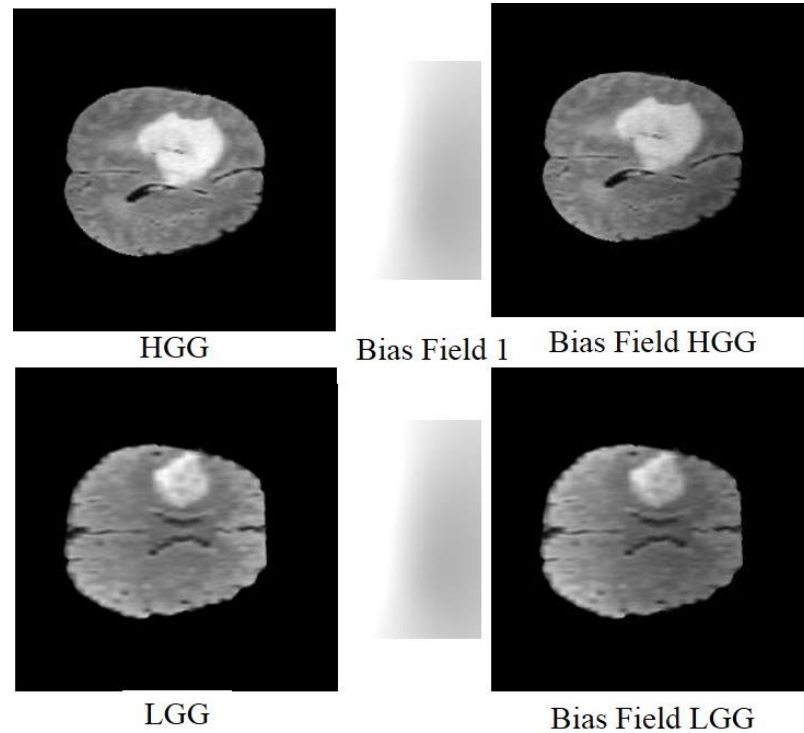
Figure 5.6 Superimposition of longitudinal bias field on the HGG and LGG MR Images respectively

From the images depicted in Figure 5.5 and 5.6 we can visually analyze that a smooth variation of the caused by both the bias fields across MR Images. In the circular bias field, the darker region is present in outer circular formation and in the central area lighter intensity are present. From the outer to the central region there is a smooth variation of the gray values. On superimposing this bias field, the images generated also show the similar change in comparison to the original image. In the longitudinal images we can observe smooth variation from darker region to lighter from right side of the image to the left side. Similar variation is observed in the images generated by this field on MR images on comparing with the original image.

To provide a better insight to this variation we have studied the histogram of the original and IIH images. The original image depicted in Figure 5.7 and Figure 5.8 is a high grade glioma MR image that is been superimposed with the longitudinal image and bias field degraded MR image is generated. The histogram for original and its

degraded image (i.e. image with longitudinal and circular bias effect) are shown in Figure 5.9 and Figure 5.10.
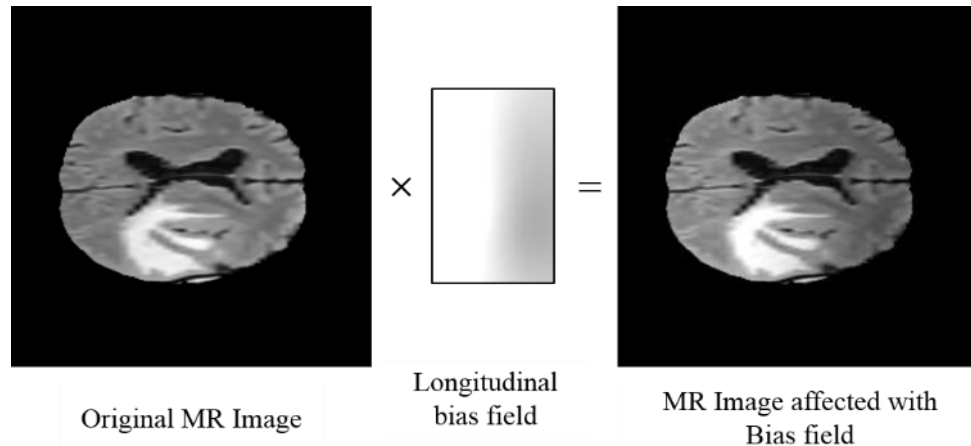
Figure 5.7 Effect of longitudinal bias field on the MR Image
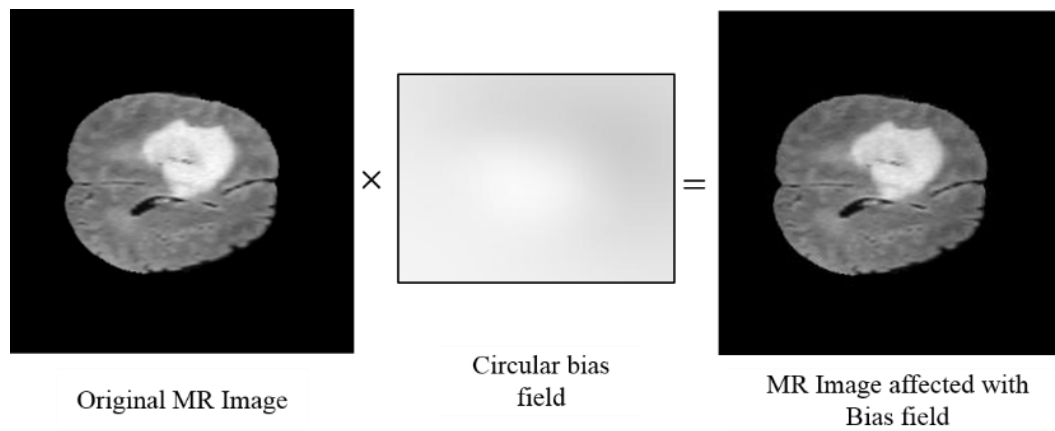
Figure 5.8 Effect of circular bias field on the MR Image

In the histograms of both images we analyze the effect of bias field gray image. The x-axis in the histogram represent the gray value and y-axis represent the frequency or the number of pixels. The gray values of the original image have been normalized so, the pixel values are in the scale of 0-1 range.

(a)

(b)
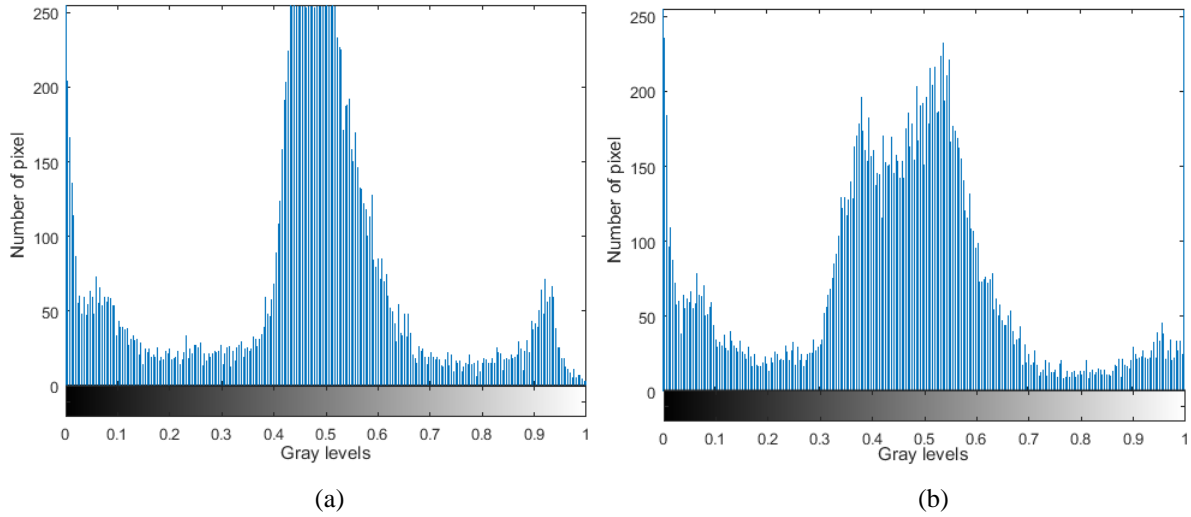
Figure 5.9 (a) Histogram of original MR Image, (b) Histogram of MR Image with longitudinal bias effect

(a)

(b)
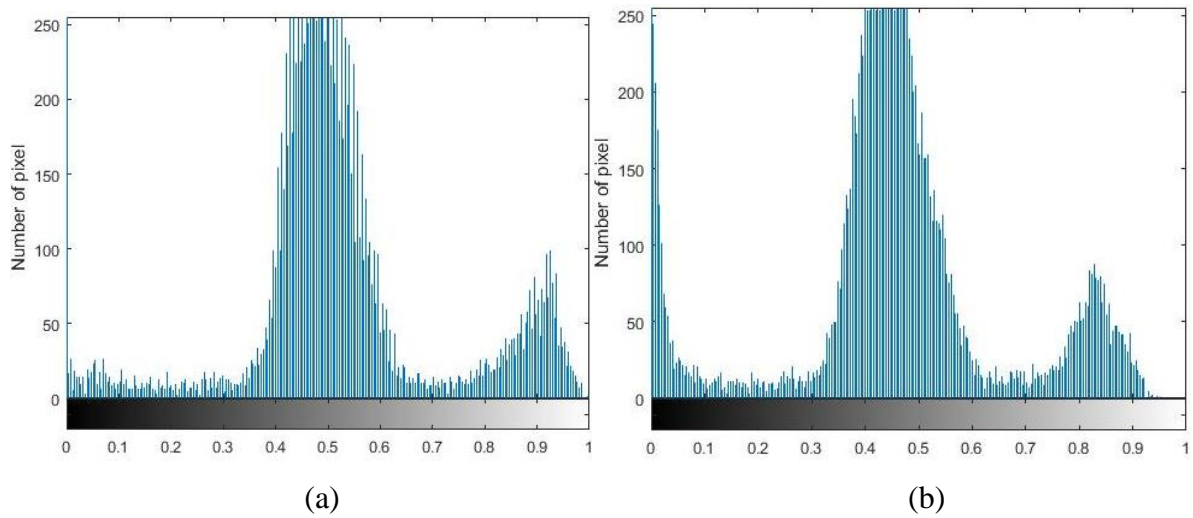
Figure 5.10 (a) Histogram of original MR Image, (b) Histogram of MR Image with circular bias effect

By observing both the histogram distribution the following analyses are made:

i.   The bias field spreads all the pixels towards the darker region. This is caused due to the multiplying bias factor that is in the range of 0-1. All the pixel values change their original values and become smaller.

ii. Due to the reduction in the intensity values the variance gets increased hence, the spread of the histogram is observed in Figure 5.9 (b) and Figure 5.10 (b). At higher gray value the spread is higher in comparison to the lower values. As variance is defined by the minimum bias times the constant gray value.

iii. Both the histograms have equal number of pixels but there is reduction in the peaks. This is due to the increase in variance that cause decrement of the peaks.

iv. A gradual or smooth variation can be observed as we go from the darker (left) side of the intensity scale towards the lighter (right) side of the intensity scale.

Finally, it is observed that smooth variation of this intensity distribution makes the composition of bias field intricate and difficult to remove. Consequently, it causes application of certain image processing methods as segmentation difficult.

5.3 PROPOSED METHODOLOGY

As previously studied the effect of the bias field cause severe degradation in the accuracy of segmentation results. Most of the segmentation method including graph cut method depend on the pixel intensity distribution of the MR Image. Any disturbance in the intensity uniformity directly affect the process of segmentation. In our proposed methodology we have applied the proposed GBKS GC method to the images affected by bias field. The experiment is conducted on some dataset with HGG and LGG MR Images as addressed in Chapter 1. The complete methodology is depicted in Figure 5.11 that also shows image result at each step of proposed method. All the steps involved in proposed methodology are explained in detail.
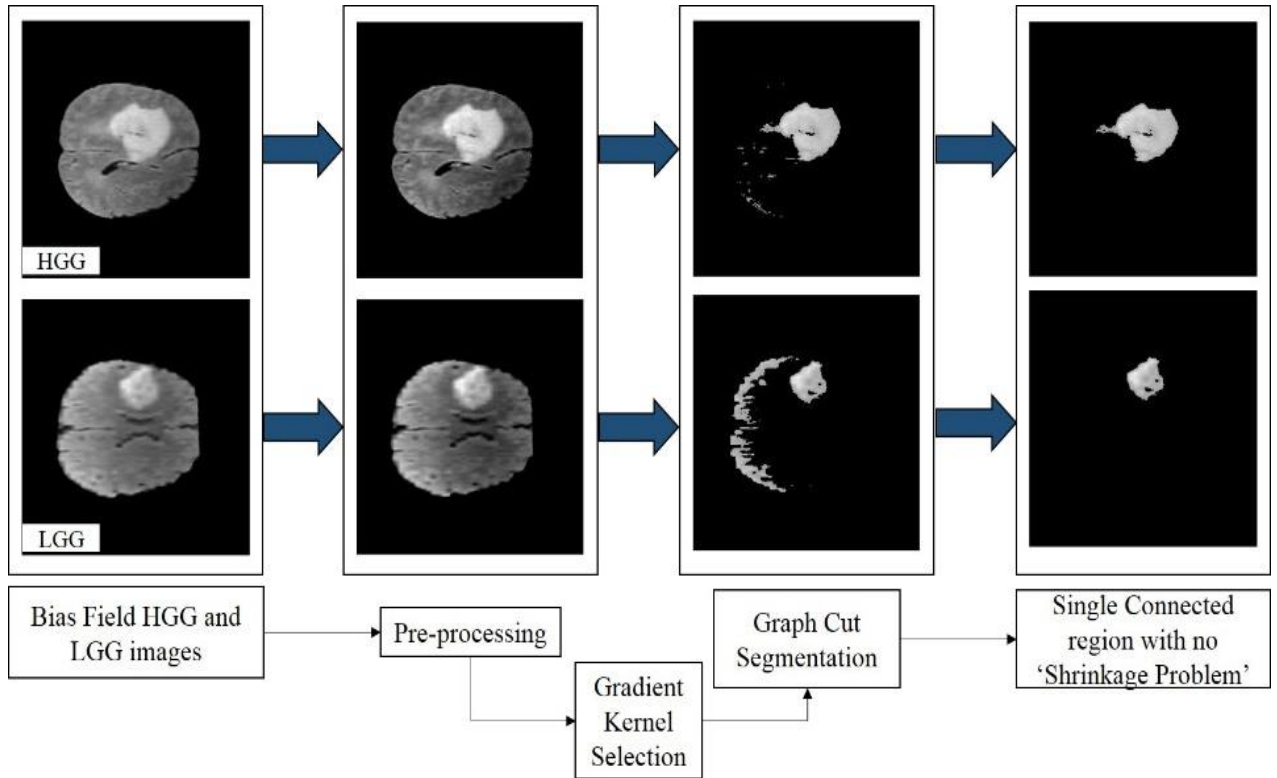
Figure 5.11 Segmentation of MRI employing GBKS GC method applied on the bias field images

5.3.1   Input bias field MR images

The input MR images include HGG and LGG MR bias field images that are of size 240×240. In the Figure 5.12 we have used longitudinal slice for creating the bias field image. As the longitudinal slice are of size 128×80 so they are resized to 240×240 and superimposed with all input Flair MR Images as shown in Figure 5.12.
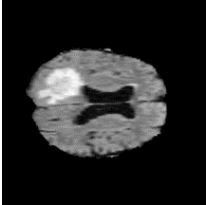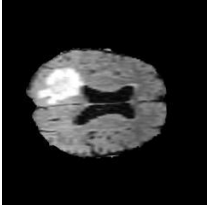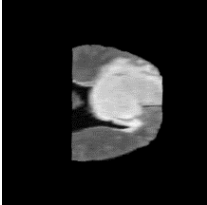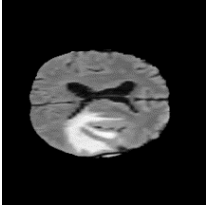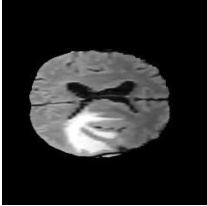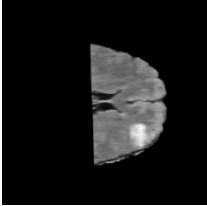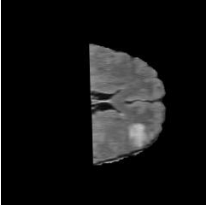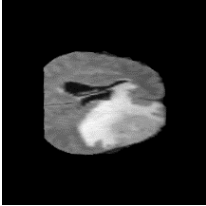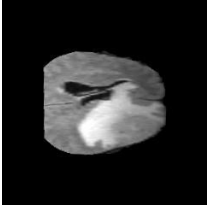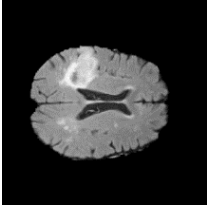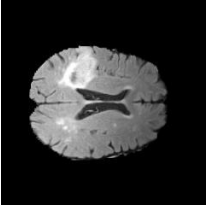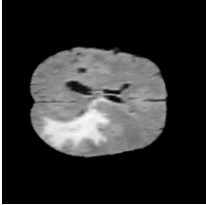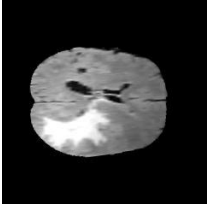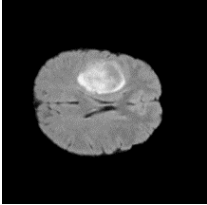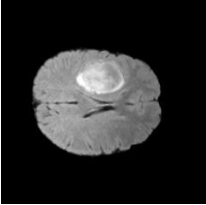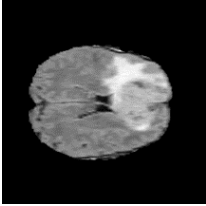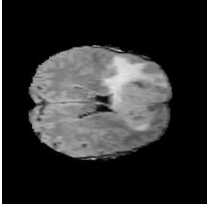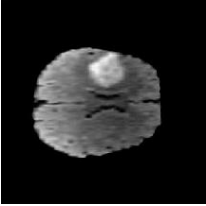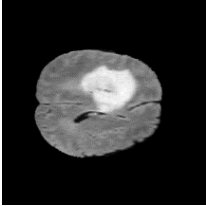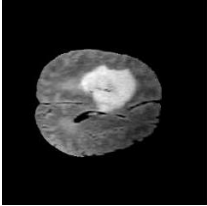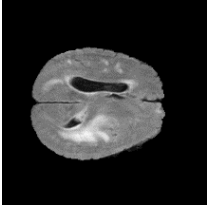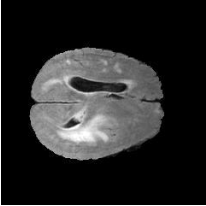
Original HGG MRI	Bias field HGG image	Original LGG MRI	Bias field LGG image

Figure 5.12 . Input bias field HGG and LGG images with longitudinal bias effect
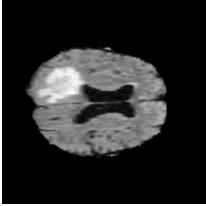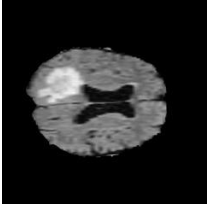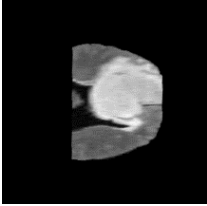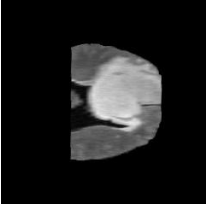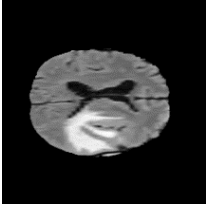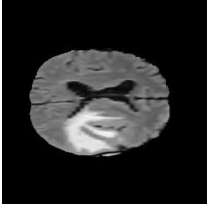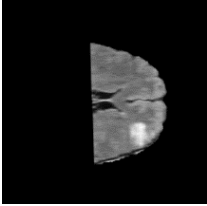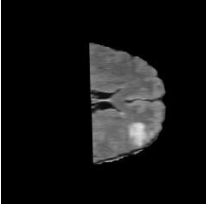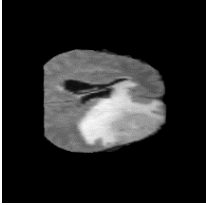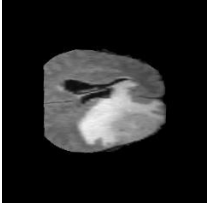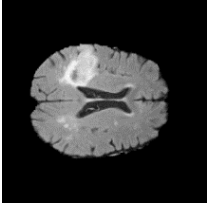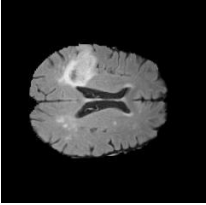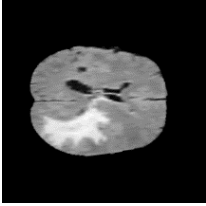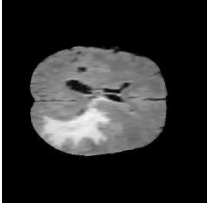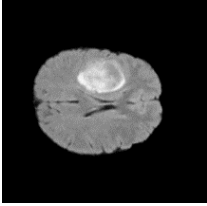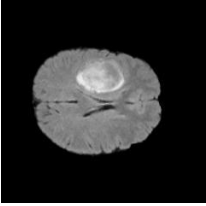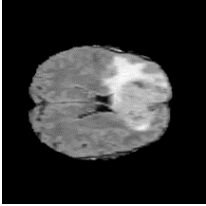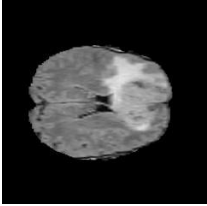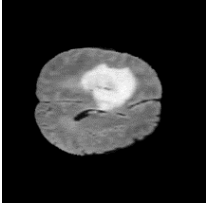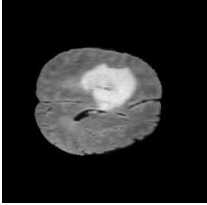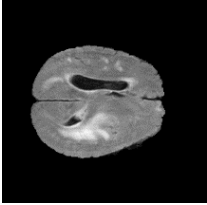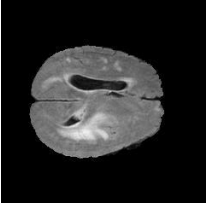
Original HGG MRI	Bias field HGG image	Original LGG MRI	Bias field LGG image

Figure 5.13 Input bias field HGG and LGG images with circular bias field

The complete input image set with the longitudinal and circular bias field effect is created for HGG and LGG images are shown in Figure 5.12 and Figure 5.13.

5.3.2 Pre-processing

The pre-processing is done to reduce the memory space used by the input images. The bias field images have pixel intensity in the ranges of 0-65025. This size of the images is large and takes a large amount of the memory space. These images are intensity normalized to the pixel intensity with the range of 0-255.

5.3.3 Seed selection

The images obtained after intensity normalization are used for seed selection. This step is achieved by proposed GBKS technique that is explained in detail in Algorithm 5.1. The selection of the kernels is totally intensity dependent and the abrupt changes in these values play an essential role for the selection. The potential kernels are selected using this technique and given to the graph cut segmentation method.

Algorithm 5.1.

Input: MR Flair Image

Output: Kernel points, Kernel Co-ordinates

Begin

Step 1: Read an image: I of size $m \times n$.

Step 2: Divide the MR image in two horizontal halves: $I : \{I_{11}, I_{12}\}$.

Step 3: Selection of the kernels: $\{o_1, o_2, o_3, \dots\}, \{b_1, b_2, b_3, \dots\}$.

3.1 Initialization of the intensity mean:

Set number of kernel k.

Vectorize the image:

$\hat{I}_{11} : \left[p_{i_1}, p_{i_2}, p_{i_3}, \dots\right]_{L \times 1}$

---

where, $L = m * \frac{n}{2}$

Extract all the non-zero pixel values of $\hat{I}_{11}$ in a new vector $\hat{H}$.

From the vector $\hat{H}$ obtain the range of pixel intensity lying between $p_{LI_{11}}(Low)$ and $p_{HI_{11}}(High)$.

Calculate initial weighted arithmetic mean:

$$\mu_{I_{11}} = (1:K) * \frac{w}{K}$$

where, $w = p_{HI_{11}}$ is the fixed weight assigned.

3.2 Obtain the locations $A_l(x, y)$ in $\hat{I}_{11}$ containing minimum distance a with $\mu_{I_{11}}$.

$$a = \left(\left| \hat{H}_{11l} - \mu_{I_{11}}(k) \right| \right)$$

Calculate the current means K as expressed in Eq. (2).

Adaptive mean calculation:

$$\mu_{I_{11K}} = \mu_{I_{11K(current)}} = \mu_{I_{11K(current)}} + \mu_{I_{11}}$$

Do the same for $\{I, I_{12}\}$ and obtain μ_{I_K} and $\mu_{I_{12K}}$ for I and I_{12} respectively:

3.3 Calculate change in the gradient from the mean of pixel intensity values as given in Eq. (3) and Eq. (4):

Calculate the amount of negative slopes as expressed in Eq. (5) and Eq. (6).

If $NS > NS^{-1}$

Divide the image $I_{11}:\{I_{11/4}, I_{11/4}^{-1}\}$

Else

Divide the image $I_{12}:\{I_{12/4}, I_{12/4}^{-1}\}$

End

Split the image further r in vertical halves.

Go to step 3.1 and repeat up to 3.3 till 2 level division of the complete image.

Step 4: Threshold the quadrant part of the image into binary form: $I_{1/4}$.

Step 5: Extract all the original pixel values which are the potential kernels from the thresholded image: $O = \{o_1, o_2, o_3, \dots\}$.

Step 6: Find and store the location of the selected kernel values: $[X, Y]$.

where, $X = \{X_{o_1}, X_{o_2}, X_{o_3}, \dots\}; Y = \{Y_{o_1}, Y_{o_2}, Y_{o_3}, \dots\}$ are kernel location.

End

5.3.4 Graph cut segmentation

The potential kernels are utilized by the graph cut algorithm for the following purposes: initialization of the algorithm, evaluation of the object and background kernel points, the kernel site location for removing the shrinkage problem. The kernel points are given to graph cut algorithm and segmentation is performed as described in Chapter 3. The kernel site location obtained from Algorithm 5.1 aids in the removal of erroneous region. The algorithm developed for removing the shrinkage problem is given in Algorithm 5.2. Hence an accurate tumor is extracted for both the HGG and LGG images.

Algorithm 5.2. Single confined object region

Input: Kernel co-ordinates.

Output: Single confined object region.

Begin

Step 1: By comparing the weights the labelling is performed to partition one complete MR brain image into a segmented image.

$$r_k = \begin{cases} 0 & Object \\ 1 & Background \end{cases}$$

Step 2: Obtain the location or the co-ordinates from Algorithm 5.1.

$$X = \{X_{o_1}, X_{o_2}, X_{o_3}, \dots\}; Y = \{Y_{o_1}, Y_{o_2}, Y_{o_3}, \dots\}$$

Step 3: For the stored locations $[X, Y]$ find the neighbouring pairs $\left(n_{o_x}, n_{o_y}\right)$

Step 4: Calculate similarity.

$$s\left(n_{o_x}, n_{o_y}\right)$$

$$S = S \cup s\left(n_{o_x}, n_{o_y}\right);$$

Step 4: Calculate neighboring pixels with similar property.

$$N = \left\{\left(n_{o_x}, n_{o_y}\right) : s\left(n_{o_x}, n_{o_y}\right) = \max(S)\right\};$$

Step 4: Obtain the single confined object region.

$$C_R = \left\{n_{o_x} \cup n_{o_y}\right\};$$

End

5.4 RESULTS

In this section the validation of obtained result is shown by providing: images of segmented tumor from bias field MRI, quantitative analysis of extracted tumor and validation by extracting tumor from real patient images.

5.4.1 Validation with bias field MRI

The segmentation result of the Bias field HGG and LGG MR Images after applying proposed GBKS GC depicted in Figure 5.14 and Figure 5.15. In Figure 5.14 the results are shown for MR Images with longitudinal bias field and in Figure 5.15 results are depicted for MR Images with circular bias field. Here, we have shown results for seven MR images of both grades and type of bias field. The, segmented results are shown in last column of Figure 5.14 and Figure 5.15 respectively as per Algorithm 5.1 and Algorithm 5.2. These results confirm the accurate extraction of the tumor and also prove that proposed GBKS GC is an effective and robust algorithm. It is observed that even with intensity inhomogeneity the tumor is perfectly extracted and fallacious segmentation is also not present.
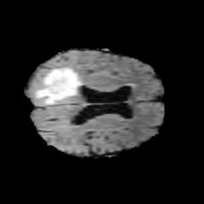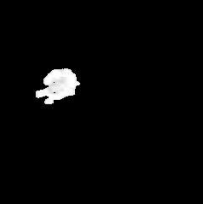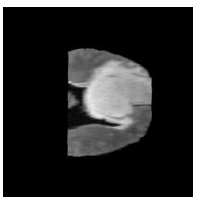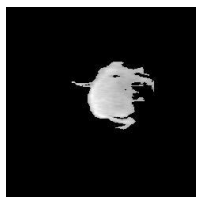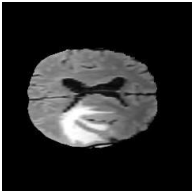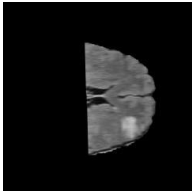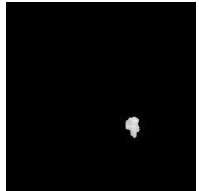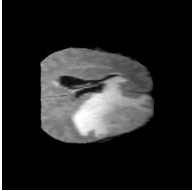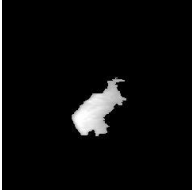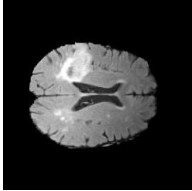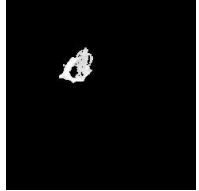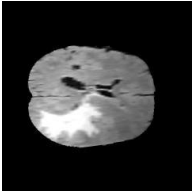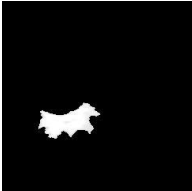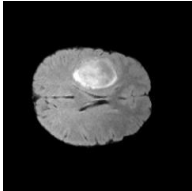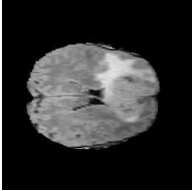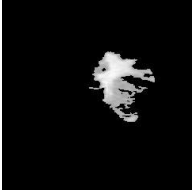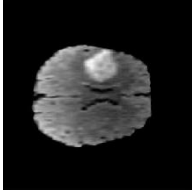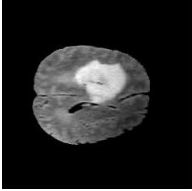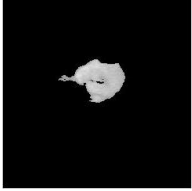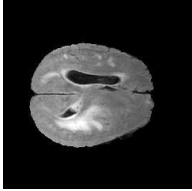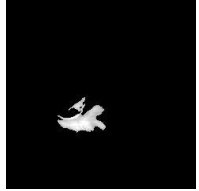
Bias field HGG MRI	Segmented tumor	Bias field LGG MRI	Segmented tumor

Figure 5.14 GBKS GC method applied on longitudinal bias field HGG and LGG MRI
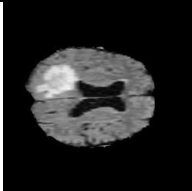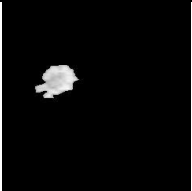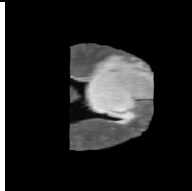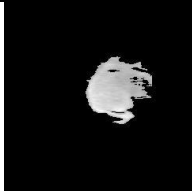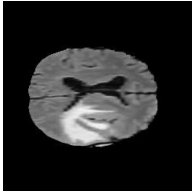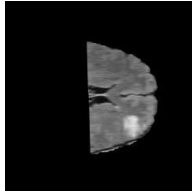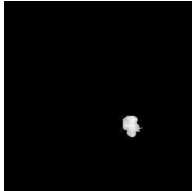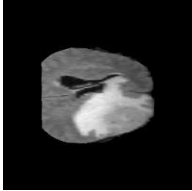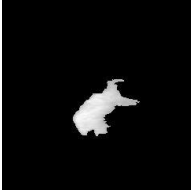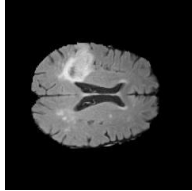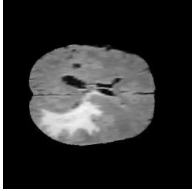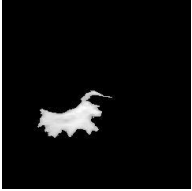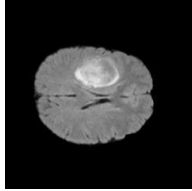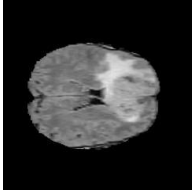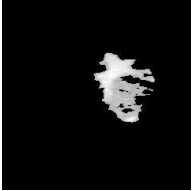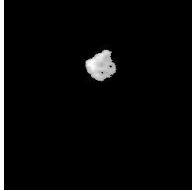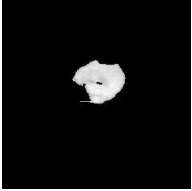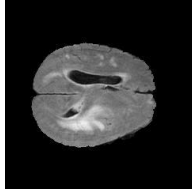
Bias field HGG image	Segmented tumor	Bias field LGG image	Segmented tumor

Figure 5.15 GBKS GC method applied on circular bias field HGG and LGG MRI

5.4.2 Quantitative analysis of tumor segmentation

For analyzing the effect of bias field on these images MSE and CC values are evaluated that are tabulated in Table 5.1 for 10 images of each grade. The average values for these parameter are tabulated in Table 5.2 for complete dataset of MRI. The MSE is evaluated between the extracted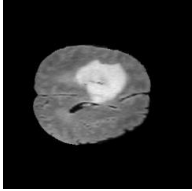 tumor region obtained from original MRI and bias field MRI with respect to their respective ground truth. Similarly, CC is also evaluated for with and without bias field. For a good segmentation of tumor region MSE value should be nearer to 1 and CC value should be nearer to 1.

Table 5.1 Results for 10 HGG and LGG images respectively depicting the effect of bias field

MSE (HGG)		CC (HGG)		MSE (LGG)		CC (LGG)	
Without bias field	With bias field	Without bias field	With bias field	Without bias field	With bias field	Without bias field	With bias field
0.004	0.013	0.903	0.938	0.011	0.011	0.935	0.934
0.007	0.007	0.923	0.924	0.001	0.002	0.889	0.909
0.002	0.009	0.950	0.869	0.001	0.004	0.904	0.936
0.001	0.030	0.890	0.784	0.005	0.008	0.899	0.869
0.005	0.008	0.936	0.910	0.001	0.008	0.958	0.848
0.011	0.019	0.904	0.857	0.002	0.005	0.949	0.720
0.008	0.015	0.905	0.867	0.002	0.008	0.849	0.937
0.007	0.011	0.844	0.871	0.009	0.009	0.903	0.915
0.005	0.016	0.950	0.871	0.002	0.002	0.888	0.841
0.005	0.009	0.930	0.842	0.002	0.021	0.959	0.701

On observing Table 5.2 it is inferred that even with the IIH caused due to bias field of MRI machine the average MSE values are closer to 0 and are not very significantly larger than values attained for Images without bias field. Also, average CC values obtained are also closer to 1 and are not very low in comparison to the CC value obtained for images without bias field images.

All the results infer a favorable output as the tumor is accurately extracted. These results depict an effective and robust framework of proposed GBKS GC technique.

Table 5. 2 Comparison of average MSE and CC with and without bias field

	MSE		CC	
	Without bias field	**With bias field**	**Without bias field**	**With bias field**
HGG	0.008±0.004	0.013±0.001	0.899±0.031	0.877±0.04
LGG	0.006±0.005	0.006±0.005	0.919±0.044	0.861±0.079

5.4.3   Validation with MR Images (IGMC SHIMLA)

To provide a better validation the proposed algorithm is also applied on the real patient images. As detailed previously in Chapter 1 these real patient images are obtained from Government hospital, IGMC, Shimla. These results are shown in Figure 5.16 with the stepwise performance of the proposed technique.

The effect of the bias field is observed as a gradual change in the intensity is seen on comparing with the original MR image. In addition, tumor region is accurately extracted even with the effect of bias field. There is no erroneous region observed and a single connected tumor region is obtained. The extracted tumor is validated with the tumor region marked by expert radiologist as shown with a red arrow in Figure 5.16.

Because the real patient images are corrupted with IIH so our proposed methodology is able to extract the tumor effectively even from bias field MR images.
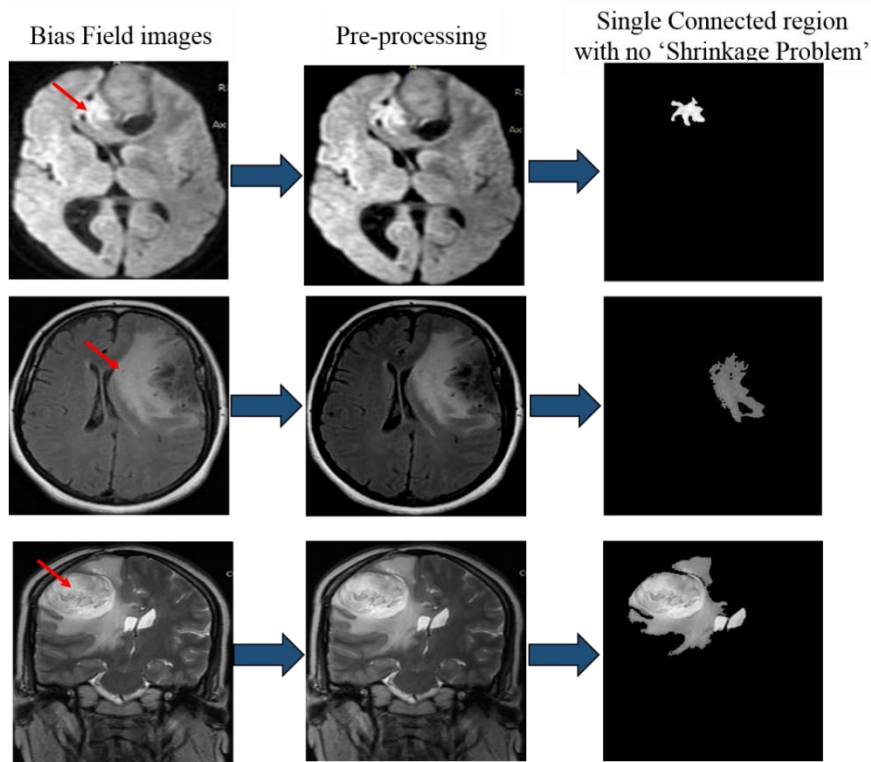

Figure 5.16 GBKS GC method applied on real patient images with bias field

5.5   CONCLUSION

The image characteristic encompasses features that are required for providing diagnosis. Any change in these characteristics can alter diagnosis and intensity inhomogeneity is the main cause of such degradation. This degradation caused by bias field are a major cause of disturbance in MR Images. Hence, extraction of tumor region becomes difficult from such images as this process completely depends on pixel intensity. In Chapter 4 proposed GBKS GC algorithm is applied on the MR Images without any noise. In this Chapter we are able to validate the robust nature of the algorithm as it is able to extract the tumor region from bias field images and real time images also. The obtained results depict that proposed GBKS GC technique is a robust and effective algorithm for extracting the target regions. Although proposed GBKS GC is based on abrupt changes

in intensity values but it is clearly observed that working of this algorithm has not been hindered. This is because it majorly identifies the gradients of complete intensity scale present between symmetrical half of MR Image. Even the coordinates of extracted kernel point have provided a strength and intactness in extracting the tumor region.

MRI scans consists of various sequences that define different regions of the brain by varying the parameters of MR machine. To identify the sequences that is able to provide full characterization of tumor type is difficult due to the complex brain structure. Hence, detection of the best sequence is covered in Chapter 6 that is able to grade glioma with highest accuracy.

CHAPTER 6

DESIGN OF MR SEQUENCE DETECTOR FOR EFFECTIVE GLIOMA GRADING

CHAPTER 6

DESIGN OF MR SEQUENCE DETECTOR FOR EFFECTIVE GLIOMA GRADING

The accurate extraction of glioma from different MR images is obtained as given in the previous chapters. To provide complete characterization of glioma and degree of malignancy in these extracted tumor regions, glioma grading is required. This histology grading is done according to WHO [246] for retrieving critical information related to prognosis and treatment planning. MRI scans have different sequences that represent different characteristic information of HGG and LGG [247] tumors. The selection of sequence is difficult as it requires high level knowledge for identifying the degree of malignancy present in one of MR sequences. On basis of this information, sequence is chosen and glioma grading is performed. In this chapter, a system model is developed that is able to detect the optimal sequence for glioma grading. In the proposed model, feature selection and extraction is performed using t-test. The most effective imaging attributes are used for classification of each sequence using machine learning.

6.1   MRI SEQUENCES

In clinical tumor imaging MRI is an important tool for diagnosis, characterization and continuous monitoring of the tumors. All the sequence of MR images represent different hyper intense regions that provide diagnosis of tumor. The T2 sequence that includes spin echo and fluid-attenuated inversion-recovery (FLAIR) reflect prolongation of transverse relaxation times related to increased tissue water content and ultrastructure [248]. The contrast enhancement is mainly administered for intravenous gadolinium that is reflected in the image by accumulation of paramagnetic compound in interstitium. This occurs due to the increased blood brain barrier permeability that is related to the necrosis and neovascularization [249]. Mostly inspection is done by expert radiologist visually and the evaluation is done on linear measurements of enhancing tumor components.

6.2   PROPOSED METHODOLOGY

The procedural steps of proposed Computer-aided design (CAD) system for the binary classification of HGG and LGG tumors from MR brain image is illustrated in Figure 6.1. The steps involved in this methodology are: pre-processing, segmentation, overlapping, feature extraction, feature selection and classification. In the first step pre-processing is done to reduce memory space of image by scaling gray-level pixels in the range 0-255. Then, segmentation is done by utilizing the novel approach GBKS GC proposed by Dogra *et al.* [250]. In this technique GC segmentation method is enhanced by automatically selecting the kernel values and effectively partitioning the tumor region from MR brain image. This method also avoids the limitation of shrinkage problem in GC. From extracted tumor region, a binary image is formed as the tumor mask. In order to obtain the tumor region from all sequences, this tumor mask is overlapped with each of the original tumor sequence.
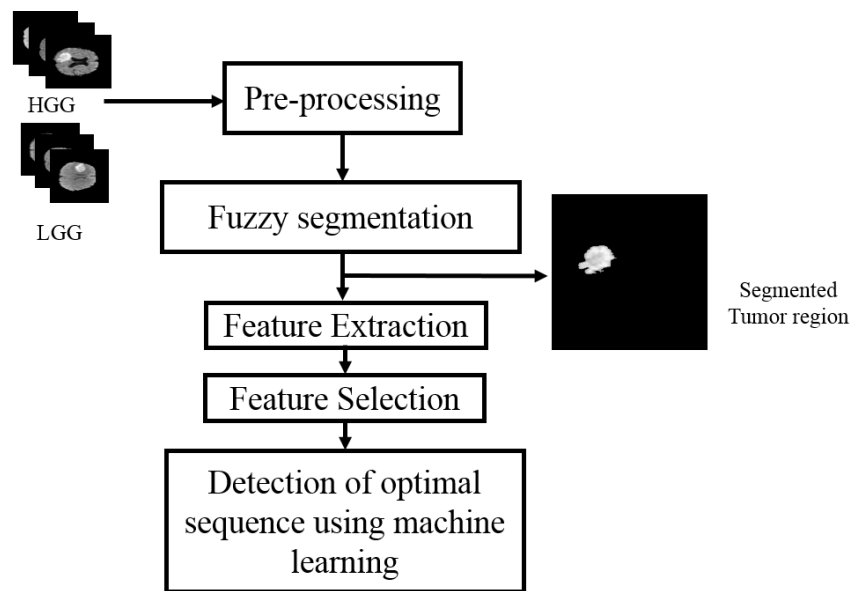

Figure 6. 1 Proposed methodology for classification of the HGG and LGG tumor

The most appropriate and prominent features are selected by using IBM Statistical Package for Social Sciences Statistics (SPSS) [251]. These features help in classification

of glioma regions. The classification is performed by applying two machine learning techniques: SVM and kNN [252].

The classification is performed on extracted features set obtained from all sequences of MR Images. Finally, input feature set is classified into HGG and LGG tumor classes.

6.2.1 Segmentation

In GC segmentation approach, image is interpreted as graph where pixels are nodes or vertices of the graph. To identify pixel intensity lying in the tumor region regional penalty of each pixel is calculated. Based on these penalties weights are assigned and correct labels are assigned to each pixel according to their property. The MAP-MRF framework [253] is formulated for the label assignment. In GC segmentation, cut refers to the partitioning of vertices into two groups representing the regional characteristics. These partitions are referred as object region or ROI and remaining portion is labelled as background region. The best cut is obtained by minimizing the energy function given in Equation 6.1.

$$E(L) = \lambda \sum_{p \in P} R_p(l_p) + \sum_{\{p,q\} \in N} B_{pq}(l_p, l_q) \tag{6.1}$$

L_p is the labels of pixels p in image for which penalty is calculated by regional term $R_p(L_p)$. Pixels p, q belongs to the neighboring pixels N, λ is a positive constant term and provide a relative contribution. Regional term in the energy equation reaches to a minimum value if the labelling is correctly done. The second term is boundary term which tends to give minimum value when two neighboring pixels p, q are different. Large value of the boundary term signifies similarity of the neighboring pixels. Seed points calculated by the proposed algorithm are used for initialization. GBKS GC technique selects these seed points and performs the segmentation of tumor. This technique removes limitation of shrinkage bias in GC with automatic selection of seed points, providing an effective tumor extraction is obtained. Hence, the segmentation in this research work is performed using the same technique and results obtained for

the MR Images are given in Figure 6.2 and Figure 6.3 for the HGG and LGG MR brain images.
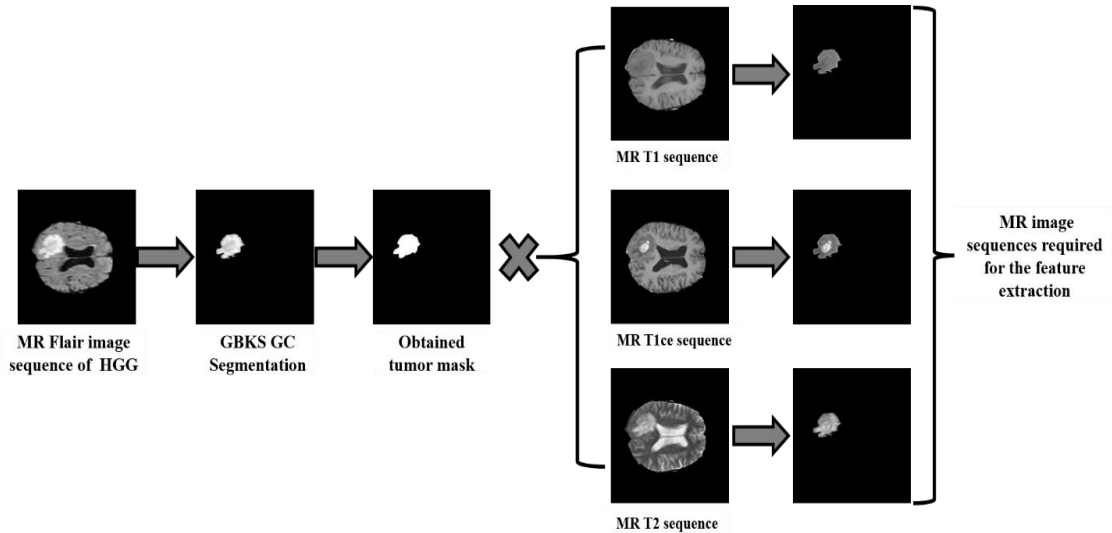

Figure 6. 2 Segmentation of the tumor region from flair sequence of HGG dataset. The tumor mask is obtained from this sequence and overlapped with the original images of T1, T1ce and T2 sequences of the MR images
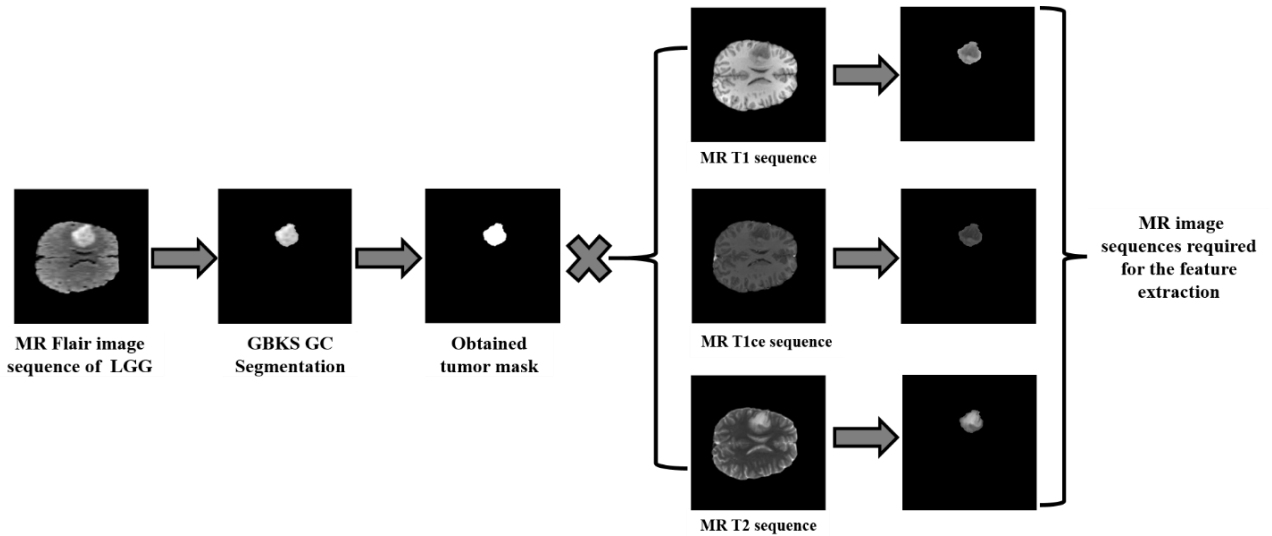

Figure 6. 3 Segmentation of the tumor region from flair sequence of LGG dataset. the tumor mask is obtained from this sequence and overlapped with original images of T1, T1ce and T2 sequences of MR Images.

Extraction of the tumor region from all sequences present in dataset is illustrated in Figure 6.3. Dogra *et al.* [250] in their proposed algorithm used Flair sequence of the

MR image for performing segmentation, due to its property of maintaining the high contrast difference among normal and abnormal region of brain. The segmented tumor region is validated with the ground truth provided in dataset. Once the tumor region is segmented, its respective tumor mask is generated in binary form representing tumor region as white colored portion. This obtained tumor mask is overlapped with all the original sequences of the MR brain images that are: T1, T1ce and T2. After performing this overlap, the tumor regions of remaining sequences are obtained. All these extracted regions are subjected to feature extracted for obtaining the image texture properties.

6.2.2   Imaging Feature Extraction

Various high level statistics from the tumor region such as color, contrast, shape and texture are an essential requirement for the classification [254]. Among these features the texture analysis is the most important feature that gives a human visual perception to the machine learning system to effectively improve the ACC. This task becomes problematic due to the complex and diverse tissue structure of the brain. A total of 18 first order and second order statistical imaging features are computed. The minimum intensity and maximum intensity provides the measure of variation and diversity present in the pixel intensity of image. The features such as mean intensity, eccentricity and centroid of pixel intensity values provide measure of central tendency. Kurtosis, skewness and Inverse Difference Moment (IDM) are histogram shape based features of the image. Skewness reveals information about the symmetry of grey level values around the mean, whereas Kurtosis gives information about peaks of the pixel intensity distribution in histogram. IDM is a measure of the local homogeneity of an image. It may have a single or a range of values so as to determine whether the image is textured or non-textured.

First-order statistics features provide information related to gray level distribution of the image but not about relative position of the various gray levels within image. Second-order statistics features do this where pixels are considered in pairs. Two

parameters or more, such as relative distance and orientation among pixels, are used. The second order statistical features calculated are the Gray Level Co-occurrence Matrix (GLCM) and Grey-Level Run-Length Matrix (GLRM) features [255]. Contrast feature is a measure of intensity of a pixel and its neighbor over the image.

Energy can be defined as quantifiable amount of the extent of pixel pair repetitions. Energy is a parameter to measure the similarity of an image. If energy is defined by Haralicks GLCM feature, then it is also referred to as angular second moment. Correlation feature describes the spatial dependencies between the pixels. Homogeneity returns a value that measures closeness of the distribution of elements in GLCM to GLCM diagonal. The range is in [0 1]. Homogeneity is 1 for a diagonal GLCM.GLRM is represented in the form of a matrix for geometrical features. It gives a measure of the intensity of pixels along given direction mentioned as Run length. GLRM has two dimensions. Here each element is represented as the number of elements j with intensity i, in given direction ş. Thus, given a direction, the run-length matrix estimates for each gray level value how many times the run occur.

Gray Level Non-Uniformity (GLN) measure the distribution of runs over the gray values (Galloway, 1975) [256]. The feature value is low when runs are equally distributed along grey levels. Thus a lower value indicates higher similarity in intensity values. Run Length Non-Uniformity (RLN) measures the distribution of runs over the run lengths (Galloway, 1975) [256].

The feature value is low when runs are equally distributed along run lengths. Short Run Emphasis (SRE) measures the distribution of short runs. Higher value indicates fine textures. Long Run Emphasis (LRE) measures the distribution of long runs. Higher value indicates coarse textures. Run Percentage (RP) feature is the ratio between total number of observed runs in the image and total number of possible runs if all runs had a length of one. Imaging features utilized in this work are formulated in Table 6.1.

Table 6. 1 Imaging attributes for feature extraction

First Order Statistical Features

Intensity based	Formulas	Histogram based	Formulas
Minimum intensity	$I_{min} = \min(I(x,y))$	Kurtosis	$I_{Kurtosis} = \left(\frac{1}{m \times n}\right)\frac{\sum(I(x,y)-M)}{SD^3}$
Maximum intensity	$I_{max} = \max(I(x,y))$	Skewness	$I_{Skewness} = \left(\frac{1}{m \times n}\right)\frac{\sum(I(x,y)-M)^3}{SD^3}$
Mean intensity	$I_{mean} = \text{mean}(I(x,y))$	IDM	$I_{IDM} = \sum_{x=0}^{m-1}\sum_{y=0}^{n-1}\frac{1}{1+(x-y)^2}I(x,y)$
Eccentricity	$I_{Eccentricity} = c/a$	Entropy	$I_{Entropy} = -\sum_{x=0}^{m-1}\sum_{y=0}^{n-1}I(x,y)\log_2 I(x,y)$
Centroid	$I_{Centroid} = \frac{1}{i}\sum_{j=1}^{i}x_j$		

Second Order Statistical Features

GLCM	Formulas	GLRM	Formulas
Contrast	$I_{Contrast} = \sum_{x=0}^{m-1}\sum_{y=0}^{n-1}(x,y)^2 I(x,y)$	GLN	$I_{GLN} = \sum_{l=1}^{L}\left[\sum_{g=0}^{G-1}P(g,l)\right]^2$
Energy	$I_{Energy} = \sqrt{\sum_{x=0}^{m-1}\sum_{y=0}^{n-1}I^2(x,y)}$	RLN	$I_{RLN} = \sum_{g=0}^{G-1}[\sum_{l=1}^{L}P(g,l)]^2$
Correlation	$I_{Corr} = \frac{\sum_{x=0}^{m-1}\sum_{y=0}^{n-1}(x,y)\,I(x,y) - M_x M_y}{SD_x SD_y}$	SRE	$I_{SRE} = \sum_{g=0}^{G-1}\sum_{l=1}^{L}\frac{P(g,l)}{l^2}$
Homogeneity	$I_{Homo} =$	LRE	$I_{LRE} = \sum_{g=0}^{G-1}\sum_{l=1}^{L}P(g,l)l^2$

$$\sum_{x=0}^{m-1}\sum_{y=0}^{n-1}\frac{I(x,y)}{1+(x-y)^2}$$	RP	$$I_{RP} = \frac{}{\sum_{g=0}^{G-1}\sum_{l=1}^{L}\frac{1}{P(g,l)l}}$$

* $I(x,y)$ is the grayscale image and $x \neq y$; $M = \left(\frac{1}{m \times n}\right)\sum_{x=0}^{m-1}\sum_{y=0}^{n-1}I(x,y)$, $SD = \sqrt{\left(\frac{1}{m \times n}\right)\sum_{x=0}^{m-1}\sum_{y=0}^{n-1}(I(x,y)-M)^2}$, $P(g,l)$ is the probability of specific run length, g denotes gray value, l is the length, c is distance from center of focus, a is distance from focus to vertex, i is total number of data point in extracted region, x_j different data point in extracted region.

6.2.3 Statistical analysis for feature selection

Only some of the prominent features are selected for effectively improving the ACC of the diagnosis. This selection is performed using *t*-test. In this selection, the significance of all imaging features is observed and selection is made respectively. The general equation for the *t*-test is presented in Equation 6.2.

$$p = \begin{cases} p > 0.05; \; weakly \; significant \\ 0.01 < p \leq 0.05; \; moderately \; significant \\ p \leq 0.05; \; strongly \; significant \end{cases} \tag{6.2}$$

where p is the significance value. All the values below 0.05 represent significant difference between HGG and LGG (p<0.05) and are strongly significant features. The values above 0.05 represents weakly significant features (p>0.05).

6.2.4 Detection of optimal sequence using machine learning

After imaging feature reduction, these features are submitted to the classification procedure for determining glioma grade from extracted tumor region. The binary classification of total population of MR images is performed by using SVM and kNN classifiers.

i. **Support Vector Machine (SVM):** SVM is the most effective linear classifier with good mathematical intuition that was given by V. N. Vapnik in 1933 [257]. It is a supervised learning technique applied to 1-n class classification problem that is

based on the finding of the decision surface. This decision surface is formed by the support vectors that are the closest and the equidistant points to this plane. A graphical understanding of the SVM is shown in Figure 6.4 where (x, y) are the feature attributes
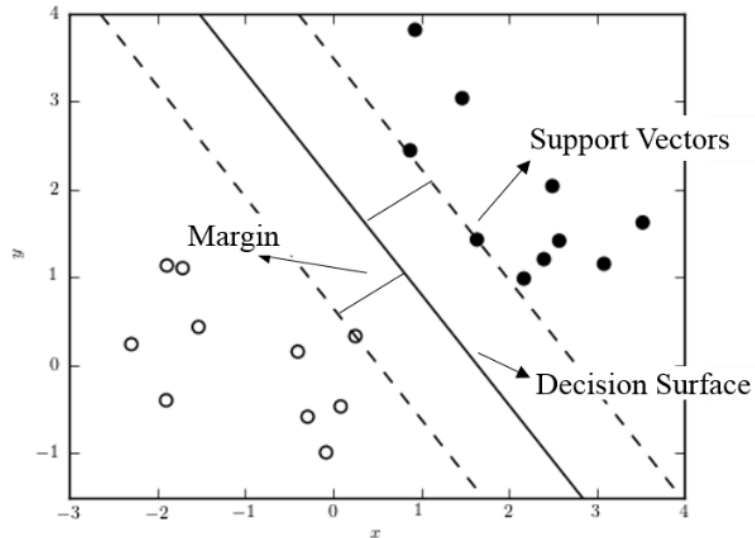
.

Figure 6.4 Graphical presentation of SVM technique

The distance of a point (x_i, y_j) from decision boundary is defined as function margin as given in Equation 6.3.

$$\gamma^i = y_i(w^T x_i + b) \tag{6.3}$$

where, w^T are the hyperplane parameter that are normal to surface of decision boundary, x_i is the point that is mapped to higher dimensional space and b is constant. If the point is further away from the surface, we have higher confidence in classification of the point. So, larger functional margin means more confidence in predicted class of that point.

ii. **k-Nearest Neighbor (kNN):** Another supervised technique used particularly for the classification purpose is kNN [258]. The main idea for this method is that it has similar output for similar training samples. It is one of the most extensively used

lazy learning approach. Given a set of *n* training examples, upon receiving a new instance to predict, the kNN classifier will identify k nearest neighboring training examples of the new instance. Then, it assigns class label depending upon maximum number of neighbors to new instance. The distance between training and testing vector is calculated by different distance metric measurement technique such as Euclidean distance. Consider $X_i = \{x_1, x_2, \ldots, x_{iN}\}$ and $X_j = \{x_1, x_2, \ldots, x_{jN}\}$ the sample population, thus to measure the similarity between them the distance is calculated as given.

$$Dist(X_i, X_j) = \sqrt{\sum_{m=1}^{N}(x_{im} - x_{jm})^2} \tag{6.4}$$

We can then consider the similarity of two different points to distance between them in a space under by evaluating the Euclidean distance. The way in which applied algorithm decides which of the points from training set are enough similar to the point considered when choosing class to estimate for a new observation is to pick the k closest data points to the new observation, and to take the most common class among these.

6.2.5   Performance Metric

The obtained results are verified by evaluating the performance metric. ACC and error rate of the classification outcomes are verified by evaluating the performance metric. These metrics describe efficiency of the classification that are based on terms mentioned in Table 6.2 of the possible outcomes.

i. TP is the HGG class predicted in the presence of LGG class of glioma.
ii. TN is the LGG class predicted in the absence of HGG class of glioma.
iii. FP is the classification result when HGG class in absence of LGG class.
iv. FN is the classification result when LGG class is present in absence of HGG class.

The performance metric used are: sensitivity, specificity, ACC and error rate. Sensitivity represents the percentage of recognition of actual HGG class. Specificity value defines the percentage of recognition of actual LGG class. ACC is the degree of correctly prediction made by the total number of predictions made. The error rate (ERR) is the amount of predicted class that have been incorrectly classified by a decision model. The overall classification is also provided by the Area Under the Curve (AUC) that represents better classification if the area under the curve is more. All of these performance metrics are evaluated for T1, T2, Flair and T1ce sequences and their respective accuracies are observed.

Table 6. 2 Possible outcomes for parameter evaluation

Actual class	Predicted class	
	HGG/0	**LGG/1**
HGG/0	TN	FP
LGG/1	FN	TP

6.3   RESULTS AND DISCUSSION

Glioma grading identification from the MR Images is a complex process due to the intricate intensity distribution in the tumor region. In this paper have developed a technique for extracting the tumor region and classifying these regions of all the sequences in HGG and LGG classes. The proposed approach for segmentation is performed by GBKS GC technique developed by Dogra *et al.* [250] and classification is implemented on working platform of Matlab. All the imaging features selected from Figure 6.6 are employed in the process of classification.

6.3.1 Segmentation

The segmentation performed in the proposed method provides the accurate extraction of the Glioma from the MR images. The novel technique proposed by Dogra *et al.* [250] provides an automatic segmentation and removes the major limitation of shrinkage problem from the conventional GC technique. The segmentation is performed on the Flair sequence and from obtained extracted region, the mask is formed. This mask is utilized in extracting the tumor region from the rest of sequences by multiplying it with the original images of these sequences. The highlighted region indicated in Figure 6.5 represents the tumor regions of all the sequences obtained from GBKS GC segmentation.

Extracted Imaging Features: {Intensity based; Histogram based; GLCM; GLRM}
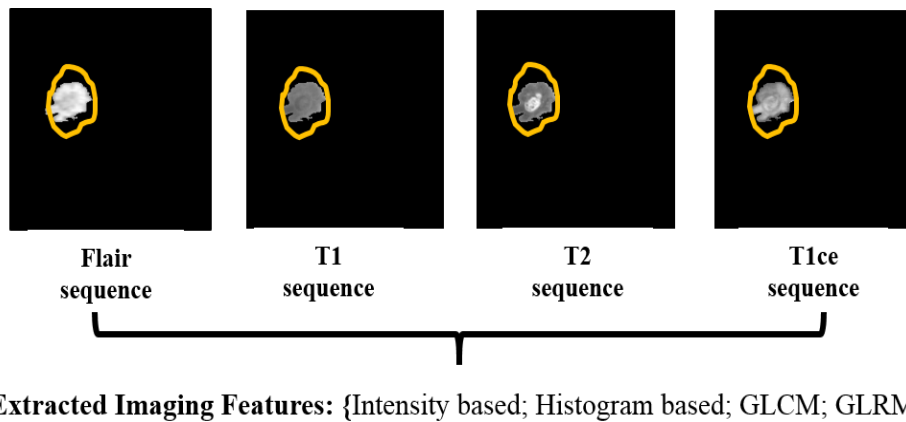
Figure 6. 5 Extracted imaging features from Flair, T1, T2 and T1ce sequence of the extracted HGG tumor

6.3.2 Feature extraction and selection

Imaging features extracted from various sequences of tumor region and the process of feature selection is accomplished using *t*-test. This *t*-test is performed on all the imaging attributes as listed in Table 6.1. The *p*-values are evaluated for each imaging

features and are listed in Table 6.3. Based on Equation 6.2 the selection of most significant features is made.

TABLE 6. 3 *p*-values evaluated of imaging attributes.

First Order Statistical Features			
Intensity based	***p*-value**	**Histogram based**	***p*-value**
Minimum intensity	0.001	Kurtosis	0.381
Maximum intensity	0.18	Skewness	0.53
Mean intensity	0.001	IDM	0.78
Eccentricity	0.038	Entropy	0.69
Centroid	0.001		
Second Order Statistical Features			
GLCM	***p*-value**	**GLRM**	***p*-value**
Contrast	0.649	GLN	0.053
Energy	0.528	RLN	0.004
Correlation	0.46	SRE	0.003
Homogeneity	0.34	LRE	0.001
		RP	0.059

These features are selected as shown in Figure 6.6, are provided to the classification process. The p values obtained for respective imaging features are illustrated in Figure

6.6. From this representation it is clear that, all the features having p value below 0.05 represent a significant difference between HGG and LGG ($p<0.05$).
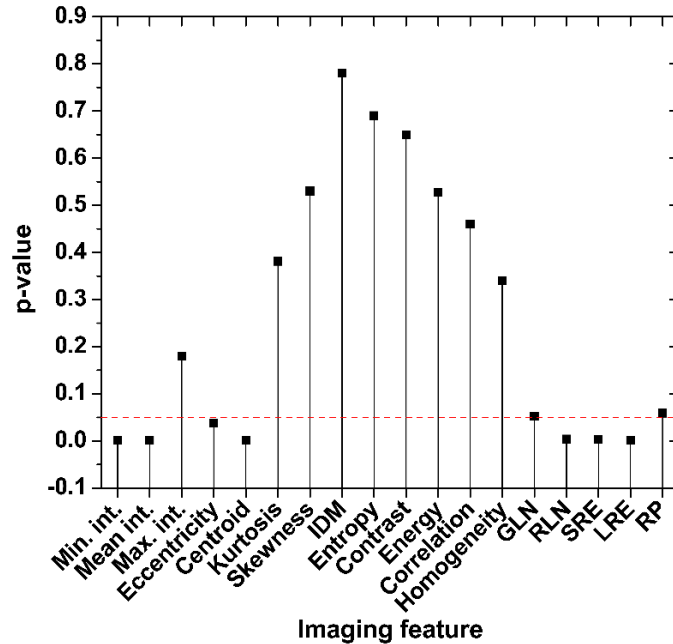
Figure 6. 6 Stem plot of *p* values of 18 imaging features

So, these are selected as prominent features in comparison to features that are discarded. The dash line represents critical value where *p* equals to 0.05 and is responsible for the feature selection. Selected prominent features are minimum intensity, maximum intensity, eccentricity, centroid, RLN, SRE and LRE.

6.3.3   Detection of optimal sequence

A five-fold cross validation of classifying HGG and LGG tumors by applying two different classification methods (SVM and kNN) using most prominent features are obtained from *t*-test. All these classifications are performed on different MR image sequences and they investigate the most potential sequence that generates highest ACC for the proposed work. All the sequences comprise different intensity distribution and

the same remains true for HGG and LGG tumors. This is due to enhancing region that is present in LGG tumor that can only be visualized in one of the MR image sequences.

i. **SVM classification:** The results presented in Table 6.4 shows performance metric evaluated for binary classification of HGG and LGG tumors by applying SVM classifier for all sequences. The SVM classifier utilizes prominent imaging features for performing the classification.

Table 6. 4 Performance metric for binary classification using SVM classifier

	SVM Classifier		
	Sensitivity	Specificity	Error rate
Flair	0.75	0.96	0.26
T1	0.53	0.78	0.30
T2	0.63	0.87	0.24
T1ce	0.95	0.98	0.07

Among all four sequences, the highest values are attained for sensitivity and specificity on applying SVM classifier are 0.96 and 0.98 respectively forT1ce sequence. The error rate attained for T1ce is 0.07 that is lowest in comparison to others. The evaluated results present the most efficient binary SVM classification performed on T1ce sequence. Other than the performance metric evaluated in Table 6.4 the ROC curves are also illustrated in Figure 6.7 for all the sequences.
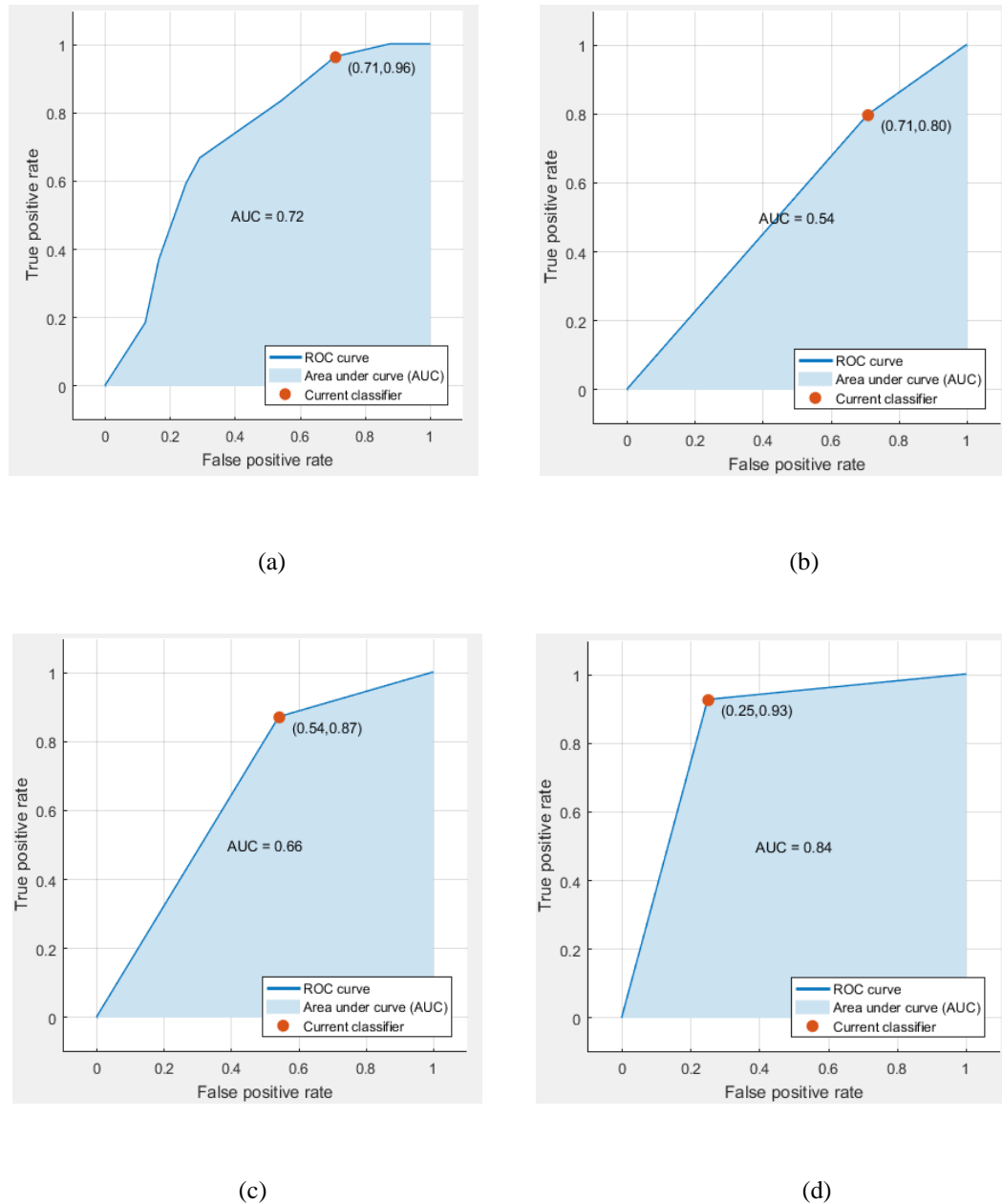
(a)

(b)

(c)

(d)
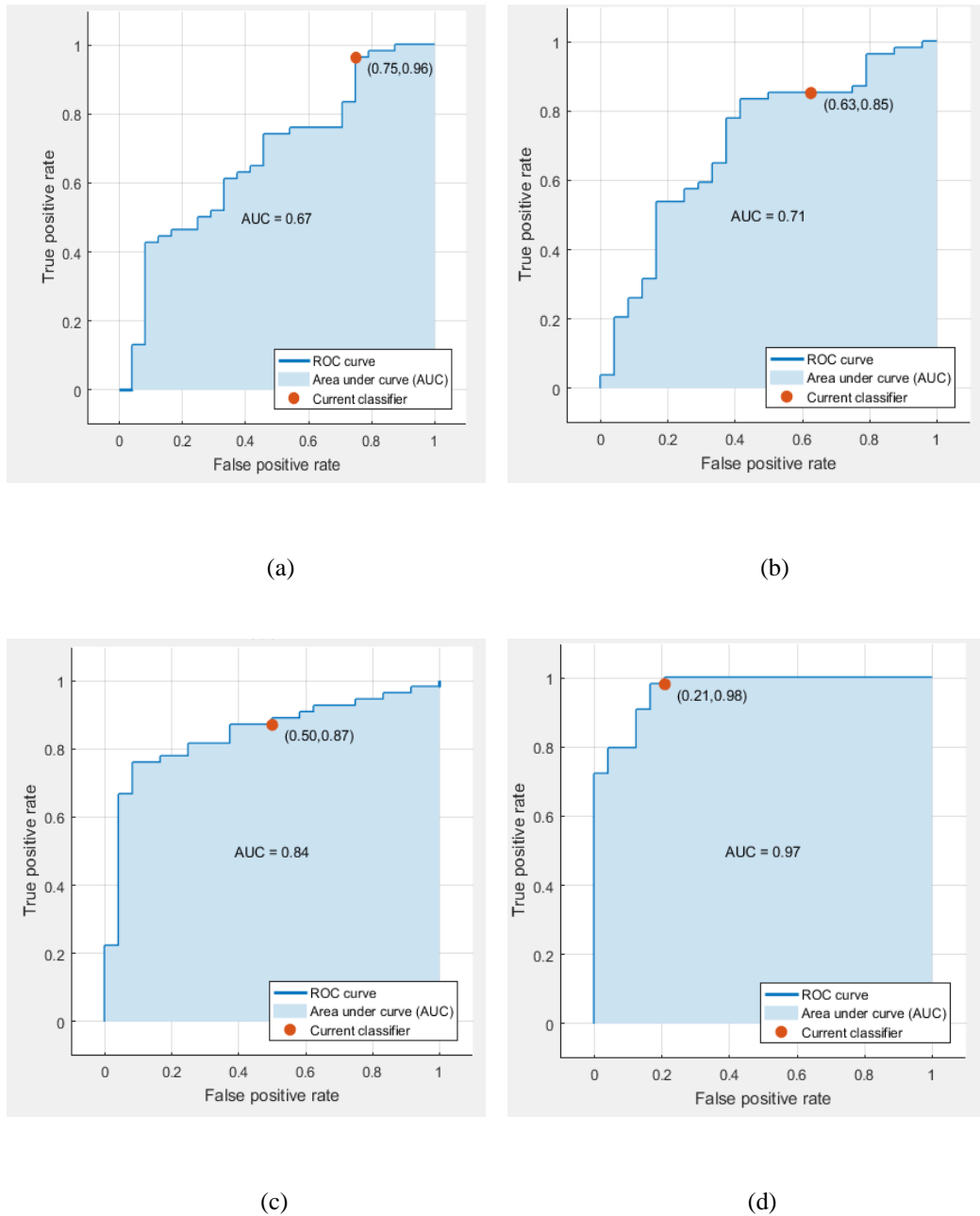
Figure 6. 7 ROC curves for binary classification of HGG and LGG tumors using SVM classifier for the following sequence: (a)Flair, (b) T1, (c) T2 and (d) T1ce

These ROC depict the true positive rate as a function of the false positive rate for diverse cut-off points. Best classification has a ROC curve with highest area under the curve (AUC). On analyzing the AUC for all sequences in Figure 6.7, the T1ce sequence depict

highest AUC of 0.97. Whereas, the AUC for Flair, T1 and T2 sequences are 0.67, 0.71 and 0.84 respectively.

ii. **kNN classification:** The kNN classifier is used for performing binary classification and the evaluated performance metric are presented in Table 6.5. The sensitivity, specificity and error rate are calculated for all the sequences. On observing the values in Table 6.5, it is inferred that a maximum value for sensitivity and specificity (0.82 and 0.93 respectively) is attained for T1ce sequence. Even the error rate achieved by the kNN classifier is lowest for T1ce sequence that is 0.12.

Table 6. 5 Performance metric for binary classification using kNN classifier

	kNN Classifier		
	Sensitivity	Specificity	Error rate
Flair	0.77	0.96	0.24
T1	0.49	0.79	0.36
T2	0.61	0.87	0.25
T1ce	0.82	0.93	0.12

(a)

(b)

(c)

(d)

Figure 6. 8 ROC curves for binary classification of HGG and LGG tumors using kNN classifier for the following sequence: (a) Flair, (b) T1, (c) T2 and (d) T1ce

All these values signify best binary classification on the T1ce sequence. The ROC curve plotted for all these sequences are depicted in Figure 6.8. The AUC attained by classifier for Flair, T1, T2 and T1ce sequences are 0.72, 0.54, 0.66 and 0.84

respectively. These values easily present that the most efficient binary classification is only provided by the T1ce sequence.

6.4   COMPARATIVE ANALYSIS

This paper presents a binary classification of the high grade glioma and low grade glioma tumors from the MR Images. This classification solely depends on the features extracted from the segmented tumor regions. Hence, the accurate segmentation of the tumor region is critically important, that is achieved in the proposed model by applying GBKS GC segmentation [250]. After the segmentation is performed, extracted tumor regions from all the sequences are obtained. But, it is ambiguous to identify the best sequence that provides accurate classification results. In the prosed model SVM and kNN classifiers are employed for performing the binary classification. In Table 6.6, the ACC obtained by both the classifier on all sequences are illustrated.

Table 6. 6 ACC attained by SVM and kNN classifier on all sequences

	SVM	kNN
Flair	76.9%	75.6%
T1	71.8%	69.2%
T2	75.6%	71.9%
T1ce	**94.9%**	**91%**

It is observed that T1ce sequence generates the maximum ACC values of 94.9% and 91% for the SVM and kNN classifiers. Hence, it is inferred that in comparison to all the sequences of MR images, the best ACC is achieved only with T1ce sequence.

The Table 6.7 illustrates the comparison of AUC and ACC values of the proposed models with the state of art techniques applied for the HGG and LGG tumor

classification. It is depicted form the attained values that our proposed models outperform the existing technique.

Table 6. 7 Comparative analysis of the proposed models with the existing technique for HGG and LGG tumor in MR Images.

Proposed model	AUC	ACC
GBKS GC+SVM	**97%**	**94.6%**
GBKS GC+kNN	84%	91%
Zacharaki *et al.* [259]	89.6%	87.8%

Zacharaki *et al.* [259] proposed a computer assisted classification method combining conventional MRI and perfusion MRI for differential diagnosis. Authors have provided the high grade and low grade glioma binary classification using SVM method and the extracted features include texture and shape feature from the ROIs.

6.5   CONCLUSION

The main goal of detection of the most appropriate sequence for classification is accomplished in this chapter. After the tumor extraction from the complex brain MR Images, it is essential to classify the malignancy of disease in order to prevent invasive diagnosis and provide better patient treatment planning. The complete set of MRI sequences provides different characteristic information of the brain anatomy from MR Images. Hence, all the imaging attributes are extracted from these images and by applying t-test the most prominent features are selected. Using these features a computer assisted algorithm is developed that uses machine learning algorithm to provide good binary classification with an ACC of 94.6%. In future, multi classification of tumor can be done that will provide the stages of both grades of tumor.

CHAPTER 7

CONCLUSION AND FUTURE WORK

CHAPTER 7

CONCLUSION AND FUTURE WORK

This chapter concludes complete research work regarding glioma segmentation by improving the graph cut technique. We present our conclusion, contribution and future course of research in the field of medical segmentation.

7.1   CONCLUSION

The primary goal of this research work includes development of robust, accurate and computational efficient algorithm for extraction of tumor region from complex MRI brain scans. The presented algorithms are able to provide better tumor characterization. After an exhaustive literature review as given in Chapter 2 GC image segmentation technique is opted due to its popularity in the field of medical analysis. In this research work the limitations of this techniques are eliminated to improve the accuracy of segmentation and provide a simpler mathematical computation.

Exhaustive literature review of GC method revealed that prior information of brain anatomy is required for an automatic initialization of this algorithm, which are assumed or provided by experts as described in the literature. So, to address this issue three novel approaches are developed that demonstrate accurate selection of seed values and tumor extraction. The obtained results inferred that selected seed values were able to successfully extract the tumor region with a simpler mathematical computation. The techniques were also automated and removed the complexity in subjectivity of expert.

Other than the problem of seed selection in GC technique the open research issue of shrinkage problem is addressed in this research work is stated in IEEE Review in Biomedical Engineering. This is a major limitation of GC that causes occurrence of some erroneous region leading to fallacious segmentation. A novel automatic approach termed GBKS GC is proposed that is able to eliminate this problem completely. This

technique facilitates three simultaneous goals of automatic initialization, removal of shrinkage problem and accurate tumor extraction. The qualitative and quantitative results validate the extracted tumor with respect to its shape, size and location.

Later, for IIH problem in MRI, the same GBKS GC framework was adopted for validating its robustness in real time application. IIH is caused due to MR machine at magnetic field above 3T. An effective and accurate segmentation results are obtained from proposed GBKS GC method on the standard database as well as on real patient MR Images from Government hospital, IGMC. The results inferred that tumor region is effectively extracted as validated by quantitative comparison with ground truth and identified by expert radiologist. These results demonstrate GBKS GC as an improved, effective and robust framework with low computation.

For better diagnosis glioma grading is necessary in order to provide better treatment planning of patient. It is difficult to identify the most accurate sequence for glioma grading as MRI scans consist of four different sequences that provide different textural features of tumor region. An effective sequence selection model is finally developed employing machine learning that is able to detect the optimal sequence for providing glioma grading with highest accuracy. All the results obtained by the proposed techniques are well compared with state of art technique employing same dataset for their research work. The results also represented in terms of percentage improvement of proposed technique over others.

7.2   CONTRIBUTION

The main contributions in this research work comprises following aspects:

i.   An exhaustive literature review of all the image segmentation techniques in the field of biomedical images is carried out. All the theoretic approaches with their pros and cons for segmentation are reviewed. The detailed survey on evolvement of GC technique with its major advantages over the other exiting techniques are

listed. From the complete literature survey we are able to conclude with the key requirements for performing brain tumor segmentation.

ii. Three efficient techniques are presented for seed selection to develop an automatic and semi-automatic initialization to the existing graph cut technique for tumor segmentation. The selected seed values are able to provide not just the tumor extraction but also the priori information regarding location of tumor.

iii. The open research issue of shrinkage problem is also addressed by developing a novel GBKS GC technique for its eradication. This technique is able to provide a simultaneous goals of automatic initialization, accurate seed selection and eradication of shrinkage problem with very low mathematical complexity. This technique improves segmentation accuracy and validates location, shape and size of the tumor.

iv. Real time application of GBKS GC in noisy environment and on real patient images is also achieved. The extraction of tumor is difficult from bias field images that are produced at ultra-high magnetic fields causing IIH. GBKS GC is able to accurately extract tumor regions from such difficult images. It is successfully implemented on real patient MR images with different patient profile and tumor type. The accuracy of these results depicts an effective and robust framework of GBKS GC.

v. For better diagnosis a system model is proposed that uses machine learning for detecting the optimal sequence for glioma grading. The most optimal sequence is identified with highest accuracy using binary classifiers that are SVM and kNN.

7.3 FUTURE SCOPE

This research work is able to provide an accurate binary segmentation of glioma tumor. In future following areas in segmentation can be explored: i) multi-object segmentation of tumor region for providing better understanding of tumor characterization, ii)

complex medical segmentation problem by using deep learning, iii) Hybrid method for medical image segmentation that provides graph cut to be more flexible and powerful, iv) multi-modality co-segmentation.

LIST OF PUBLICATIONS

LIST OF PUBLICATIONS

JOURNALS

1. Dogra, J., Jain, S., and Sood, M., 2020. Novel Graph Cut Based GBKS Technique for Tumor Detection and Extraction from Medical Images. *IET Image Processing,* vol. 14, no. 1, pp. 84-93. **(SCI)** <u>**IF: 2.004**</u>

2. Dogra, J., Jain, S., and Sood, M., 2020. Glioma extraction from MR images employing Gradient Based Kernel Selection Graph Cut technique. *The Visual Computer*, Springer, vol. 36, no. 5, pp. 875-891. **(SCI)** <u>**IF: 1.415**</u>

3. Dogra, J., Jain, S., Sharma, A., Kumar, R. and Sood, M., 2020. Brain Tumor Detection from MR Images Employing Fuzzy Graph Cut Technique. *Recent Patents on Computer Science, Bentham Science,* vol. 13, no. 3, pp. 362-369. (**ESCI/Scopus)**

4. Dogra, J., Jain, S., and Sood, M., 2020. Novel Seed Selection Techniques for MR Brain Image Segmentation using Graph Cut. *Computer Method in Biomechanics and Biomedical Engineering: Imaging and Visualization,* vol. 8, no. 4, pp. 389-399.
(ESCI/Scopus)

5. Dogra, J., Jain, S., and Sood, M., 2019. Glioma Classification of MR brain tumor employing Machine Learning. *International Journal of Innovative Technology and Exploring Engineering*, vol. 8, no. 8, pp. 2676-2682. **(Scopus)**

6. Dogra, J., Jain, S., and Sood, M., 2018. Segmentation of MR Images using Hybrid k Mean-Graph Cut Technique. *Journal of Procedia Computer Science*, vol. 132, pp. 775-784, 2018. **(Scopus)**

7. Dogra, J., Jain, S., and Sood, M., 2018. Improved Method for Analyzing MRI Brain Images. *Network Biology*, vol. 8, no. 1, pp. 1-11. **(Clarivate Analytics)**

CONFERENCES

1. Dogra, J., Jain, S., and Sood, M., 2019. Analysis of Graph Cut Technique for Medical Image Segmentation. 3rd International Conference on Advanced Informatics for Computing Research (ICAICR), Shimla, pp. 451-463. **(Scopus)**

2. Dogra, J., Jain, S., and Sood, M., 2017. Segmentation of Magnetic Resonance Images of Brain using Thresholding Techniques. 4th IEEE International Conference on Signal Processing, Computing and Control (ISPCC), Wakhnaghat, pp. 311-315. **(Scopus)**

REFERENCES

REFERENCES

[1] DeAngelis L. M., "Brain tumors", The New England journal of medicine, vol. 344, no. 2., pp. 114-123, January, 2001.

[2] Mohan G., and Subashini M. M., "Medical Imaging with Intelligent Systems: A Review", Deep Learning and Parallel Computing Environment for Bioengineering Systems. Academic Press, vol. 22, no. 10, pp. 53-73, 2019.

[3] Reblin M., Sahebjam S., Peeri N. C., *et al.*, "Medical Cannabis Use in Glioma Patients Treated at a Comprehensive Cancer Center in Florida", Journal of palliative medicine, vol. 22, no. 10., September 2019.

[4] Kohler B. A., Ward E., McCarthy B. J., *et al.*, "Annual report to the nation on the status of cancer, 1975–2007, featuring tumors of the brain and other nervous system", Journal of the national cancer institute, vol. 103, no. 9, pp. 714-736, 2011.

[5] Logeswari T., and Karnan M., "An improved implementation of brain tumor detection using segmentation based on hierarchical self-organizing map", International Journal Computer Theory and Engineering, vol. 2, no. 4, pp. 1793-8201, August 2010.

[6] Abd-Ellah M. K., Awad A. I., Khalaf A. A. M., *et al.*, "Classification of brain tumor MRIs using a kernel support vector machine. Building Sustainable Health Ecosystems", 6th International Conference on Well-Being in the Information Society, vol. 636, pp. 151–60, 2016.

[7] Singh A., Bajpai S., Karanam S., *et al.*, "Malignant brain tumor detection", International Journal Computer Theory of Engineering, vol. 4, no. 5, pp. 1002-1006, December 2012.

[8] Dasgupta A., Gupta T., and Jalali R., "Indian data on central nervous tumors: A summary of published work", South Asian journal of cancer, vol. 5, no. 3, pp. 147-153, September 2016.

[9] Asirvatham J. R., Deepti A. N., Chyne R., *et al.*, "Pediatric tumors of the central nervous system: A retrospective study of 1,043 cases from a tertiary care center in South India", Child's Nervous System, vol. 27, no. 8, pp. 1257-63, August 2011.

[10] Jaiswal J., Shastry A. H., Ramesh A., *et al.*, "Spectrum of primary intracranial tumors at a tertiary care neurological institute: a hospital-based brain tumor registry", Neurology India, vol. 64, no. 3, pp. 494–501, 2016.

[11] Jha P, Suri V, Singh G, *et al.*, "Characterization of molecular genetic alterations in GBMs highlights a distinctive molecular profile in young adults" Diagnostic Molecular Pathology vol. 20, no. 4, pp. 225-32, December 2011.

[12] Norhashimah M. S., Syed Abu Bakar S. A. R., Sobri Muda A., *et al.*, "Review of brain lesion detection and classification using neuroimaging analysis techniques" Journal Teknologi, vol. 74, no. 6, pp. 73–85, April 2015.

[13] Schad, L.R., Bluml, S., Zuna, I., "MR tissue characterization of intracranial tumors by means of texture analysis", Magnetic Resonance Imaging, vol. 11, no. 6, pp. 889–896, March 1993.

[14] Lauterbur P., "Image formation by induced local interactions: examples employing nuclear magnetic resonance", Nature, vol. 242, pp. 190–191, 1973.

[15] Mansfield P., "Multi-planar image formation using NMR spin echoes" Journal of Physics C: Solid State Physics, vol. 10, no. 3, L55, 1977.

[16] Sprawls P. "Magnetic resonance imaging: principles, methods, and techniques", Medical Physics Publishing, Madison, 2000.

[17] Prados F., Cardoso M. J., Yiannakas M. C., *et al.*, "Wheeler-Kingshott CA2 OS. Fully automated grey and white matter spinal cord segmentation", Scientific Report 6, Article no. 36151, October 2016.

[18] Corso J, Sharon E, Dube S, *et al.*, "Efficient multilevel brain tumor segmentation with integrated Bayesian model classification", IEEE Transaction of Medical Imaging, vol. 27, no. 5, pp. 629–40, 2008.

[19] Sorensen A. G., Batchelor T. T., Wen P. Y., *et al.*, "Response criteria for glioma" Nature Clinical Practice Oncology 5, pp. 634–644, August 2008.

[20] Galanis E., Buckner J. C., Maurer M. J., *et al.*, "Validation of neuroradiologic response assessment in gliomas: Measurement by RECIST, two-dimensional, computer-assisted tumor area, and computer-assisted tumor volume methods" Neuro-Oncology, vol. 8, no. 2, pp. 156–165, April 2006.

[21] Wen P. Y., Macdonald D. R., Reardon D. A., *et al.*, "Updated response assessment criteria for high-grade gliomas: response assessment Neuro-Oncology Working Group", Journal Clinical Oncology, vol. 28, no. 11, pp. 1963-1972, April 2010.

[22] Rogowska J., "Overviewand fundamentals of medical image segmentation", In Handbook of medical imaging, processing and analysis, pp. 69–85, October 2000.

[23] Gibbs P., Buckley D. L., Blackband S. J., *et al.*, "Tumour volume determination from MR images by morphological segmentation", Physics in Medicine and Biology, vol. 41, no. 11, p. 2437, June 1996.

[24] Leedham, G., Varma, S., Patankar, A., at al., "August. Separating text and background in degraded document images-a comparison of global thresholding techniques for multi-stage thresholding", In Proceedings of Eighth IEEE International Workshop on Frontiers in Handwriting Recognition, pp. 244-249, 2002.

[25] Haralick R. M., Shapiro L. G., "Image segmentation techniques", Computer Vision Graphics and Image Processing, vol. 29, no. 1, pp. 100–132, January1985.

[26] Kuo W. F., Lin C. Y., Sun Y. N., "Brain MR images segmentation using statistical ratio: mapping between watershed and competitive hopfield clustering network algorithms", Computer Methods and Programs in Biomedical, vol. 91, no. 3, pp. 191–198, September 2008.

[27] Gies V., Bernard T. M., "Statistical solution to watershed oversegmentation", In proceeding of International conference on image processing IEEE, vol. 3., pp. 1863–1866, October 2004.

[28] Coleman G. B., Andrews H. C., "Image segmentation by clustering" Proceeding in IEEE, vol. 67, no. 5, pp. 773–785, May 1979.

[29] Balafar M., "Fuzzy c-mean based brain MRI segmentation algorithms", Artificial Intelligence Review, vol. 41, no. 3, pp. 441–449, March 2014.

[30] Yang X., Fei B., "A multiscale and multiblock fuzzy c-means classification method for brain MR images" Medical Physics, vol. 38, no. 6, pp. 2879–2891, June 2011.

[31] MacQueen, J., "Some methods for classification and analysis of multivariate observations", Proceedings of the fifth Berkeley symposium on mathematical statistics and probability, vol. 1, no. 14, June 1967.

[32] Zadeh, L. A., "Fuzzy sets", Information and control, vol. 8, no. 3, pp. 338-353, June 1965.

[33] Bezdek, J C., Coray C., Gunderson R. *et al.*, "Detection and characterization of cluster substructure i. linear structure: Fuzzy c-lines", SIAM Journal on Applied Mathematics, vol. 40, no. 2, pp. 339-357, April 1981.

[34] Murray D. W., Kashko A., and Buxton H., "A parallel approach to the picture restoration algorithm of Geman and Geman on an SIMD machine", Image and Vision Computing, vol. 4, no. 3, pp. 133-142, August 1986.

[35] Warfield S. K., Kaus M., Jolesz F. A., *et al.*, "Adaptive, template moderated, spatially varying statistical classification", Medical Image Analysis, vol. 4, no. 1, pp. 43–55, March 2000.

[36] Buller D., Buller A., Innocent P. R., *et al.*, "Determining and classifying the region of interest in ultrasonic images of the breast using neural networks," Artificial Intelligence in Medicine, vol. 8, no. 1, pp. 53–66, February 1996.

[37] Kohonen T., "Learning vector quantization", In Self-organizing maps, vol. 30, pp. 245-261, 2001, Berlin, Heidelberg.

[38] Chi D., "Self-Organizing Map-Based Color Image Segmentation with k-Means Clustering and Saliency Map", ISRN signal processing, vol. 2011, Article ID 393891, p 18.

[39] Osher S., and Sethian J. A., "Fronts propagating with curvature-dependent speed: algorithms based on Hamilton-Jacobi formulations", Journal of computational physics, vol. 79, no. 1, pp. 12-49, November 1988.

[40] Kass M., Witkin A., Terzopoulos D., "Snakes: active contour models", International Journal Computer Vision, vol. 1, no. 4, pp. 321–331, January 1988.

[41] Wu Z., Leahy R., "An optimal graph theoretic approach to data clustering: theory and its application to image segmentation", IEEE Transactions on Pattern Analysis and Machine Intelligence, vol. 15, no. 11, pp. 1101–1113, November 1993.

[42] Boykov Y., Veksler O., Zabih R., "Fast approximate energy minimization via graph cuts", IEEE Transactions on pattern analysis and machine intelligence, vol. 23, no. 11, pp. 1222-1239, November 2001.

[43] Menze B. H., Jakab A., Bauer S., *et al.*, "The multimodal brain tumor image segmentation benchmark (BRATS)", IEEE transactions on medical imaging, vol. 34, pp. 1993-2024, December 2015.

[44] Menze B. H., Van Leemput K., Lashkari D., *et al.*, "A generative model for brain tumor segmentation in multi-modal images", In International Conference on Medical Image Computing and Computer-Assisted Intervention, pp. 151-159, September 2010.

[45] Hameurlaine, M., and Moussaoui A., "Survey of Brain Tumor Segmentation Techniques on Magnetic Resonance Imaging", Nano Biomed. Eng, vol. 11, no. 2, pp. 178-191, 2019.

[46] Cheng J., Huang W., Cao S., *et al.*, "Enhanced Performance of Brain Tumor Classification via Tumor Region Augmentation and Partition", PloS one, vol. 10, no. 10, October 2015.

[47] Cheng, Jun, *et al.*, "Retrieval of Brain Tumors by Adaptive Spatial Pooling and Fisher Vector Representation", PloS one, vol. 11, no. 6, 2016.

[48] Pereira S., Pinto A., Alves V., *et al.*, "Brain tumor segmentation using convolutional neural networks in MRI images", IEEE Transaction on Medical Imaging, vol. 35, no. 5, pp. 1240–1251, March 2016.

[49] Jiang J., Wu Y., Huang M. *et al.*, "3D brain tumor segmentation in multimodal MR images based on learning population-and patient-specific feature sets" Computerized Medical Imaging and Graphics, vol. 37, no. 7-8, pp. 512-521, October 2013.

[50] Joshi A. J., Porikli F. and Papanikolopoulos N., "Multi-class active learning for image classification" IEEE Conference on Computer Vision and Pattern Recognition, pp. 2372-2379, June 2009.

[51] Kotsiantis, S. B., Zaharakis I., and. Pintelas P., "Supervised machine learning: A review of classification techniques", Emerging artificial intelligence applications in computer engineering, vol. 160, pp. 3-24, June 2007.

[52] Bull, D., Joy I., Bagwell S., *et al.*, "Supporting good health: the role of the charity sector", UK: New Philanthropy Capital, October 2014.

[53] Hamamci, A., Kucuk N., Karaman K, *et al.*, "Tumor-cut: segmentation of brain tumors on contrast enhanced MR images for radiosurgery applications", IEEE transactions on medical imaging, vol. 31, no. 3, pp. 790-804, December 2011.

[54] Chen X. and Pan L., "A Survey of Graph Cuts/Graph Search based Medical Image Segmentation", IEEE Reviews in Biomedical Engineering, vol. 11, pp. 112-124, January 2018.

[55] Vicente S., Kolmogorov V., and Rother C., "Graph cut based image segmentation with connectivity priors", IEEE Conference on Computer Vision and Pattern Recognition, pp. 1-8, June 2008.

[56] Tustison N. J., Avants B. B., Cook P. A., *et al.*, "N4ITK: improved N3 bias correction" IEEE transactions on medical imaging, vol. 29, no. 6, pp. 1310, June 2010.

[57] Bouwmans T., Silva C., Marghes C., "On the role and the importance of features for background modeling and foreground detection", Computer Science Review, vol. 28, pp. 26–91, May 2018.

[58] Wang X., Wang D., Yao Z., *et al.*, "Machine learning models for multi parametric glioma grading with quantitative result interpretations", Frontiers in neuroscience, vol. 12, 2018.

[59] Muerle T., "Experimental evaluation of techniques for automatic segmentation of objects in a complex scene", Pictorial Pattern Recognition, pp 3–13, 1968.

[60] Woods K., "Genetic Algorithms: Colour Image Segmentation Literature Review", Max Wertheimer. Laws of organization in perceptual forms (partial translation). Hayes Barton Press, 1938. 3, 58, 59. 2007

[61] Wertheimer M., "A source book of Gestalt theory", W. D. Ellis edition, p.1-11, (1938).

[62] Cheng M. M., Zhang G. X., Mitra N. J., *et al.*, "Global contrast based salient region detection" In Proceeding of Computer Vision and Pattern Recognition (CVPR), 2011 IEEE Conference on, pp. 409–416, 2011.

[63] Carreira J. and Sminchisescu C., "Constrained parametric min-cuts for automatic object segmentation", In Proceeding of Computer Vision and Pattern Recognition (CVPR), pp. 3241–3248, 2010.

[64] Arbelaez P., Maire M., Fowlkes C., *et al.*, "Contour detection and hierarchical image segmentation", IEEE Transaction on Pattern Analysis and Machine Intelligence, vol. 33, no. 5, pp. 898–916, May 2011.

[65] Shotton J., Winn J. M., Rother C., *et al.*, "TextonBoost: Joint appearance, shape and context modeling for multi-class object recognition and segmentation", In Proceeding on Computer Vision ECCV, pp. 1–15, May 2006.

[66] Everingham M., Van Gool L., Williams C. K. I., *et al.*, "The pascal visual object classes (voc) challenge", International Journal of Computer Vision, vol. 88, no. 2, June 2010.

[67] Meilă M., "Comparing clusterings—an information based distance", Journal of multivariate analysis, vol. 98, no. 5, pp. 873-895, May 2007.

[68] Martin D. R., Fowlkes C., Tal D., *et al.*, "A database of human segmented natural images and its application to evaluating segmentation algorithms and measuring ecological statistics" In Proceeding on Computer International Conference on Vision (ICCV), pp. 416–425, 2001.

[69] Mundy J. L., "Object recognition in the geometric era: A retrospective", Toward category level object recognition, pp. 3–28, 2006.

[70] Uijlings J. R. R., Van de Sande K. E. A., Gevers T., "Selective search for object recognition", International journal of computer vision, vol. 104, no. 2, pp. 154–171, 2013.

[71] Alexe B., Deselaers T., and Ferrari V., "Classcut for unsupervised class segmentation In Proceeding on Computer Vision–ECCV, pp. 380–393, 2010.

[72] Shotton J., JWinn. M., Rother C., *et al.*, "TextonBoost: Joint appearance, shape and context modeling for multi-class object recognition and segmentation", In Proceeding on Computer Vision-ECCV, pp. 1–15, May 2006.

[73] Lafferty J., McCallum A., and Pereira F. C. N., "Conditional random fields: Probabilistic models for segmenting and labeling sequence data", 2001.

[74] Arbeláez P., Hariharan B., Gu C., *et al.*, "Semantic segmentation using regions and parts" In Proceeding on Computer Vision and Pattern Recognition, pp. 3378–3385, 2012.

[75] http://eduscol.education.fr/numerique/tout-le-numerique/veille-education-numerique/juillet-2018/moteur-de recherche-darticles-scientifiques. Retrieved on December 2018.

[76] Salman Y. M., "Modified technique for volumetric brain tumor measurements", Journal of Biomedical Science and Engineering, vol. 2, no. 1, p. 16, February 2009.

[77] Hung M. C., Wu J., Chang J. H., *et al.*, "An efficient k-means clustering algorithm using simple partitioning", Journal of Information and Science and Engineering, vol. 21, no. 6, pp. 1157–1177, November 2005.

[78] Cai W., Chen S., Zhang D., "Fast and robust fuzzy c-means clustering algorithms incorporating local information for image segmentation", Pattern Recognition, vol. 40, no. 9, pp. 825–38, March 2007.

[79] Zalik K R., "An efficient k-means clustering algorithm", Pattern Recognition Letters, vol. 29, no. 9, pp. 1385–1391, July 2008.

[80] Rabeh A. B., Benzarti F, Amiri H., "Segmentation of brain MRI using active contour model" International Journal of Imaging System and Technology, vol. 27, no. 1, pp. 3-11, March 2017.

[81] Meier R., Knecht U., Loosli T., *et al.*, "Clinical evaluation of a fully-automatic segmentation method for longitudinal brain tumor volumetry", Scientific Report 6, Article no. 23376, March 2016.

[82] Hasan A, Meziane F, Aspin R, *et al.*, "Segmentation of brain tumors in MRI images using three-dimensional active contour without edge", Symmetry, vol. 8, no. 11, p. 132.

[83] El-Dahshan E. S. A., Mohsen H. M., Revett K., *et al.*, "Computer-aided diagnosis of human brain tumor through MRI: a survey and a new algorithm", Expert System Application, vol. 41, no. 11, pp. 5526–5545, 2014.

[84] Moeskops P., Viergever M. A., Mendrik A. M., *et al.*, "Automatic segmentation of MR brain images with a convolutional neural network", IEEE Transaction on Medical Imaging, vol. 35, no. 5, pp. 1252–1261, March 2016.

[85] Soltaninejad M., Yang G., Lambrou T., *et al.*, "Automated brain tumour detection and segmentation using superpixel-based extremely randomized trees in FLAIR MRI", International Journal on Computer Assisted Radiology Surgery, vol. 12, no. 2, pp. 183–203, February 2017.

[86] Saouli R., Akil M., Kachouri R., "Fully automatic brain tumor segmentation using end-to-end incremental deep neural networks in MRI images", Computer methods and programs in biomedicine, vol. 166, pp. 39–49, November 2018.

[87] Soltaninejad M, Yang G., Lambrou T., *et al.*, "Supervised learning based multimodal MRI brain tumour segmentation using texture features from supervoxels" Computer methods and programs in biomedicine, vol. 157, pp. 69–84, April 2018.

[88] Ilunga-Mbuyamba E., Cruz-Duarte J. M., Avina-Cervantes J. G., *et al.*, "Active contours driven by cuckoo search strategy for brain tumour images segmentation" Expert System Application, vol. 56, pp. 59–68, September 2016.

[89] Lok K. H., Shi L., Zhu X., *et al.*, "Fast and robust brain tumor segmentation using level set method with multiple image information", Journal of X-Ray Science and Technology, vol. 25, no. 2, pp. 301–312, January 2017.

[90] Mahata N., Kahali S., Adhikari S. K, *et al.*, "Local contextual information and gaussian function induced fuzzy clustering algorithm for brain MR image segmentation and intensity inhomogeneity estimation", Applied Soft Computer, vol. 68, pp. 586–96, July 2018.

[91] Derraz F., Beladgham M, Khelif M., "Application of active contour models in medical image segmentation", In Proceeding on International Conference on Information Technology: Coding and Computing, vol. 2, pp. 675–81, April 2004..

[92] Meier R., Knecht U., Loosli T., *et al.*, "Clinical evaluation of a fully-automatic segmentation method for longitudinal brain tumor volumetry", Scientific Report 6, Article no. 23376, March 2016.

[93] Gordillo N., Montseny E., Sobrevilla P., "State of the art survey on MRI brain tumor segmentation", Magnetic Resonanace Imaging, vol. 31, no. 8, pp. 1426–1438, October 2013.

[94] Otsu N., "A threshold selection method from gray-level histograms" IEEE Transaction on System Man Cybernetics, vol. 9, no. 1, pp. 62-66, January 1979,

[95] SungY-C., Han K-S., Song C-J., *et al.*, "Threshold estimation for region segmentation on MR image of brain having the partial volume artifact", In proceedings on 5th international conference on signal processing proceedings, WCCC-ICSP, vol. 2, pp 1000–1009, August 2000.

[96] Stadlbauer A., Moser E., Gruber S., *et al.*, "Improved delineation of brain tumors: an automated method for segmentation based on pathologic changes of 1H-MRSI metabolites in gliomas", NeuroImage, vol. 23, no. 2, pp. 454–461, October 2004.

[97] Kim D. Y., Park J. W., "Connectivity-based local adaptive thresholding for carotid artery segmentation using MRA images", Image and Vision Computing, vol. 23, no. 14, pp. 1277–87, December 2005.

[98] Shanthi K., Kumar M. S., "Skull stripping and automatic segmentation of brain MRI using seed growth and threshold techniques" In proceeding International conference on intelligent and advanced systems, pp 422–426, November 2007.

[99] Taheri S., Ong S., Chong V., "Level-set segmentation of brain tumors using a threshold-based speed function" Image and Vision Computing, vol. 28, no. 1, pp. 26–37, January 2010.

[100] Sujan M., Alam N., Abdullah S., *et al.*, "A segmentation based automated system for brain tumor detection", International Journal on Computer Application, vol. 153, no. 10, pp. 41–9, November 2016;.

[101] Ilhan U., Ilhan A., "Brain tumor segmentation based on a new threshold approach" Procedia Comput Science, vol. 120, pp. 580–587, January 2017.

[102] Pavlidis T., and Liow Y-T., "Integrating region growing and edge detection", IEEE Transactions on Pattern Analysis and Machine Intelligence, vol. 12, no. 3, pp. 225-233, March 1990.

[103] Kallergi, M., Woods, K., Clarke, L. P., *et al.*, "Image segmentation in digital mammography: comparison of local thresholding and region growing algorithms", Computerized medical imaging and graphics, vol. 16, no. 5, pp. 323-331, September 1992.

[104] Gambotto, J. P., "A new approach to combining region growing and edge detection", Pattern Recognition Letters, vol. 14, no. 11, pp. 869-875, November 1993.

[105] Adams R., and Bischof L., "Seeded region growing", IEEE Transactions on pattern analysis and machine intelligence, vol. 16, no. 6, pp. 641-647, June 1994.

[106] Zhu S. C. and Yuille A., "Region competition: Unifying snakes, region growing, and Bayes/MDL for multiband image segmentation", IEEE transactions on pattern analysis and machine intelligence, vol. 18, no. 9, pp. 884-900, September 1996.

[107] Tremeau A., and Borel N., "A region growing and merging algorithm to color segmentation", Pattern recognition, vol. 30, no. 7, pp. 1191-1203, July 1997.

[108] Fan J., Yau D. K., Elmagarmid, A. K., *et al.*, "Automatic image segmentation by integrating color-edge extraction and seeded region growing", IEEE transactions on image processing, vol. 10, no. 10, pp. 1454-1466, October 2001.

[109] Zhao, Yu Qian, *et al.*, "Retinal vessels segmentation based on level set and region growing", Pattern Recognition, vol. 47, no. 7, pp. 2437-2446, 2014.

[110] Lu X., Wu, J., Ren, X., *et al.*, "The study and application of the improved region growing algorithm for liver segmentation", Optik-International Journal for Light and Electron Optics, vol. 125, no. 9, pp. 2142-2147, May 2014.

[111] Rouhi, R., Jafari, M., Kasaei, S., *et al.*, "Benign and malignant breast tumors classification based on region growing and CNN segmentation", Expert Systems with Applications, vol. 42, no. 3, pp. 990-1002, February 2015.

[112] Kuo W-F., Lin C-Y., Sun Y-N., "Brain MR images segmentation using statistical ratio: mapping between watershed and competitive hopfield clustering network algorithms", Computer Methods Programs Biomedicine, vol. 91, no. 3, pp. 191–198, September 2008.

[113] Li N, Liu M, Li Y., "Image segmentation algorithm using watershed transform and level set method", In proceedings on IEEE international conference on acoustics, speech and signal processing, vol .1, pp I–613, April 2015.

[114] Gies V., Bernard T. M., "Statistical solution to watershed oversegmentation", In proceeding on International conference on image processing, vol. 3, pp. 1863–1866, October 2004.

[115] Bleau A., Leon L. J., "Watershed-based segmentation and region merging" Computer Vision Image Understanding, vol. 77, no. 3, pp. 317–370, March 2000.

[116] Bhattacharya M., Das A., "A study on seeded region based improved watershed transformation for brain tumor segmentation, 2008.

[117] Ratan R., Sharma S., Sharma S., "Multiparameter segmentation and quantization of brain tumor from MRI images", Indian Journal of Science and Technology, vol. 2, no. 2, pp. 11–15, February 2009.

[118] Chen, C. W., Luo J., and Parker K. J., "Image segmentation via adaptive K-mean clustering and knowledge-based morphological operations with biomedical

applications", IEEE transactions on image processing, vol. 7, no. 12, pp. 1673-1683, December 1998.

[119] Ng, H. P., Ong, S. H., Foong, K. W. C., *et al.*, "Medical image segmentation using k-means clustering and improved watershed algorithm", Southwest Symposium on Image Analysis and Interpretation, pp. 61-65, March 2006.

[120] Fahim, A. M., Salem, A. M., Torkey, F. A., *et al.*, "An efficient enhanced k-means clustering algorithm", Journal of Zhejiang University-Science A, vol. 7, no. 10, pp. 1626-1633, October 2006.

[121] Purohit, Pallavi, and Ritesh Joshi. "A new efficient approach towards k-means clustering algorithm." International Journal of Computer Applications, vol. 65, no. 11, 2013.

[122] Despotović I., Goossens B., and Philips W., "MRI segmentation of the human brain: challenges, methods, and applications", Computational and mathematical methods in medicine, 2015.

[123] Rahi A., "MRI segmentation by K-mean clustering method and detection of leasions", Inernational Journal of science and research (IJSR), vol. 4, issue 6, pp.2484-2492, June 2015

[124] Dhanachandra, N., Manglem, K., & Chanu, Y. J., "Image segmentation using K-means clustering algorithm and subtractive clustering algorithm", Procedia Computer Science, vol. 54, pp. 764-77, January 2015.

[125] Clark, M. C., Hall, L. O., Goldgof, D. B. *et al.*, "MRI segmentation using fuzzy clustering techniques", IEEE Engineering in Medicine and Biology Magazine, vol. 13, no. 5, pp. 730-742, November 1994.

[126] Pedrycz W., and Waletzky J., "Fuzzy clustering with partial supervision", IEEE Transactions on Systems, Man, and Cybernetics, Part B (Cybernetics), vol. 27, no. 5, pp. 787-795, September 1997.

[127] Iyer, N. S., Kandel A, and Schneider M., "Feature-based fuzzy classification for interpretation of mammograms" Fuzzy Sets and Systems, vol. 114, no. 2, pp. 271-280, September 2000.

[128] Ahmed, M. N., Yamany, S. M., Mohamed, N., *et al.*, "A modified fuzzy c-means algorithm for bias field estimation and segmentation of MRI data", IEEE transactions on medical imaging, vol. 21, no. 3, pp. 193-199, March 2002.

[129] Chuang, K. S., Tzeng, H. L., Chen, S., *et al.*, "Fuzzy c-means clustering with spatial information for image segmentation", computerized medical imaging and graphics, vol. 30, no. 1, pp. 9-15, January 2006.

[130] Krishnapuram R., and Kim J., "A note on the Gustafson-Kessel and adaptive fuzzy clustering algorithms", IEEE Transactions on Fuzzy systems, vol. 7, no. 4, pp. 453-461, August 1999.

[131] Benaichouche A. N., Oulhadj H., and Siarry P., "Improved spatial fuzzy c-means clustering for image segmentation using PSO initialization, Mahalanobis distance and post-segmentation correction", Digital Signal Processing, vol. 23, no. 5, pp. 1390-1400, 2013.

[132] Wells W. M., Grimson W. E. L., Kikinis R., *et al.*, "Adaptive segmentation of MRI data" IEEE Transaction Medical Imaging, vol. 15, no. 4, pp. 429–442, August 1996.

[133] Held K., Kops E. R., Krause B. J., *et al.*, "Markov random field segmentation of brain MR images", IEEE Transaction Medical Imaging, vol. 16 no. 6, pp. 878–886, December 1997.

[134] Leemput V., Maes, F. K., Vandermeulen, D., *et al.*, "Automated model-based tissue classification of MR images of the brain", IEEE Transaction Medical Imaging, vol. 18, no. 10, pp. 897–908.

[135] Capelle A. S., Alata O., Fernandez C., *et al.*, "Unsupervised segmentation for automatic detection of brain tumors in MRI", In Proceedings of international conference on image processing, vol. 1, pp. 613–616.

[136] Pham D. L., Xu C., Prince J. L., "Current methods in medical image segmentation" Annual Review of Biomedical Engineering, vol. 2, no. 1, pp. 315–337, August 2000.

[137] Gering D. T., Grimson W. E. L., Kikinis R., "Recognizing deviations from normalcy for brain tumor segmentation", In International Conference on Medical Image Computing and Computer-Assisted Intervention, pp. 388-395, September 2002.

[138] Tran, T. N., Wehrens, R., & Buydens, L. M., "Clustering multispectral images: a tutorial" Chemometrics and Intelligent Laboratory Systems, vol. 77, no. 1–2, pp. 3–17, May 2005.

[139] Warfield S. K., Kaus M., Jolesz F. A., *et al.*, "Adaptive, template moderated, spatially varying statistical classification", Medical Image Analysis, vol. 4, no. 1, pp. 43–55, March 2000.

[140] Cocosco C. A., Zijdenbos A. P., Evans A. C., *et al.*, "A fully automatic and robust brain MRI tissue classification method", Medical Image Analysis, vol. 7, no. 4, pp. 513–527, December 2003.

[141] Khalid N. E. A., Ibrahim S., Haniff P., "MRI brain abnormalities segmentation using knearest neighbors (k-NN)", International Journal of Computer Science and Engineering, vol. 3, no. 2, pp. 980–990, February 2011.

[142] Steenwijk M. D., Pouwels P. J., Daams M., *et al.*, "Accurate white matter lesion segmentation by k nearest neighbor classification with tissue type priors (kNN-TTPs)", NeuroImage: Clinical, vol. 3, pp. 462–469, January 2013.

[143] Ozkan M., Dawant B. M., Maciunas R. J., "Neural-network based segmentation of multi-modal medical images: a comparative and prospective study", IEEE Transaction on Medical Imaging, vol. 12, no. 3, pp. 534–544, September 1993.

[144] Chaplot S., Patnaik L., Jagannathan N., "Classification of magnetic resonance brain images using wavelets as input to support vector machine and neural network", Biomed Signal Processing Control, vol. 1, no. 1, pp. 86–92, January 2006.

[145] Kavitha A. R., Chellamuthu C., Rupa K., "An efficient approach for brain tumour detection based on modified region growing and neural network in MRI images", In proceedings on international Conference on Computing, Electronics and Electrical Technologies (ICCEET), pp. 1087–1095, March 2012.

[146] Damodharan S., Raghavan D., "Combining tissue segmentation and neural network for brain tumor detection", International Arab Journal of Information Technology, vol. 12, no. 1, pp. 42–52, January 2015.

[147] Wang S., Zhang Y., Dong Z., *et al.*, "Feed-forward neural network optimized by hybridization of PSO and ABC for abnormal brain detection", International Journal of Imaging System and Technology, vol. 25, no. 2, pp. 153–64, June 2015.

[148] Muhammad N., Fazli W., Sajid A. K., "A simple and intelligent approach for brain MRI classification", Journal of Intelligent & Fuzzy Systems, vol. 28, no., 3, pp. 1127–35, January 2015.

[149] Sharma M., Purohit G. N., Mukherjee S., "Information retrieves from brain MRI images for tumor detection using hybrid technique K-means and artificial neural network(KMANN)", Networking communication and Data Knowledge Engineering, pp. 145-157, 2018.

[150] Vijayakumar C., Damayanti G., Pant R., *et al.*, "Segmentation and grading of brain tumors on apparent diffusion coefficient images using self-organizing maps", Computerized Medical Imaging and Graphics, vol. 31, no. 7, pp. 473–484.

[151] Reddick W. E., Glass J. O., Cook E. N., *et al.*, "Automated segmentation and classification of multispectral magnetic resonance images of brain using artificial neural networks", IEEE Transaction on Medical Imaging, vol. 16, no. 6, pp. 911–918.

[152] Murugavalli S., Rajamani V., "An improved implementation of brain tumor detection using segmentation based on neuro fuzzy technique", Journal of Computer Science, vol. 3, no. 11, pp. 841–846, 2007.

[153] Tayel M. B., Abdou M. A., *et al.*, "A neuro-difference fuzzy technique for automatic segmentation of region of interest in medical imaging. In: Proceedings of the twenty third national radio science conference, pp 1–7, March 2014.

[154] Wells W., Grimson W. E. L., Kikinis R., *et al.*, "Adaptive segmentation of MRI data" Inproceedings on Computer vision, virtual reality and robotics in medicine, pp. 59–69, March 2014.

[155] Li C., Xu C., Gui C., *et al.*, "Distance regularized level set evolution and its application to image segmentation", IEEE Transaction Image Processing, vol. 19, no. 12, p. 3243, August 2010.

[156] Rajendran A., Dhanasekaran R., "Fuzzy clustering and deformable model for tumor segmentation on MRI brain image: a combined approach", Procedia Engineering, vol. 30, pp. 327–333, January 2012.

[157] Cobzas D., Birkbeck N., Schmidt M., *et al.*, "3D variational brain tumor segmentation using a high dimensional feature set", In Proceedings of the 2007 IEEE 11th international conference on computer vision, pp. 14–21, October 2007.

[158] Prastawa M., Bullitt E., Moon N., *et al.*, "Automatic brain tumor segmentation by subject specific modification of atlas priors", Academic radiology, vol. 10, no. 12, pp. 1341–1348, December 2003.

[159] Ho S., Bullitt E., Gerig G., "Level-set evolution with region competition: automatic 3-D segmentation of brain tumors", In Proceedings of 16th international conference on pattern recognition, vol. 1., p. 10532, August 2002.

[160] Sethian J. A., "Level set methods, evolving interfaces in geometry, fluid mechanics computer vision, and materials sciences", Cambridge: Cambridge university press, vol. 3, January 1996.

[161] Gui L., Lisowski R., Faundez T., *et al.*, "Morphology-driven automatic segmentation of MR images of the neonatal brain", Medical Image Analysis, vol. 16, no. 8, pp. 1565–1579, December 2012.

[162] Wang L., Shi F., Li G., *et al.*, "Segmentation of neonatal brain MR images using patch-driven level sets", NeuroImage, vol. 84, pp. 141–158, January 2014.

[163] Kass M., Witkin A., Terzopoulos D., "Snakes: active contour models", International Jounal of Comput Vision, vol. 1, no. 4, pp. 321–331, January 1988.

[164] Terzopoulos D., Witkin A. P., Kass M., "Constraints on deformable models: recovering 3D shape and nonrigid motion", Artificial Intelligence, vol. 36, no. 1, pp. 91–123, August 1988.

[165] Cohen L. D., Cohen I., "Finite-element methods for active contour models and balloons for 2-D and 3-D images", IEEE Transaction on Pattern Analysis and Machine Intelligence, vol. 15, no. 11, pp. 1131–1147, November 1993.

[166] Chan T. F., Vese L. A., "Active contours without edges", IEEE Transaction Image Processing, vol. 10, no. 2, pp. 266–277, February 2001..

[167] Kichenassamy S., Kumar A., Olver P., *et al.*, "Gradient flows and geometric active contour models", In Proceedings of fifth international conference on computer vision, pp 810–815, June 1995.

[168] Malladi R., Sethian J. A., Vemuri B. C., "Shape modeling with front propagation: a level set approach", IEEE Transaction on Pattern Analysis Machine Intelligence, vol. 17, no. 2, pp. 158–175, Feburary 1995.

[169] Caselles V., Kimmel R., Sapiro G., "Geodesic active contours", International Journal of Computer Vision, vol. 22, no. 1, pp. 61–79, February 1997.

[170] Li C., Huang R., Ding Z., *et al.* "A level set method for image segmentation in the presence of intensity inhomogeneities with application to MRI", IEEE Trans Image Process, vol. 20, no. 7, April 2007.

[171] Huang A., Abugharbieh R., Tam R., "Initiative ADN *et al.* (2009) A hybrid geometric-statistical deformable model for automated 3-D segmentation in brain MRI", IEEE Transaction on Biomedical Engineering, vol. 56, no. 7, pp. 1838–1848.

[172] Sagiv C., Sochen N. A., Zeevi Y. Y., "Integrated active contours for texture segmentation", IEEE Transaction on Image Processing, vol. 15, no. 6, pp. 1633–1646.

[173] Ilunga-Mbuyamba E., Avina-Cervantes J. G., Garcia-Perez A., *et al.*, "Localized active contour model with background intensity compensation applied on automatic MR brain tumor segmentation", NeuroComputing, vol. 220, pp. 84–97.

[174] Wu Z., Leahy R., "An optimal graph theoretic approach to data clustering: theory and its application to image segmentation" IEEE Transactions on Pattern Analysis and Machine Intelligence, vol. 15, no. 11, pp. 1101–1113, November 1993.

[175] Boykov Y., Veksler O. and. Zabih R, "Fast approximate energy minimization via graph cuts" In proceeding on International Conference on Computer Vision, pp. 377–384, November 1999

[176] Yuri Y. B., Jolly M. P., "Interactive Graph Cuts for optimal Boundary & Region Segmentation of Objects in N-D Images", Proceedings of International Conference on Computer Vision, vol. 1, pp.105-112, July 2001.

[177] Freedman D., Zhang T., "Interactive graph cut based segmentation with shape priors" IEEE computer society conference on CVPR, vol.1, pp.755-762, June 2005.

[178] Yuri Y. B., Lea G. F., "Graph Cuts and Efficient N-D Image Segmentation," International Journal of Computer Vision, vol.70, no.2, pp.109-131, November 2006.

[179] Furnstahl P., Schweizer A., Nagy L., *et al.*, "Automatic and robust forearm segmentation using graph cuts" IEEE inter symposium on ISBI, pp.77-80, May 2008.

[180] Nhat V., Manjunath B. S., "Shape prior segmentation of multiple objects with graph cuts" IEEE conference on CVPR, pp.1-8, June 2008.

[181] Zhou J., Ye M., Zhang X, "Graph cut segmentation with automatic editing for Industrial images" Inter conference on ICICIP, pp.633-637, August 2010.

[182] Wu X., Xu W., Li L., *et al.*, "An Interactive Segmentation Method Using Graph Cuts for Mamographic Masses", International conference on iCBBE, pp.1-4, May 2011.

[183] Li Z., Wu X., Chang S., "Segmentation using superpixels: a bipartite graph partitioning approach" In proceeding on IEEE International Conference on Computer Vision and Pattern Recognition, pp. 789-796, June 2012.

[184] Mahapatra D. and Buhmann J. M., "Prostate MRI segmentation using learned semantic knowledge and graph cuts", IEEE transactions on bio-medical engineering, vol. 61, pp. 756-64, November 2013.

[185] Ju W., Xiang D., Zhang B., *et al.*, "Random Walk and Graph Cut for Co-Segmentation of Lung Tumor on PET-CT Images" IEEE Transactions on Image Processing, vol. 24, pp. 5854-5867, October 2015.

[186] Pauchard, Y., Fitze, T., Browarnik, D., *et al.*, "Interactive graph-cut segmentation for fast creation of finite element models from clinical CT data for hip fracture prediction. Computer methods in biomechanics and biomedical engineering", vol. 19, no. 16, pp. 1693-1703, December 2016.

[187] Fang L, Cunefare D, Wang C, *et al.*, "Automatic segmentation of nine retinal layer boundaries in OCT images of non-exudative AMD patients using deep learning and graph search" Biomedical Optics Express, vol. 8, no. 5, pp. 2732, May 2017.

[188] Gamechi, Z. S., Arias-Lorza, A. M., Pedersen, J. H., *et al.*, "Aorta and pulmonary artery segmentation using optimal surface graph cuts in non-contrast CT", Society of Photo-Optical Instrumentation Engineers (SPIE) Conference Series, vol. 10574, p. 105742D, March 2018.

[189] Arias Lorza, A. M., Van Engelen, A., Petersen, J., *et al.*, "Maximization of regional probabilities using Optimal Surface Graphs: Application to carotid artery segmentation in MRI", Medical physics, vol. 45, no. 3, pp. 1159-1169, March 2018.

[190] Castaño, M., García, H. F., Porras-Hurtado, *et al.*, "Enhanced Graph Cuts for Brain Tumor Segmentation Using Bayesian Optimization" In Iberoamerican Congress on Pattern Recognition, pp. 774-782, November 2018.

[191] Song, X., Wang, Y., Feng, Q., *et al.*, "Improved graph cut model with features of superpixels and neighborhood patches for myocardium segmentation from ultrasound

image" Mathematical Biosciences and Engineering, vol. 16, no. 3, pp. 1115-1137, January 2019.

[192] Reza M. N., Na I. S., Baek S. W., *et al.*, "Rice yield estimation based on K-means clustering with graph-cut segmentation using low-altitude UAV images", Biosystems engineering, vol. 177, pp. 109-121, January 2019.

[193] Zhang F. Z., Wang J. P., & Jiang W., "An integrative classification model for multiple sclerosis lesion detection in multimodal MRI", Statistics and its Interface, vol. 12, no. 2, pp. 193-202, January 2019.

[194] Patel D., Vankawala F., & Bhatt B., "A Survey on Identification of Glioblastoma Multiforme and Low-Grade Glioma Brain Tumor Type", In 2019 International Conference on Communication and Signal Processing (ICCSP), pp. 0335-0339, April 2019.

[195] Subashini, M. M., Sahoo, S. K., Sunil, V., *et al.*, "A Non-Invasive Methodology for the Grade Identification of Astrocytoma Using Image Processing and Artificial Intelligence Techniques", Expert Systems with Applications, vol. 43, pp. 186-196, January 2016.

[196] Polly F. P., Shil S. K., Hossain M. A., *et al.*, "Detection and Classification of HGG and LGG Brain Tumor Using Machine Learning," International Conference on Information Networking (ICOIN), January 2018.

[197] Gupta N., Bhatele P., & Khanna P., *et al.*, "Identification of Gliomas from Brain MRI through Adaptive Segmentation and Run Length of Centralized Patterns," Journal of Computational Science, vol. 25, pp. 213-220, March 2018.

[198] Arakeri M. P., Reddy G.R.M., "Computer-aided diagnosis system for tissue characterization of brain tumor on magnetic resonance images", Signal Image and Video Processing, vol. 9, pp. 409-425, February 2013.

[199] Li G., Yang J., Ye C., *et al.*, "Degree prediction of malignancy in brain glioma using support vector machines", Computer Biology Medicine, vol. 36, pp. 313-325, March 2006.

[200] Alfonse M. and Salem A. B. M., "An automatic classification of brain tumors through MRI using support vector machine," Egyptian Computer Science Journal, vol. 40, pp. 11-21, September 2016.

[201] Ahuja R. K., Magnanti T. L., and Orlin J. B., "Network Flows: Theory, Algorithms, and Applications", Prentice-Hall, pp. 1-83, January1993.

[202] Ford L. R. and Fulkerson D. R., "Flows in Networks", Princeton University Press, vol. 59, 1962.

[203] Goldberg A. V. and Tarjan R. E., "A new approach to the maximum flow problem", Journal of the Association for Computing Machinery, vol. 35, no. 4, pp. 921–940, October 1988.

[204] Edmonds J. and Karp R. M., "Theoretical improvements in algorithmic efficiency for network flow problems", Journal of the ACM, vol. 19, no. 2, pp. 248–264, April 1972.

[205] Goldberg A. V. and Tarjan R. E. "A new approach to the maximum flow problem", Journal of the Association for Computing Machinery, vol. 35, no. 4, pp. 921–940, October 1988.

[206] Cherkassky B. V. and Goldberg A. V., "On implementing push-relabel method for the maximum flow problem", In proceeding on International Conference on Integer Programming and Combinatorial Optimization, pp. 157-171, 1994.

[207] Geman S. and Geman D., "Stochastic relaxation, gibbs distributions, and the Bayesian restoration of images", IEEE Transactions on Pattern Analysis and Machine Intelligence, vol. 6, pp. 721–741, November 1984.

[208] Greig D. M., Porteous B. T., and Seheult A. H., "Exact maximum a posteriori estimation for binary images", Journal of the Royal Statistical Society. Series B., vol. 51, no. 2pp. 271–279, 1989.

[209] Boykov Y., Veksler O., and. Zabih R., "Markov random fields with efficient approximations" In proceeding on IEEE Conference on Computer Vision and Pattern Recognition, pp. 648–655, June 1998.

[210] Szeliski R., Zabih R., Scharstein D., *et al.*, "A comparative study of energy minimization methods for Markov random fields with smoothness-based priors", IEEE Transactions on Pattern Analysis and Machine Intelligence, vol. 30, no. 6, pp. 1068–1080, 2008.

[211] Kolmogorov V. and Rother C., "Comparison of energy minimization algorithms for highly connected graphs", In proceeding on 9th European Conference on Computer Vision, pp. 1–15, May 2006.

[212] Kohli P., "Minimizing Dynamic and Higher Order Energy Functions using Graph Cuts", Oxford Brookes University, Oxford, United Kingdom, 2007.

[213] Kohli P., Kumar M. P., and Torr P. H. S., "P3 & beyond: Solving energies with higher order cliques", In proceeding on Computer Vision and Pattern Recognition, pp. 1–8, June 2007.

[214] Kolmogorov V. and Rother C., "Minimizing non-submodular functions with graph cuts -a review", IEEE Transactions on Pattern Analysis and Machine Intelligence, vol. 29, no. 7, pp. 1274–1279, July 2007.

[215] Komodakis N., "Optimization Algorithms for Discrete Markov Random Fields, with Applications to Computer Vision", PhD thesis, University of Crete, Heraklion, Crete, 2006.

[216] Komodakis N., Tziritas G., and Paragios N., "Fast, approximately optimal solutions for single and dynamic MRFs", In proceeding on Computer Vision and Pattern Recognition, pp. 1–8, June 2007.

[217] Ishikawa H., "Higher-order clique reduction in binary graph cut", In proceedings on Computer Vision and Pattern Recognition, pp. 2993–3000, June 2010.

[218] Ishikawa H., "Exact optimization for Markov random fields with convex priors", IEEE Transactions on Pattern Analysis and Machine Intelligence, vol. 25:1333–1336, 2003.

[219] Kolmogorov V., "Graph Based Algorithms for Scene Reconstruction from Two or More Views", PhD thesis, Cornell University, USA, 2004.

[220] Kolmogorov V. and Zabih R., "What energy functions can be minimized via graph cuts?", IEEE Transactions on Pattern Analysis and Machine Intelligence, vol. 26, no. 2, pp. 147–159, May 2004.

[221] Dufour A., Shinin V., Tajbakhsh S., *et al.*, "Segmenting and tracking fluorescent cells in dynamic 3-D microscopy with coupled active surfaces", IEEE Transactions on Image Processing, vol. 14, no. 9, pp. 1396–1410, September 2005.

[222] Adams R. and Bischof L., "Seeded region growing", IEEE Transactions on pattern analysis and machine intelligence, vol. 16, no. 6, pp. 641-647, June 1994.

[223] Manousakas I. N., Undrill P. E., Cameron G. G., *et al.*, "Split-and-merge segmentation of magnetic resonance medical images: performance evaluation and extension to three dimensions", Computers and Biomedical Research, vol. 31, no. 6, pp. 393-412. December 1998.

[224] Grady, L., Schiwietz, T., Aharon, S., *et al.*, "Random walks for interactive organ segmentation in two and three dimensions: Implementation and validation", In Medical image computing and computer-assisted intervention (MICCAI), pp. 773–780, October 2005.

[225] Kwon D., Shinohara R. T., Akbari H., *et al.*, "Combining generative models for multifocal glioma segmentation and registration", In proceeding on International Conference on Medical Image Computing and Computer-Assisted Intervention, pp. 763-770, September 2014.

[226] Rosenfeld, A., and Pfaltz, J. L., "Sequential operations in digital picture processing", Journal of the ACM, vol. 13, no.4, pp. 471-494, October 1966.

[227] Park, C., Huang, J. Z., Ji, J. X., *et al.*, "Segmentation, inference and classification of partially overlapping nanoparticles", IEEE transactions on pattern analysis and machine intelligence, Vol. 35, no. 3, pp. 1-1, August 2012.

[228] Rao, B. D., & Goswami, M. M., "A comprehensive study of features used for brain tumor detection and segmentation from MR images" In Proceeding on Innovations in Power and Advanced Computing Technologies (i-PACT), pp. 1-6, April 2017.

[229] Nyúl, L. G., Udupa, J. K., and Zhang, X., "New variants of a method of MRI scale standardization", IEEE Trans. Med. Imag., vol. 19, no. 2, pp. 143–150, February 2000.

[230] Shah, M., Xiao, Y., Subbanna, N., *et al.*, "Evaluating intensity normalization on MRIs of human brain with multiple sclerosis", Medical image analysis, vol. 15, no. 2, pp. 267–282, April 2011.

[231] Dogra, J., Jain, S., and Sood, M., "Segmentation of MR Images using Hybrid kMean-Graph Cut Technique", Procedia Computer Science, vol. 132, pp. 775-784, January 2018.

[232] Muthupillai, R., Lomas D. J., Rossman P. J., *et al.*, "Magnetic resonance elastography by direct visualization of propagating acoustic strain waves", Science, vol. 269, no. 5232, pp. 1854-1857, September 1995.

[233] Holsinger A. E., Wright R. C., Riederer S. J., *et al.*, "Real-time interactive magnetic resonance teimaging", Magnetic resonance in medicine, vol. 14, no. 3, pp. 547-553, June 1990.

[234] 3 Katti G., Ara S. A., and Shireen A., "Magnetic resonance imaging (MRI)–A review", International journal of dental clinics, vol. 3, no. 1, March 2011.

[235] Herrera S. L., "Inferring axon diameters using magnetic resonance imaging oscillating gradient spin echo sequences", 2018.

[236] International Commission on Non-Ionizing Radiation Protection. Guidelines for limiting exposure to time-varying electric and magnetic fields (1 Hz to 100 kHz). Health physics, vol. 99, no. 6, pp. 818-836, December 2010.

[237] Jin J., "Electromagnetic analysis and design in magnetic resonance imaging", Routledge, February 2018.

[238] Despotović I., Goossens B., and Philips W., "MRI segmentation of the human brain: challenges, methods, and applications", Computational and mathematical methods in medicine, 2015.

[239] Hou Z., "A review on MR image intensity inhomogeneity correction. International journal of biomedical imaging", 2006.

[240] 9 Juntu J., Sijbers J., Van Dyck D., and Gielen J., "Bias field correction for MRI images" In Computer Recognition Systems, pp. 543-551, 2005.

[241] Tustison N. J., Avants B. B., Cook P. A., *et al.*, "N4ITK: improved N3 bias correction" IEEE transactions on medical imaging, vol. 29, no. 6, pp. 1310, June 2010.

[242] D'agostino E., Maes F., Vandermeulen D., *et al.*, "Aviscous fluid model for multimodal non-rigid image registration using mutual information" In Proceedings of the Medical Image Computing and Computer Assisted Intervention (MICCAI '02), pp. 541–548, December 2002.

[243] Sled J. G., Zijdenbos A. P., and Evans A. C., "A nonparametric method for automatic correction of intensity non uniformity in MRI data" IEEE Transactions on Medical Imaging, vol. 17, no. 1, pp. 87–97, February 1998.

[244] Lewis E. B., and Fox N. C., "Correction of differential intensity inhomogeneity in longitudinal MR images" NeuroImage, vol. 23, no. 1, pp. 75–83, September 2004.

[245] Shattuck D. W., Sandor-Leahy S. R., Schaper K. A., *et al.*, "Magnetic resonance image tissue classification using a partial volume model" NeuroImage, vol. 13, no. 5, pp. 856–876, May 2001.

[246] Louis, D. N., Ohgaki, H., Wiestler, O. D., *et al.*, "The 2007 WHO classification of tumours of the central nervous system" , in Acta neuropathological, vol. 114, no. 2, pp. 97-109, August 2007.
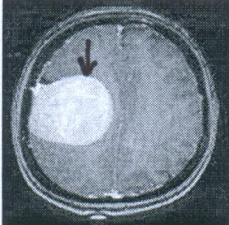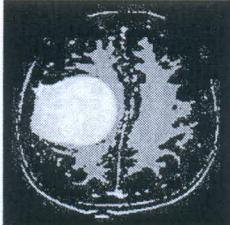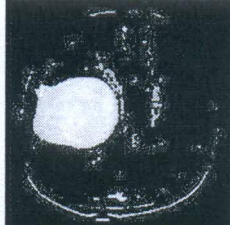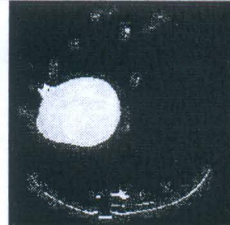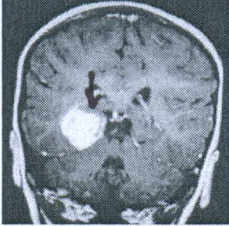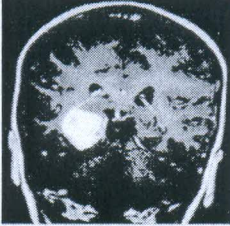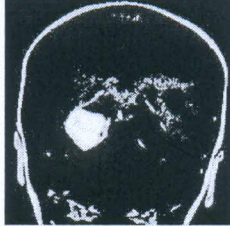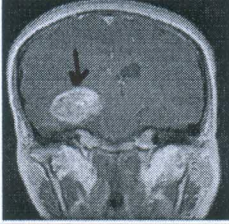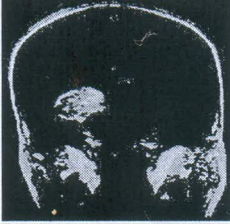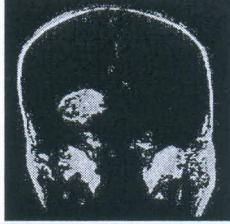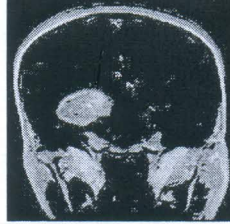
[247] Kreth, F. W., Faist, M., Rossner, R., *et al.*, "Supratentorial World Health Organization grade 2 astrocytomas and oligoastrocytomas: a new pattern of prognostic factors", Cancer, Vol. 79, no. 2, pp. 370-379, January 1997.

[248] Upadhyay, N., and Waldman, A., "Conventional MRI evaluation of gliomas", The British journal of radiology Vol. 84, no. 2, pp. S107-S111, December 2011.

[249] Biron K. E., Dickstein D. L., Gopaul R., and Jefferies, W. A., "Amyloid triggers extensive cerebral angiogenesis causing blood brain barrier permeability and hypervascularity in Alzheimer's disease", PloS one, vol. 6, no. 8, e23789, August 2011.

[250] Dogra, J., Jain, S., and Sood, M., "Glioma extraction from MR images employing Gradient Based Kernel Selection Graph Cut technique", The Visual Computer, vol. 35, no. 10, pp. 1-17, May 2019.

[251] Bryman, A., and Cramer, D., "Quantitative data analysis with IBM SPSS 17, 18 & 19: A guide for social scientists", Routledge, August 2012.

[252] Abusamra, H., "A comparative study of feature selection and classification methods for gene expression data of glioma", Procedia Computer Science, Vol. 23, pp. 5-14, January 2013.

[253] Kolmogorov, V., and Boykov, Y., "What metrics can be approximated by geo-cuts, or global optimization of length/area and flux" In Proceedings on the 10th IEEE International Conference on Computer Vision, Vol. 1, pp. 564–571, October 2005.

[254] Haralick, R. M., Shanmugam, K., and Dinstein, I. H., "Textural features for image classification", IEEE Transactions on Systems, Man and Cybernetics, vol. 3, no. 6, pp. 610–621, November 1973.

[255] Skogen, K., Schulz, A., Dormagen, J. B., *et al.*, "Diagnostic performance of texture analysis on MRI in grading cerebral gliomas", European journal of radiology, vol. 85, no. 4, pp. 824-829, April 2016.

[256] Galloway, M. M., "Texture analysis using grey level run lengths", Computer Graphics and Image Processing, vol. 4, no. 2, pp. 172–179, June 1975.

[257] Vapnik V., Levin E., and Cun Y. L., "Measuring the VC-dimension of a learning machine", Neural computation, vol. 6, no. 5, pp. 851-876, September 1994.

[258] Zhang, M. L., and Zhou, Z. H., "A k-nearest neighbor based algorithm for multi-label classification", GrC, vol. 5, pp. 718-721, July 2005.
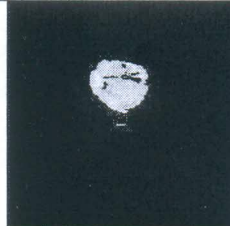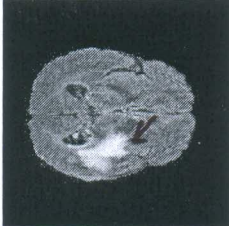
[259] Zacharaki, E. I., Wang, S., Chawla, S., *et al.*, "Classification of brain tumor type and grade using MRI texture and shape in a machine learning scheme", Magnetic Resonance in Medicine: An Official Journal of the International Society for Magnetic Resonance in Medicine, Vol. 62, no. 6, pp. 1609-1618, December 2009.

APPENDICES

Validation of our proposed tumor segmentation technique by the expert radiologists
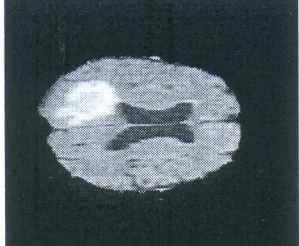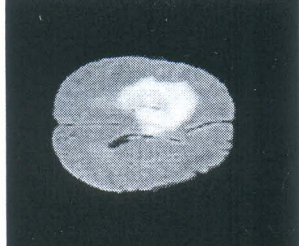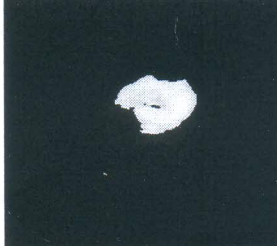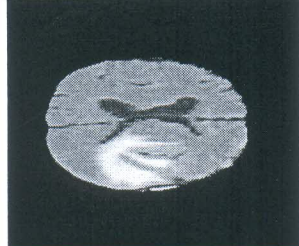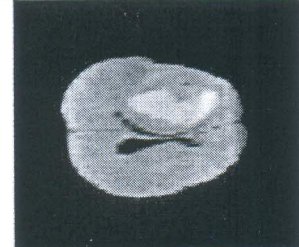
The experiments were conducted by Jyotsna Dogra (PhD Scholar, JUIT, Wakhnaghat) on Figshare and BraTS dataset using proposed techniques (CBSS, KMSS). The simulations and analysis were conducted under the supervision of Dr. Meenakshi Sood (Associate Professor, NITTTR, Chandigarh) and Dr. Shruti Jain (Associate Professor, JUIT, Wakhnaghat).

Original Image (Figshare dataset)	CBSS	KMSS	FUZZY	Validation by Expert Radiologist
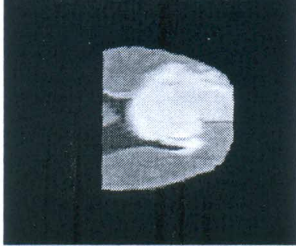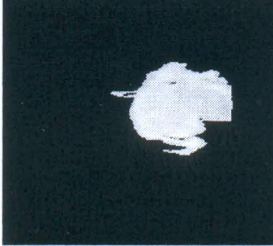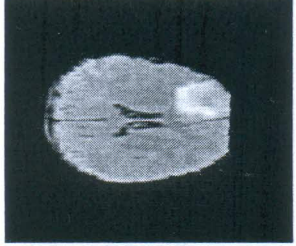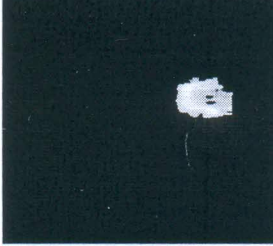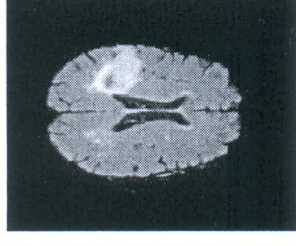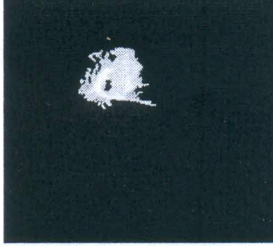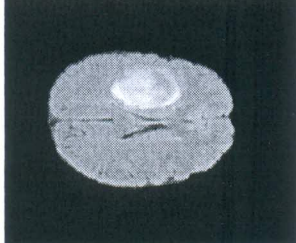
Original Image (BraTS Dataset)	CBSS	KMSS	FUZZY	Validation by Expert Radiologist

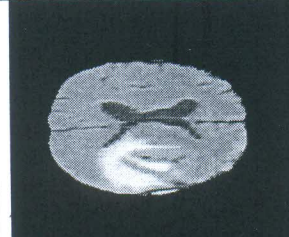**Validation of our proposed tumor segmentation technique by expert radiologists**
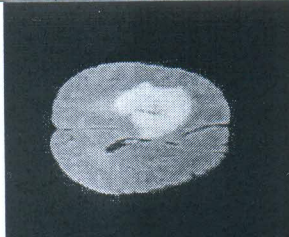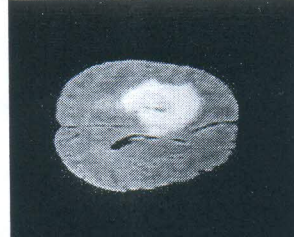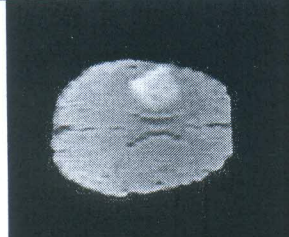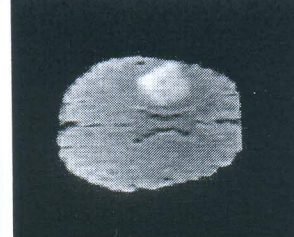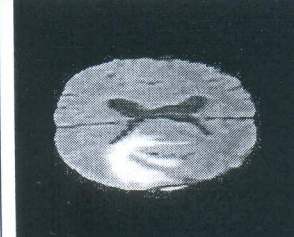
The experiments were conducted by Jyotsna Dogra (PhD Scholar, JUIT, Wakhnaghat) on BraTS dataset using proposed GBKS GC technique. The simulations and analysis were conducted under the supervision of Dr. Meenakshi Sood (Associate Professor, NITTTR, Chandigarh) and Dr. Shruti Jain (Associate Professor, JUIT, Wakhnaghat).

Original Image (HGG) (BraTS dataset)	GBKS GC	Validation by Expert Radiologist
		Dr. A. SOOD (Radiologist) DDU, ZH, SHIMLA
		Dr. A. SOOD (Radiologist) DDU, ZH, SHIMLA
		Dr. A. SOOD (Radiologist) DDU, ZH, SHIMLA
		Dr. A. SOOD (Radiologist) DDU, ZH, SHIMLA
		Dr. A. SOOD (Radiologist) DDU, ZH, SHIMLA

Validation of our proposed tumor segmentation technique by expert radiologists

Original Image (LGG) (BraTS dataset)	GBKS GC	Validation by Expert Radiologist
		Dr. A. SOOD (Radiologist) DDU, ZH, SHIMLA
		Dr. A. SOOD (Radiologist) DDU, ZH, SHIMLA
		Dr. A. SOOD (Radiologist) DDU, ZH, SHIMLA
		Dr. A. SOOD (Radiologist) DDU, ZH, SHIMLA
		Dr. A. SOOD (Radiologist) DDU, ZH, SHIMLA

Validation of our proposed tumor segmentation technique by expert radiologists

Original Image (BraTS Dataset)	Bias Field Image	Bias Field MR Images	Validation by Expert Radiologist
			Dr. A. SOOD (Radiologist) DDU, ZH, SHIMLA
			Dr. A. SOOD (Radiologist) DDU, ZH, SHIMLA
			Dr. A. SOOD (Radiologist) DDU, ZH, SHIMLA